The climate change potential of steel support structures for offshore wind turbines

MSc Industrial Ecology
Franciscus Huinink
May 2021

TU Delft

Universiteit Leiden

The climate change potential of steel support structures for offshore wind turbines

An assessment of monopile and jacket support structure steel mass and greenhouse gas emission development for offshore wind turbines in the North Sea

Franciscus Huinink
A MSc Industrial Ecology Master thesis
May 2021

Student number:	Delft: 4169042, Leiden: S2242923	
First supervisor	Dr. E.G.M. Kleijn	Leiden University Institute of Environmental Sciences (CML) Section: Future Resources
Second supervisor	Dr. A. Jarquin Laguna	TU Delft Dept of Maritime and Transport Technology (3ME) Section: Offshore and Dredging Engineering

Summary

Offshore wind electricity generation will play a key role in the transition to a sustainable energy sector. In 2020, the European Commission presented their Offshore Renewable Energy Strategy which includes 300 GW of offshore wind capacity by 2050 (European Commission, 2020). In the past few decades, turbine rated power has steadily increased from 0.5 MW turbines in the 1990's to almost 10 MW in 2019 (Wind Europe, 2019). The water depth at wind farm development sites also increases. For 2019, the average water depth of the EU's offshore wind turbines (OWTs) was 33 meters, while it was 25 meter in 2015 and 10 meter in 2000 (Wind Europe, 2020; Rodriguez et al., 2015). As a result, the size and mass of bottom-founded OWT support structures rapidly increase too.

This research focusses on the steel mass development of OWT structural support components like the tower, substructure and foundation considering a trend of higher power turbines and exploitation at increasing water depth. Support structure components form the majority of an OWT's mass and are commonly made of low-alloyed steel (Lourens, 2019b; Hoving, 2017; Igwemezie et al., 2019). A drawback of this material is the high energy intensity associated with steelmaking. Traditional steelmaking is also highly greenhouse gas (GHG) emission intensive, as fossil fuels are consumed to convert iron-ore to metallic iron, which is the bulk element in steel (Yang, 2019). The question emerges how the increase in support structure size affects the steel use of future structures and the relation between a wind turbine's steel use and associated GHG emissions and its electricity production. After all, the overlying goal of the energy transition as envisioned by the European Union is to reduce the emissions associated with electricity generation.

The research follows an initial design approach, to estimate initial dimensions of monopile and jacket support structures for 5 reference offshore wind turbines. For simplicity, initial dimensions are based on design rules-of-thumb hence no ultimate, serviceable or fatigue limit states are considered. Reference turbines of 5, 8, 10, 15 and 20 MW rated power are included in the model, as these can be expected to be commercially available up to 2050. A Water depth range of 20-80 meters is taken into account. Considering available development zones and environmental conditions, the study focusses on the North Sea region.

For monopiles, the location of the natural frequency is used as a design driver to determine the tower and monopile diameter and plate thickness. For 130 combinations of water depth, turbine rated power and soil conditions, initial monopile and tower dimensions were obtained of which 35 combinations showed to be within manufacturing and crane lifting constraints. For 5, 8 and 10 MW turbines, dimensions of viable monopile designs were found for water depths up to 60, 50 and 40 meter respectively. No combinations supporting 15 and 20 MW turbines were found within design constraints. Model results show that monopile support structure mass increases linearly with respect to water depth.

For jacket structures, member slenderness and constant bay geometry are used as design drivers to determine member length, diameter and plate thickness. In total, 126 out of 170 design combinations resulted in jacket support structure dimensions within design constraints. For 5, 8, 10 and 15 MW turbines, dimensions of jacket structures were found for water depths up to 70 meter, while this was 60 meter for the 20 MW turbine. Model results show that jacket support structure mass follows a second-order polynomial increase for increasing water depth. Overall, jacket structures show to be less steel intensive than monopile support structures considering their upfront steel requirements.

During decommissioning, steel that is part of the foundation and embedded in soil cannot be economically recovered and is therefore left at sea (Lourens, 2019b). For jackets, it is found that a higher share of the support structure steel mass can be retrieved, namely 75-95%. For monopiles, this

is 50-60%. Steel is not a scarce material, but several alloying elements used in steel for offshore use, like niobium and titanium, are on the EU's list of critical raw materials. The model results are used to estimate and compare support structure steel requirements and steel losses for a 500 MW wind farm at 20, 40 and 60 meters depth. For a 500 MW wind farm at 40 meter depth, approximately 34.000 ton steel loss can be avoided by using jackets rather than monopile support structures. Subsequently, 730 ton of niobium loss could be avoided which is almost 1% of annual global niobium production.

Considering the climate change potential of OWT support structures, GHG emissions that emerge during steelmaking and recycling are taken into account. A GHG emission indicator of 1.22 tCO2-eq/t steel is derived with the aim to reflect European steel production processes. GHG emissions that emerge during transport, manufacturing and assembly or during the making of other materials than steel are not assessed in this research. A GHG emission payback time indicator is developed to provide insight into how the GHG emissions invested in support structure steelmaking compare to the GHG emissions avoided through the generation of renewable electricity. It is found that, depending on the combination of turbine rated power and water depth, for monopiles the emission payback time lies in a range of 4-9 months. For jackets this is 2-10 months. The indicator showed to become less insightful when average electricity GHG emissions approach zero. In this case the emission payback time becomes near infinite and the indicator is no longer able to differentiate between low or high GHG emission investments. In conjunction with the emission payback time, the energy payback time is assessed. The energy payback time for the assessed OWT support structures varies between 3-6 months for monopile structures and 1-5 months for jacket support structures. Overall, GHG emissions for 5 MW monopile founded OWTs' electricity generation vary between 9.4-12.8 g CO2-eq/kWh at water depths of 20-60 meter. For 5 MW jacket founded OWTs, this range is 8.1-10.2 g CO2/kWh

In order to reduce the emission intensity of the offshore wind industry, this research recommends commissioners and designers to favour jacket over monopile support structures due to (i) reduced steel intensity for initial support structure manufacturing, and (ii) a higher recovery potential of support structure steel and its rare alloying elements at end-of-life. For 5 MW OWTs it is found that the application of jacket structures reduces an OWT's total climate change potential with 15-20% compared to monopile structures.

This research expands the knowledge of support structure mass development for future OWTs by using estimates of initial dimensions considering trends in turbine rated power and water depth exploitation to derive general formulas that help estimate a support structure's initial and recoverable steel quantity. Also, it provides insight into to the contribution of bottom-founded support structures to the climate change potential of OWTs and shows that the combination of turbine rated power, water depth and support structure typology significantly influence the steel and GHG emission intensity of an offshore wind turbine.

Acknowledgements

The writing of this master thesis for the Industrial Ecology studies has truly been a challenging experience. I have learned much about the research topic but also came to learn much about myself. The work that lays before you carries my name, but has been made possible by the continuous support of my supervisors, family and friends. For this I am truly grateful.

A special word of thanks to my two supervisors Rene Kleijn and Antonio Jarquin Laguna. Your calm, warm and supporting personalities, great minds and constructed feedback have helped me very much during the journey of this thesis. Your ability to keep things light have given me the power to keep going in times that I was overwhelmed or lacked overview. Despite your busy schedules, you have always managed to show up with a smile in our many digital meetings. You have given me the space to do this research in my own pace and in my own way which has made it an extraordinary and unique experience for me, with many lessons learned. Thank you both so much for your enthusiasm and dedication. It has been a pleasure to work with you.

Next I would like to thank my family. You were there for me day and night, in good times and during times of hardship, took me in and have given me more than any person could ever ask for. Without you, I would not have been able to come to this point. You have showed me what unconditional support is like, which is something I will never forget. You enabled me to be the person I am today.

Lastly, a big thanks to my friends, housemates and loved ones, who were always there to discuss the research and, more importantly, to talk about all the other aspects of life. I have truly enjoyed all the laughs, dinners and drinks we have shared over the past years. Cheers to all of you, next round is on me.

Cis Huinink

The Hague, May 2021

Table of Contents

1. Introduction

In order to avoid global temperatures rising to irreversible levels, annual greenhouse gas (GHG) emissions have to be reduced. The energy sector is responsible for a large share of annual GHG emissions, as fossil fuels are oxidized to convert their embedded chemical energy into the electricity and heat society demands. For the European Union (EU), the energy sector was responsible for 49% of total emissions in the year 2014 (Ritchie & Roser, 2019). In order to reduce GHG emissions, the European Commission required the member states to formulate national renewable energy action plans (NREAPs) in 2010 and national energy and climate plans (NECPs) in 2019. From these plans, it becomes clear that alternative energy generating technologies, like wind and solar power, will form the basis of the EU's renewable electricity production in the future (International Energy Agency, 2019). In 2019, cumulative EU28 onshore wind turbine capacity reached 169 GW (Sönnichsen, 2020) and cumulative offshore wind turbine (OWT) capacity reached 22 GW (Wind Europe, 2020). In 2018, scenarios developed in support of the EU's long-term strategy included 240-450 GW of offshore wind capacity by 2050, significantly increasing European offshore wind capacity (European Commission, 2018). In 2020, this long-term strategy was redefined in the Offshore Renewable Energy Strategy to include 300 GW offshore wind capacity by 2050 (European Commission, 2020). Similarly, the offshore wind industry aims to develop up to 150 and 180 GW of offshore wind in the North Sea region by 2040 and 2050 respectively (NSWPH, 2019). Stated policy targets for the EU member states suggest the aim to increase the total capacity of offshore wind power to 65-85 GW by 2030 and up to 130 GW by 2040 (International Energy Agency, 2019). These prognoses all indicate a rapid expansion of the European offshore wind sector.

A shift in material use between fossil and renewable energy sources

In contrast to current fossil fuel based energy systems, renewable energy conversion systems – like OWTs – do not consume resources during operation but require a material investment upfront. Where traditional energy sources convert chemical energy from carbon-rich fuels into mechanical energy through an engine, for OWTs kinetic energy from the wind is converted to mechanical energy by the wind turbine's rotor. The kinetic energy is then converted to electrical energy by generator equipment, which is located in the nacelle of the OWT. The maximum power output of an OWT is largely dependent on the rotor swept area, where bigger rotors can convert more energy and subsequently have a higher rated power. This, however, does not mean that no materials are consumed by renewable energy sources. In order for the rotor and nacelle equipment to properly operate, supporting structures are required to keep the nacelle-rotor assembly (NRA) in place and to guarantee overall structural stability. Bigger rotors require bigger support structures, which in turn require more material.

Structural components required to construct OWTs and secondary infrastructure are manufactured onshore and transported to the construction site offshore, to be assembled on site. After approximately 20 years of operation, the OWTs are decommissioned and partly disassembled. The OWT's components are then transported back to shore. Some main components are the rotor, nacelle, tower, substructure and the foundation. Where the rotor and nacelle form the basis of the energy conversion system, the focus of this research is on the structural support components like the tower, substructure and foundation. These components form the majority of the OWT's mass and are commonly made of low-alloyed steel. Steel is a common construction material, characterised by high strength and workability and is well recyclable (Yang, 2019). However, a drawback of this material is the high energy intensity associated with steelmaking. In the conversion of iron ore to steel, high temperatures are required to convert iron ore to metallic iron, which forms the bulk element of low-

alloyed steel. Currently, these high temperatures are obtained through the burning of fuels. In summary, traditional fossil-based electricity generation equipment directly converts fuels into electricity during operation, whereas renewable electricity generators require a more sizeable upfront investment of energy – and associated GHG emissions – spend in material making but then no longer consume fuels in operation. Therefore, a shift appears in the size, location and moment of time considering the emergence of GHG emissions in electricity generation. The goal of the upcoming energy transition, is to reduce the net GHG emissions related to electricity generation to as low as reasonably possible.

Steel requirements of future OWTs and associated GHG emissions

Topham et al. (2019) show in their paper that the ratio between rated power and construction material requirements increases with higher rated-power OWTs, making larger turbines more material intensive. For example, they found that a single 4 MW OWT requires more construction steel than two 2 MW OWTs would. While it is common to assume that technological upscaling leads to increased material efficiency, the opposite seems to be the case for the steel requirements of OWT structures. This is an important phenomenon, as recent trends show a steady increase in both average and maximum OWT rated power over time, suggesting that OWT's become more steel intensive. Another facet highly relevant for offshore wind energy is the water depth of the exploitation area. Logically, for bottom-fixed structures, deeper water requires a larger size support structure which subsequently increases support structure steel requirements. However, the magnitude of these two effects, being the increase in rated power and water depth on OWT support structure steel demand, is not yet known but considered important due to the GHG emission intensity of current steel making processes.

The influence of steel requirements and its production process on the GHG emissions associated with offshore wind power becomes clear through a lifecycle analysis (LCA) study by Bonou, Laurent & Olsen (2016). Bonou et al. (2016) found that for OWTs of 4 and 6 MW, approximately 40% of total contribution to climate change (CC) was related to the embedded emissions of monopile and tower steel structures alone. Even though turbines of this size can already be considered quite large, future turbines are expected to be even larger, potentially up to four or five times this rated power. Furthermore, these larger structures are expected to be built further offshore and in deeper waters. The question emerges how this affects the steel use of these future structures and the relation between a wind turbine's steel use and associated GHG emissions. After all, the overlying goal of the energy transition as envisioned by the European Union is to reduce the emissions associated with electricity generation.

Knowledge gap

The knowledge gap that this research addresses can be found in the following four aspects:

1. Effect of upscaling of turbine rated power on material demand of OWT support structures
2. Effect of increasing water depth on material demand of OWT support structures
3. Effect of increasing support structure size and steel demand on associated GHG emissions
4. Effect of increasing support structure size on the emission and energy payback time.

With respect to the first effect, literature like the papers from Topham et al. (2019) and Shammugam et al. (2019) are found that provide analysis considering installed capacity and number of installed foundations. Topham et al. (2019) show a correlation between monopile length, weight and turbine rated power based on readily installed turbine data and provide a linear regression to describe the trend. A similar linear assumption was made by Shammugam et al. (2019) in their assessment of future

material requirements for the German offshore wind industry. However, when one compares steel requirements for a V164-8MW OWT tower at different hub heights, the tower mass seems to increase exponentially rather than the linear trend provided in the paper. This raises the question if a linear regression describes the development of support structure mass with respect to turbine rated power and water depth sufficiently.

With respect to the second effect, no literature is found that describes the effect of applying alternative support structure typologies on steel demand and associated emissions. This is important, as it is not clear if the currently prevailing monopile support structure typology is capable of supporting turbines of future magnitude and/or increased water depth. Various alternative support structure typologies exist and are applied in practice, like lattice type structures and floating foundations. In this research, focus lies on bottom-fixed support structures, specifically on monopiles and jackets of which a schematic representation is shown in Figure 1. Floating foundations are out of the scope of this work.

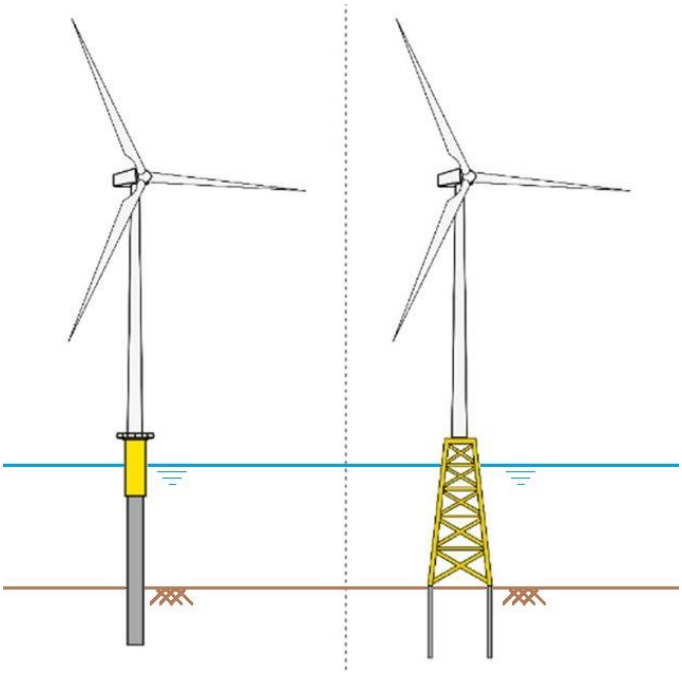

Figure 1: Schematic representation of a monopile supported OWT (left) and a jacket supported OWT (right).

As monopiles form the dominant support structure typology, only a limited number of jacket support structures is currently installed. The structures that are available for assessment are built for low to medium rated capacity turbines (<8 MW) and shallow water areas. Higher rated power OWTs (>8 MW) supported on jacket substructures have as of yet not been realised. A research approach that analyses readily installed structures to estimate steel requirements of to-be-built OWT support structures, a top-down approach, is therefore less effective. In this research an alternative approach is applied, namely a bottom-up approach. Instead of using data of existing structures, initial support structure dimensions are estimated by applying design rules-of-thumb for turbine sizes in a range of 5-20 MW, situated in water depths of 20-80 meters. To ensure that the applied design method reflects offshore structures in a sufficient degree, technical drawings of existing structures were assessed prior to the creation of a dimensioning model. An advantage of applying a bottom-up approach is that it allows to compare the two support structure typologies in similar operating and environmental conditions.

With respect to the third and fourth effect, no literature directly addressing these effects is found. Therefore, an estimate of embedded GHG emissions in support structure steel is included based on the dimensioning model results obtained in the study of the first two effects.

Aim of the research and the research question

This research touches upon the topics of technological change, dematerialisation and decarbonisation and aims to provide insight in the future requirements and related impact to the emerging technology associated with the offshore wind industry. The primary aim of this research is to provide insight in the development of steel requirements associated with bottom-founded support structures of offshore wind turbines of various sizes at various water depths. A secondary aim is to fill the knowledge gap regarding growing OWT support structure dimensions and their associated environmental impact in terms of climate change potential. Furthermore, this thesis research aims to add on the work of other authors like Topham et al. (2019) and Shammugam et al. (2019) by expanding the project scope to include jacket support structures and the geographical boundaries to the North Sea region. Novelty can be found in the application of a bottom-up approach instead of the top-down approach presented by reviewed literature. This leads to the following research question:

How do support structure steel demand and associated environmental impact evolve for offshore wind turbines in the North Sea until 2050, following trends of exploitation at increasing water depth and turbine rated power?

And the following research sub-questions:

SQ1. How does the material demand for main bottom-fixed support structure technologies like monopiles and jackets change with increasing water depth and rated power?

SQ2. What is the impact related to steel requirements of the assessed OWT support structures and what is the emission payback time?

In support of the research sub-questions, insight into available support structure typologies and the range of OWT rated power that can be expected to emerge within the temporal scope of the research is required. Therefore, the following two supporting questions are formulated.

1. *Which bottom-fixed support structure technologies are available for offshore wind turbines at various water depths until 2050?*
2. *How has the rated power of wind turbines evolved over time and what is expected until 2050?*

Structure of the report

The report is divided over five sections and several supporting addendums. In the first chapter, the introduction, a problem statement is formulated followed by the aim and main research question of this research. In the second chapter, the methods applied to the answer the research question and sub questions are elaborated. A model is created based on design rules and standards, that allows for preliminary dimensioning of monopile and jacket support structures in North Sea environmental conditions. Findings from literature analysis and the model results are covered in Chapter 3. A discussion and the interpretation of obtained results is provided in Chapter 4, followed by the limitations of this research and several suggestions for future research. Finally, in Chapter 5 the research questions are answered and the key points of this research are summarized.

2. Methods

This research combines qualitative and quantitative approaches to gain insight in the answer to the main research question as formulated in the introduction. The main steps followed throughout the research process are visualised in the research flow diagram shown in Figure 2 and are elaborated in this chapter. The first step is to perform a literature review in order to gain understanding of the past, current and future status of offshore wind within the North Sea region. Academic literature is reviewed, as are policy and industry reports. The second step is to create a model to estimate initial dimensions and structure mass for two bottom-founded support structures in various operating conditions, namely monopiles and jackets. The information gathered in the first step is used to determine model input parameters and boundary conditions. The model results are then used to provide insight into the development of steel requirements for OWTs that can expected to be built up to 2050. The third step of the research is to convert the estimated steel requirements into associated GHG emissions or, in other words, to estimate the climate change potential of OWT support structures that can be expected to emerge in the North Sea region towards 2050.

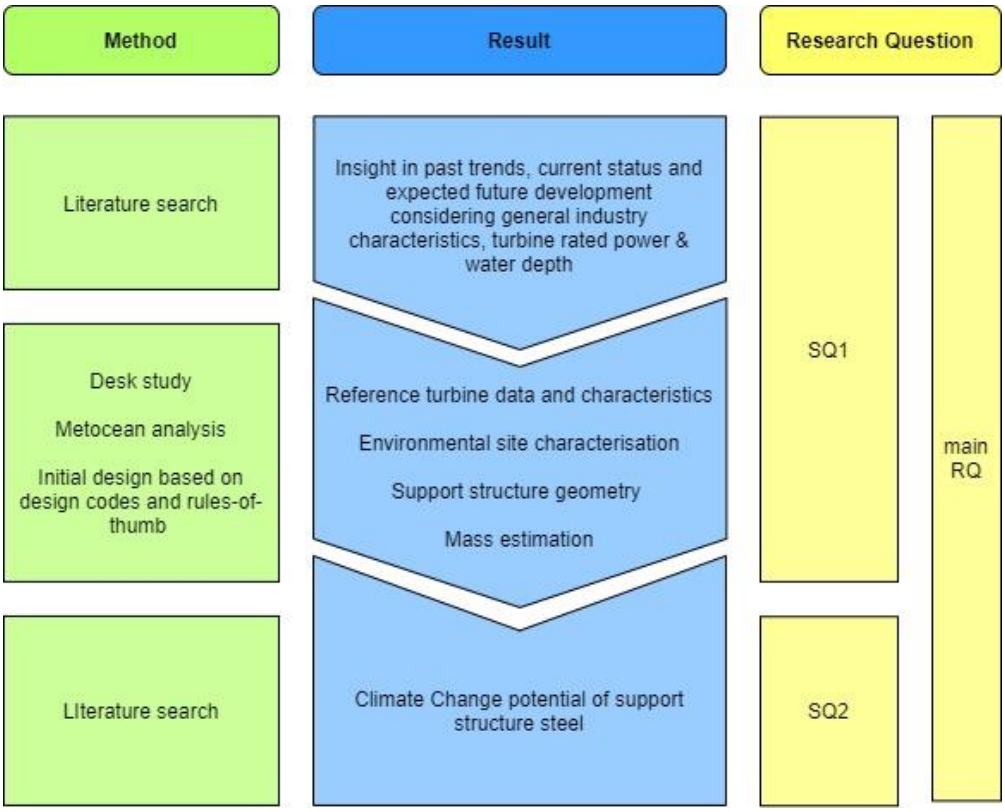

Figure 2: Visualization of the research steps, methods and results and their relation to the main and sub-questions.

2.1 Definitions

First, definitions of frequently mentioned OWT components are explained and clarified in the following parts. After that, the definitions of construction steel, GHG emissions and the emission payback time of support structures are elaborated.

2.1.1 Definitions of OWT components

A wind turbine is designed to convert kinetic energy present in wind to electrical energy used by machines and devices. Very generally, a OWT can be divided into two parts: the nacelle-rotor assembly (NRA) – also known as the hub – and the supporting structure that keeps the NRA in place. An example of this can be seen in Figure 3. The support structure allows the wind turbine to be operational and is built to withstand environmental and operational loads. It generally consists of 3 parts: the tower, substructure and foundation. In the following, a description of each of these components is presented.

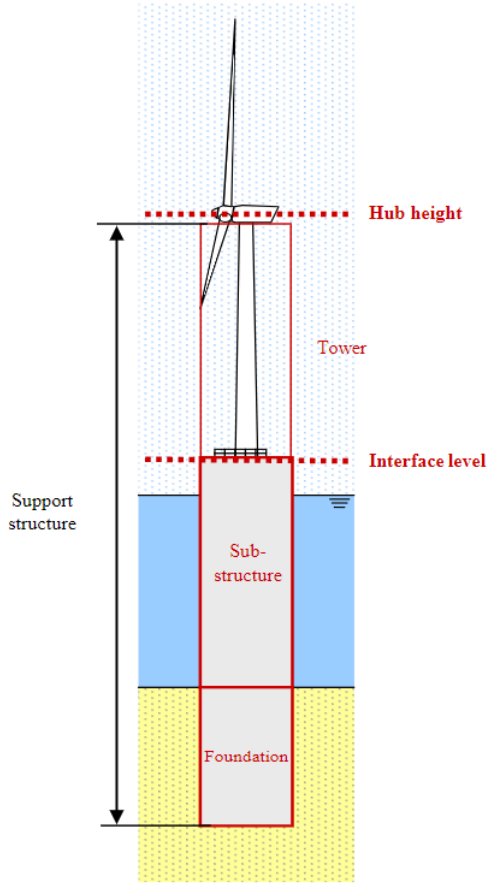

Figure 3: Overview of general OWT components. This image is obtained from Lourens (2019b).

The NRA

The NRA consists of the nacelle and the three-bladed rotor. The nacelle houses the drive train of the OWT. The drive train contains the generator and gearbox which converts the torque and rotation of the blades into electricity. OWT designs with a gearbox are currently most dominant, but designs without gearboxes do exist and are called 'direct-drive' systems. NRA configurations with gearboxes are of lighter weight, but often require more maintenance due the many moveable parts and associated risk of mechanical failure and operational downtime. Direct-drive systems are heavier than their gearbox counter parts, but require less maintenance and experience less downtime (Zaaijer, 2019).

The tower

The tower connects the NRA, at hub height, to the substructure at the interface level at the bottom part of the tower. The height of the interface level is determined as that height at which no sea water will reach, accounting for tidal difference, storm surge and extreme waves. The tower is commonly constructed from tubular cold rolled steel sections and characterized by large diameters up to 10 meters. The bottom diameter of the tower is similar to the top diameter of the substructure to allow for a streamlined design. At the tower bottom, a platform can constructed to allow for boat landings, tower access and staircases towards the hub.

Transition piece

Commonly, a transition piece (TP) is used for the connection between the tower and substructure. It has a load transferring function between the submerged section of the structure and the tower and can provide space to fit boat landings and/or a platform. A transition piece has the advantage of providing a method for inclination correction to ensure correct verticality of the tower during installation. Also, it provides a space to host electrical equipment. When a land based tower model is applied offshore, tower dimensions are copied and any difference in length is covered by a transition piece, see Appendix B in Gaertner et al. (2020).

The traditional connection technique between tower and TP is grouting, which is a form of concrete connection and acts as a glue to connect the two components together. Other, upcoming, techniques are steel bolts and slip joints. Furthermore, a new concept in support structure design is the transition-piece-less design (Lourens, 2019b). The tower is then directly connected to the substructure.

The substructure

The substructure connects the tower toe, or transition piece, to the foundation at seabed and is characterized by being largely submerged. The top of the substructure lies within the splash zone, where the effect of waves and the sea surface are most noticeable. Corrosion protection is especially important here, due to the structure's exposure to the combination of both salt water and oxygen. Multiple substructure topologies are available, where a distinction can be made between bottom founded and floating substructures. Examples of bottom founded structures are gravity base, monopiles, tripods and jacket/lattice towers. Examples of floating structures are ballast stabilized, mooring line stabilized and buoyancy stabilized devices. In section 3.1 more in-depth information is provided about various substructures.

The foundation

The foundation fixates and transfers loads on the substructure, tower and NRA to the ocean floor. The foundation used for OWT is commonly one large, or multiple smaller, steel pile(s) embedded in the soil. Other designs have been proposed such as suction buckets and suction caissons, but these are so far mostly in a conceptional stage of development (Watson et al., 2019). Several foundation installation techniques are available like hammering - using hydraulic impact hammers, vibrating - using vibratory devices, and drilling. Of these, the first two are most applied in practice (Lourens, 2019b).

The interaction between soil and structure is complex, especially for large structures. There is much uncertainty regarding soil behaviour, as soil conditions are known to vary greatly even in soils only a short distance apart. Further more, load transfer to the soil is non-linear, which requires complex models aiming to describe soil-pile behaviour (Lourens, 2019b). Research towards soil interaction is actively ongoing.

Another element typically found in offshore foundations is scour protection. As water particles move around submerged structures, increased particle velocity makes that small particle sediment, like sand, is removed around the foundation creating a hole. This has to be avoided as it negatively influences safety and stability of submerged structures. A common scour protection method is the deposition of rocks around the base of the support structure.

2.1.2 Definition of construction steel

The support structure of an OWT is predominantly made out of construction steel (Lourens, 2019b; Hoving, 2017; Igwemezie et al., 2019). Construction steel is an alloy of elemental iron and several alloying and/or tramp elements with specific properties selected for offshore use. Commonly, OWT support structures are manufactured from carbon steel with a low (<1%) carbon content. For offshore wind, type S355G8+M, S355G10+M, S420G2+M and S460G2+M construction steels are typically applied (Igwemezie et al., 2019). A description and more in-depth information about the material composition of commonly used steel alloys in offshore environments can be found in appendix A3 Steel composition and element criticality. A description of the integrated steelmaking and recycling process can be found in appendix A4 Steelmaking and the steel recycling.

2.1.3 Definition of greenhouse gas emissions

In traditional production of any type of steel, emissions are produced and emitted to the atmosphere. One of the emissions that is produced in large quantities is carbon dioxide (CO2), a green house gas (GHG). However, many more GHGs exist of which some are released in steel making processes. CO2, methane and nitrous oxide emissions are common gases that emerge during the burning of fossil fuels (EPA, 2020). Some GHGs are more potent than others, meaning that the emittance of one type of gas, like for example methane or nitrous oxide, influences global warming more than another would.

To express global warming potential (GWP), the potency of greenhouse gases are expressed relative to that of the reference greenhouse gas CO2, which has a potency of 1. Methane has a higher potency than carbon dioxide, but emerges in much smaller quantities, namely <35g CH4/t steel. The potency of Nitrous oxide is even higher, but emerges in even smaller quantities than CH4 (EPA, 2020; Lubetsky, Steiner & Faerden et al., 2006). Therefore, the total GWP of a product or process is commonly expressed in terms of CO2 equivalent GWP – or CO2-eq – to take the potency of various emerging GHGs into account and express the GWP as a single entity. The emission factor applied in the calculations of this research is elaborated in section 2.5.

2.1.4 Definition of emission payback time of support structures

As mentioned in the introduction, the goal of the energy transition is to reduce GHG emissions related to energy production. However, this does not mean that there are no GHG emissions associated with renewable energy sources. Traditionally, chemical energy embedded in fossil fuels is used to produce the heat and electricity society and industry use. As a result of the burning of these fossil fuels, GHG emissions are emitted. In contrast, renewable energy sources emit little to none GHG emissions during operation, as they convert energy present in for example solar radiation or wind. In order to construct renewable energy converters, like solar panels or wind turbines, materials are required and during the production and refining of these materials energy is consumed.

In his paper, Schleiser (2000) introduces the concept of energy payback time, which is defined as a turbine's required operational time to generate a similar amount of energy as that was spend to create the wind turbine. A similar approach is taken for the support structures assessed in this research. The energy required for material production is, at this point in time, still largely obtained from fossil fuel sources like coal and natural gas (Yang, 2019). Therefore, the emissions invested into the creation of the OWT are compared to the emission saved during the OWT's operational time and the 'emission payback time of support structures' is introduced. This is defined as 'the amount of time required for an OWT to be operational in order to equal the emissions associated with the making and refining of its embedded steel'. A reduction in steelmaking GHG emissions leads to a reduction in emission payback time. Similarly, decarbonization of the average electricity production leads to an increased emission payback time.

2.2 Scope of the research and system boundaries

In terms of system boundaries, the research context, scope and boundary conditions are specified as follows. The research context is that of material requirements for the energy transition as envisioned by the European Union. The energy transition involves many renewable energy solutions, like wind, solar and hydro power production, but this research is focused on offshore wind power production. Next, the geographical boundary is set to the North Sea region. The North Sea region covers maritime areas of six countries, being the United Kingdom, Germany, Denmark, Belgium, the Netherlands and Norway. The temporal boundary is up to the year 2050, following the scope of common policy reports.

Technical scope

Considering the technological scope, the research is focused on bottom founded OWTs. Floating support structures are shortly discussed but not further included in models created for this research. Floating support structures are expected to gain significant market share through their effect on development zone expansion and potential to reduce LCOE. However, the majority of OWT development areas within the North Sea region are situated in areas with water depths less than 100 meter. At these depths, bottom founded support structures are found to be more suitable (Perez-Collazo, Greaves & Iglesias, 2015).

Considering OWT components, the embedded steel in support structures of OWTs is analysed, but the rotor and nacelle are left out of scope. This report focuses on the steel demand of support structures and not the materials required for the NRA or power equipment. This is because the steel contribution of these components is relatively small compared to that of the support structures, while it is the dominant construction material for support structures (Topham et al., 2019; Bonou et al., 2016). Other support structure materials, like concrete, are not assessed. Secondary OWT infrastructure like offshore substations are not included in the scope of this research.

Modelling scope

The scope of modelling detail is limited to the level of initial design. Design rules-of-thumb are applied to estimate component and member dimensions. This is further elaborated later in this chapter. Calculation of forces, stresses and limit states are essential and require sufficient detail to guarantee the structural integrity of the support structure during its design life. However, for the sake of simplicity, in this work only an estimation of the initial dimensions is obtained.

Lifecycle stages and associated GHG emissions

Various lifecycle stages of an OWT are assessed. As proposed by Schleiser (2000), these various lifecycle stages of an OWT structure are:

1. Resource extraction
2. Resource transportation
3. Materials processing
4. Component manufacturing
5. Component transportation
6. Turbine construction
7. Turbine operation
8. Decommissioning
9. Turbine product disposal

Bonou et al. (2016) find that approximately 70% of total climate change contributions are related to materials production – e.g. steps 1-3 of above lifecycle stages – and little over half of that is contributed by the tower, substructure and foundation steel. GHG emissions associated with manufacturing, installation and dismantling of the support structures are limited and not taken into account in this research. Their combined effect contributes approximately 22% of the total climate change potential (Schleiser, 2000; Bonou et al., 2016). With respect to GHG emissions emerging throughout the OWT's lifecycle stages, the research includes emissions associated with steelmaking and recycling, which correspond to steps 3 and 9 of the material's lifecycle stages.

2.3 Qualitative approach: literature review

Literature review was performed to gain insight in historical development, the current status and future of the EU's offshore wind power sector. Literature is analyzed regarding development of turbine size and rated capacity, available and emerging technologies and their expected advancement within the temporal scope. Furthermore, additional information considering the levelized cost of energy, industry investments, important actors and readily installed capacity was found and is included in appendix A2 Background information wind industry. EU member state's policy targets are consulted to gain insight in future trends like the expected cumulative capacity and available development zones for offshore wind parks. A more elaborate overview of the literature review process is included in appendix A1 Literature review process.

The literature review forms the basis of the required insight to find answers to the additional questions formulated in support of the first and second research sub-questions. These are:

1. *Which bottom-fixed support structure technologies will be available for offshore wind turbines at various water depths in the North Sea until 2050?*
2. *How have water depth and rated power of wind turbines in the North Sea evolved over time and what is expected until 2050?*

2.4 Quantitative approach: support structure mass estimation model

Quantitative modelling can be done in two ways. The first is a top-down approach, which entails the analysis of existing structures and then uses extrapolation to estimate the dimensions of OWT support structures supporting larger turbines in deeper waters. The second is a bottom-up approach, where design rules and standards are applied to estimate initial dimensions of individual support structure components and sequentially the full support structure. Availability of suitable data – in terms of comparability for monopile structures and in terms of quantity with respect to jacket structures – limited the suitability of a data analysis approach. Hence, the bottom-up approach is considered to model the effect of increased turbine rated power and exploitation of deeper waters on the steel demand of OWT support structures. A mass estimation model based on initial design rules and guidelines is created for two main support structure typologies, namely monopiles and jackets. From literature assessment with respect to available support structures until 2050 and available areas for offshore wind park development, these two bottom founded typologies are considered most likely to be implemented for large scale development of OWTs.

The quantitative model forms the basis of the required insight to answer the research sub-questions, which are:

SQ1. How does the material demand for main support structure technologies change with increasing water depth and rated power?

SQ2. What is the environmental impact in terms of climate change potential related to the steel requirements of assessed OWT support structures and what is their environmental payback time?

In the following, the five steps taken to create the model and define model parameters are discussed. These are sequentially: the range of OWT rated power to be assessed, assessment of North Sea environmental conditions, an estimation of initial support structure dimensions and associated steel mass, an estimation of retrievable support structure steel at end-of-life and an estimation of the emissions associated with steel making. Lastly, the model certainty and sensitivity are presented. A more elaborate description of the modelling approach is included in appendix A5 Technical design and modelling details.

Step 1: Selection of OWTs to be assessed

Five reference turbines of varying rated capacity are selected, in a range of 5-20 MW, that can be expected to emerge within the temporal scope. Reference turbines are created by researchers and developers, to provide insight into characteristics of future OWTs. The reference turbines under assessment and their respected sources are shown in Table 1.

Table 1: Hub height and nacelle-rotor-assembly mass for the reference turbine models under assessment.

Turbine model	Hub height [m]	M_{NRA} [t]	Source
NREL-5MW-ref	90	350	Jonkman et al. (2009)
LW-8MW-ref	110	480	Desmond et al. (2016)
DTU-10MW-ref	119	677	Bak et al. (2013)
IEA-15MW-ref	150	1017	Gaertner et al. (2020)
IEA-20MW-ref	168	1730	Jensen et al. (2017)

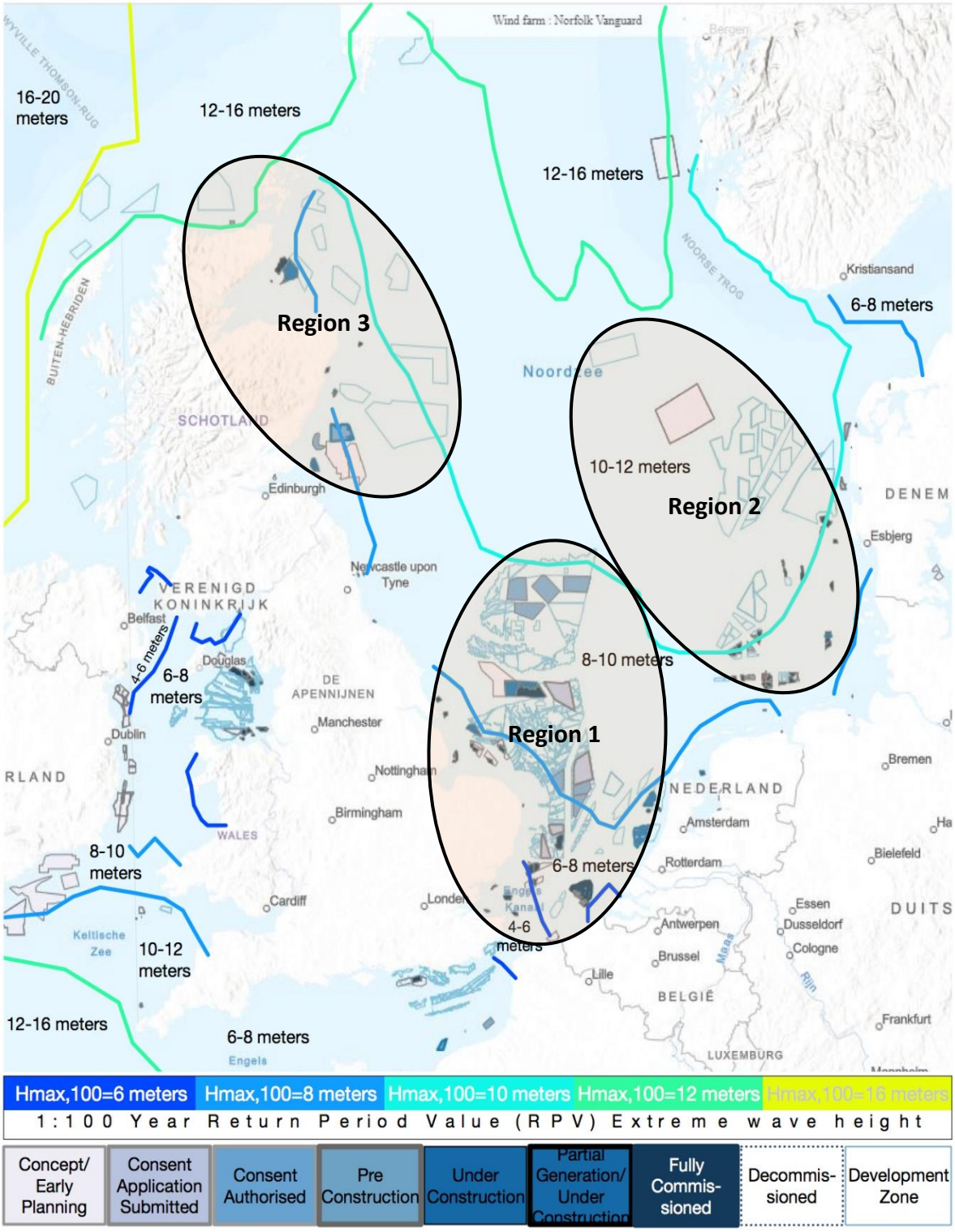

Figure 4: Selection of regions on detailed OWT development zones, including 1:100 year maximum wave height. Number indications shown black text indicate the extreme wave height in between contours.

Development zone base map is obtained from the 4Coffshore website, available at: https://www.4coffshore.com/offshorewind/.
1:100 RPV extreme wave height are obtained from the Meteorological Service of New Zealand ocean viewer and shown as contours (MetOceanView, available at: https://app.metoceanview.com/hindcast/).

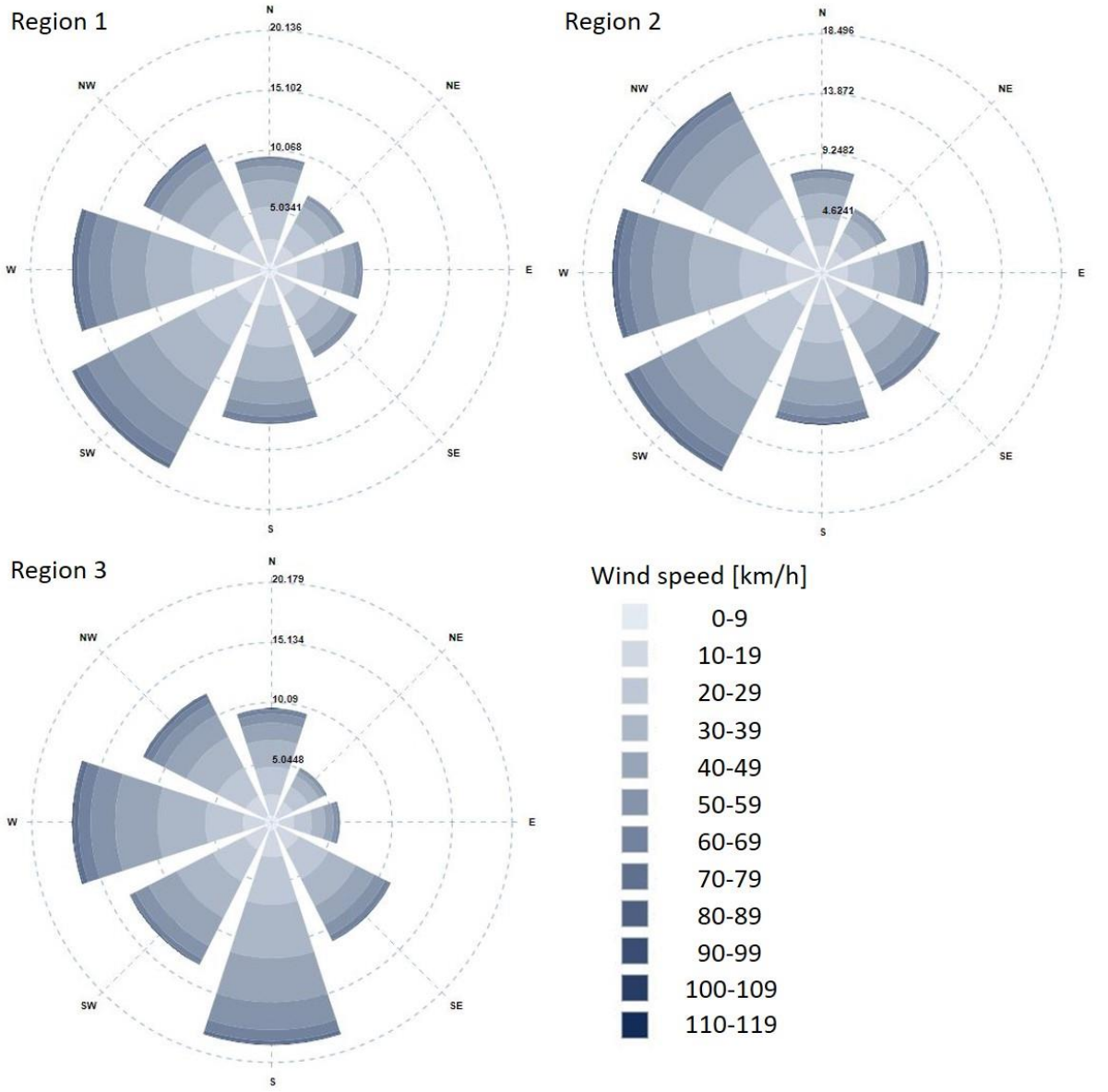

Figure 5: Wind roses for Region 1, 2 and 3 showing frequency of occurrence [%] and wind speed [km/h] in the year 2020. The figure shows wind speed and direction measured at 10 m height and for 5 minute intervals. This figure is retrieved and adjusted from the Meteorological Service of New Zealand (2020) website. Frequency of occurrence is indicated by the size of a segment, where each dashed ring represents approximately 5% occurrence. Wind direction is indicated by compass directions. Wind speed is indicated by colour.

For Region 1, the dominant wind directions are West and South-West. The 50% exceeding wind speed is 30 km/h, the 90% exceeding wind speed is 50 km/h. For region 2, the dominant wind directions are North-West, West and South-West. The 50% exceeding wind speed is 30 km/h, the 90% exceeding wind speed is 51 km/h. For Region 3, the dominant wind directions are West and South. The 50% exceeding wind speed is 33 km/h, the 90% exceeding wind speed is 54 km/h.

Step 2: Assessment of North Sea environmental conditions

Available development areas are assessed and divided into regions to account for variating environmental conditions. A trade-off between the number of required computations and variation in environmental conditions like water depth and wave height conditions was reason to define three specified regions, see Figure 4. Especially wave height conditions show a large variety within the North Sea. For example, in Region 1 the 1:100 year extreme wave height is found in a range of 6-10 meter, whereas in Region 3 this is 10-16 meter. Wave conditions are described through assessment of JOWNSWAP spectra for the three selected regions.

Wind conditions are similar in the three regions. Measured at a height of 10 meter above sea level, the 50% annually exceeded wind speed is 30-33 km/h for all three regions, see Figure 5 (Meteorological Service of New Zealand Ltd, 2020). The 90% annually superseded wind speed is 50-54 km/h. It should be noted that the wind speed is commonly higher at bigger altitudes. The wind speed can be extrapolated to higher altitudes using a power law profile. Neutral stability of the atmospheric boundary layer is assumed. The wind speed at 90 meter hub height, which corresponds with the NREL-5MW reference turbine, is approximately 35% higher than the wind speed at 10 meter height. At 170 meter hub height, for the IW-20MW reference turbine, the wind speed is approximately 50% higher than the values shown in Figure 5. For the reference turbines of 8, 10 and 15 MW rated power, the increase in wind speed is in a range of 40-45%.

Water depth conditions for each region are found through analysis of North Sea bathymetry maps and are combined with available development areas in Figure 13 on page 26. Considering soil conditions, a distinction is made between soft-medium sandy soil and medium-dense sandy soil layers.

Data sources

Relevant environmental data is obtained from multiple sources. Available wind park development zones are obtained from the 4Coffshore website. Publicly available ocean viewer tools provided by the National Oceanic and Atmospheric Administration and Meteorological Service of New Zealand (2020) are used to determine the bathymetry, wind and wave conditions in the North Sea region and complemented with the findings of a paper by Beels, Henriques & de Rouck et al. (2007). Information regarding ocean currents is obtained from a paper by Vos (2015). A report by the Alfred Wegener Institute (2009) provided insight into the sedimentation and soil conditions of the North Sea.

Step 3: Estimation of support structure dimensions and steel mass requirements

In order to estimate the overall size and dimensions of an OWT's support structure components, design rules as described by the DNVGL-ST-0126 standard are applied. General dimensions of tower and substructure are obtained and used to determine the dimensions of individual structural members for monopile and jacket substructures (DNV-GL, 2016). Monopile founded OWTs consist of a tower and monopile. Jacket founded OWTs consist of a tower, TP, jacket and foundation. A summarised description of the modelling process for these two substructure typologies is presented below.

Monopile support structures

A step-by-step initial design approach suggested by Arany, Bhattacharya & Macdonald et al. (2017) and a lecture of the TU Delft course 'Offshore Wind Farm Design' (Lourens, 2019b) are used to determine initial dimensions of monopile support structures. In this work, the location of a monopile and tower's natural frequency is used as the design driver. In order to avoid the occurrence of resonance between rotor and wave induced vibrations and to account for the dynamic nature of forces acting up OWT structures, a target design frequency is determined for 130 combinations of water depth, turbine rated capacity and soil conditions. Then, through an iterative process, monopile

dimensions are obtained using Rayleigh's method to estimate a monopile's eigenfrequency. The OWT's monopile and tower dimensions are iteratively adjusted until their natural frequency aligns with a design target frequency. The formula applied to find a monopile's eigenfrequency is:

$$(1) \quad f_{natural} = \frac{\pi}{8} * \sqrt{\frac{EI_{equivalent}}{\left(m_{top} + m_{equivalent} * L\right) * L^3}}$$

, where $f_{natural}$ is the monopile's eigenfrequency, E is the modulus of elasticity in Nm^{-2}, $I_{equivalent}$ is the moment of inertia for the combined tower and monopile combined in m^4, m_{top} is the mass of the RNA in kg, $m_{equivalent}$ is the mass per unit length in kg/m and L is the combined tower and monopile length in m.

Monopile dimensions cannot be increased indefinitely due to manufacturing limitations. Current maxima for monopile cumulative mass, length and diameter are 2250 ton, 120 meter and 11 meter respectively (Sif Group, 2018). Larger tower and monopile diameters are not yet possible to manufacture but this might be the case in the future. Same holds for the lifting capacity for cranes on board of installation ships. During a presentation by Van Oord – a company specialised in OWT installation – a maximum expected lifting capacity of 1600 and 2500 ton are mentioned for ships available now and by 2030 (Van de Brug, 2019). Therefore, the iterative dimensioning process is stopped when maximum mass, cumulative length and/or diameter of respectively 2500 ton, 130 meter and/or 12 meter were encountered.

Jacket support structures

A step-by-step initial design approach as suggested by Hoving (2017) is applied to determine initial support structure dimensions for 180 combinations of water depth, turbine size and soil conditions. The dimensions of any component follow from dimensions of components higher up. For example, the width at the tower top depends on the dimensions of an OWTs nacelle. In turn, TP dimensions depend on the bottom diameter of the tower, jacket dimensions depend on the bottom width of the TP and foundation dimensions depend on the dimensions of the jacket legs.

For jacket support structures, tower dimensions are set to be equal to those determined for the monopile support structures. To account for a streamlined design, the dimensions of the TP top are set to be equal to the diameter of the tower bottom. Transition piece dimensions are then estimated based on a paper of Lee, Gonzalez & Lee et al. (2016), using the following formula.

$$(2) \quad b_{TP} = \frac{3 * D_{tower,bottom} + 2 * D_{jacket\ leg}}{\sqrt{2}}$$

, where b_{TP} is the bottom width of the TP in m, $D_{tower,bottom}$ is the diameter of the tower bottom in m and D_{jacket} leg is the diameter of a jacket leg in m.

Next, jacket bay dimensions are determined following initial member size estimates as suggested in lectures of the TU Delft's Bottom Founded Offshore Structures course (Hoving, 2017). The width at the top of the jacket is chosen to be equal to the bottom width of the TP. Jacket bay dimensions are applied with constant geometric ratios between bays, see Figure 6. Applied formulas for jacket bay geometric ratios are as follows.

$$(3) \quad dim_{i+1} = m * dim_i\,, \quad (4) \quad m = \left(\frac{b_N}{b_0}\right)^{\frac{1}{N}}, \quad (5) \quad \tan(\theta) = \frac{h_i}{b_i - h_i \tan(\alpha)}$$

, where dim_i is the height or width of the i^{th} jacket bay in meter, dim_{i+1} is the height or width of the next adjacent jacket bay in meter and *m* is a unitless bay ratio. In equation (4), b0 is the width at the top of the first bay in meter, b_N is the width at the bottom of the last bay in meter and N is the number of bays. In equation (5), θ is the angle between a horizontal and diagonal member in degrees, b_i and h_i are the width and height in meter of the i^{th} bay respectively and α is the batter angle in degrees. The overall jacket height (h_{total}) in meter is found as equation (6) through the following substitution.

$$(6)\quad \left.\begin{cases} h_{total} = \sum_{i=1}^{N} h_i = h_1 + mh_1 + \cdots + m^{N-1}h_1 \\ h_{total} = h_1 \sum_{i=1}^{N} m^{i-1} = h_1 \dfrac{m^N - 1}{m - 1} \end{cases}\right\} \rightarrow h_1 = h_{total} * \frac{m-1}{m^N - 1}$$

Member dimensions are estimated based on slenderness constraints, as these form the dominant failure mechanism to be avoided and are therefore selected as the design driver in the dimensioning of the jacket support structures (Hoving, 2017). For a given member length (L) in meter, the diameter can be determined through equation (7) and (8).

$$(7)\quad \lambda = \frac{K * L}{r_g}, \qquad (8)\quad r_g = \sqrt{\frac{I}{A}} = \frac{D}{2\sqrt{2}}$$

, where for equation (7) λ is a unitless slenderness coefficient, L is the member length in meter, K is the effective buckling coefficient and r_g is the radius of gyration in meter. Applied buckling coefficients can be found in appendix A5 Technical design and modelling details. The radius of gyration can be found with equation (8), where I is the moment of inertia in m^4, A is the cross-sectional area in m^2 and D is the member diameter in meter.

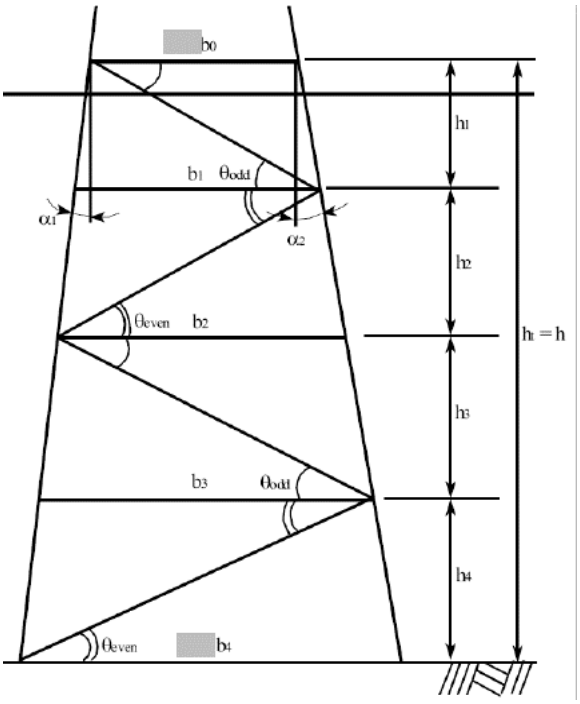

Figure 6: Schematic of OWT jacket showing relevant geometric variables. Bays, the trapezoidal sections, are chosen geometrically equal to ease manufacturing. This image is obtained from Hoving (2017).

Lastly, foundation pile dimensions are estimated based on suggestions by Arany et al. (2017) as equation (9).

$$(9)\quad L_{foundation} = minimum\begin{cases} 8.0 * \left(\frac{E_{pile} * I_{pile}}{n_h}\right)^{0.2} \\ 70 \end{cases}$$

, where E_{pile} is the Young's modulus of the steel at 210 GPa, I_{pile} is the moment of inertia and n_h is the coefficient of subgrade reaction. The diameter of the foundation piles is set to be 15 cm larger than the diameter of the jacket leg piles to allow a grouted connection.

Reference literature – like a series of detailed jacket designs by the Danish Technical University (DTU Wind, 2013) and related academic papers by Sandal, Verbart & Stolpe (2018), Natarajan, Stolpe & Wandji (2019) and Jalbi, Nikitas & Bhattacharya et al. (2019) – are assessed in order to gain additional understanding of design dimensions and considerations.

Step 4: Estimation of recoverable steel mass at end-of-life

At end-of-life, at the decommissioning stage, it is common that OWTs and their support structures are deconstructed and transported back to shore (Topham et al., 2019; Smith, Garrett & Gibberd, 2015). The NRA, tower and transition pieces are recovered, as are the submerged parts of the substructure. In-soil embedded parts of the foundation are generally left at sea and, for safety, cut-off 2 meters below the seabed such that the remaining stumps do not become exposed over time. The support structure steel retrievable at end-of-life is found as the total support structure mass subtracted by the, unrecoverable, foundation mass.

$$(10)\quad M_{retrievable} = \sum\left(M_{components}\right) - M_{foundation}$$

, where $M_{retrievable}$ is the support structure mass in tons that can be retrieved during decommissioning, $M_{component}$ is the mass of an individual support structure component in tons and $M_{foundation}$ is the mass of the soil-embedded foundation in tons that cannot be retrieved during decommissioning. The end-of-life recycling rate (EOL-RR) is applied as defined by Yang (2019).

$$(11)\quad EOL - RR(\%) = \%_{collection} * \%_{separation} * \%_{recovery}$$

Here, the collection rate ($\%_{collection}$) relates to the number of turbines returned from sea, the separation rate ($\%_{separation}$) expresses the ratio of a retrievable support structure mass to its total mass. The recovery rate ($\%_{recovery}$) relates to the losses that occur in the metallurgical recycling process, of which more information can be found in appendix A3 Steel composition and element criticality and appendix A4 Steel making and recycling.

Considering manufacturing constraints, individual members of the jackets and foundation piles have much smaller dimensions than is the case for monopile support structures. Therefore, no maximum member dimension constraints are applied. With respect to other design constraints, for jackets a maximum crane lifting capacity of 2500 tons is applied, similar to that of monopile structures.

Step 5: Estimation of emissions associated with steel making and recycling

An estimate of emissions associated with steel making and recycling is calculated following Guidelines for National Greenhouse Gas Inventories (Lubetsky, Steiner & Faerden et al., 2006). They provide a 1.5 [tCO2-eq/tFeMn-steel] factor for FeMn alloy steel as a global indicator for CO2 emissions. A more suitable value for this indicator is determined, which better reflects the EU's steel production and recycling systems and is found as 1.22 [tCO2-eq/tFeMn-steel]. In the IPCC indicator selection three

groups of GHG emissions are elaborated, namely CO2, CH4 and nitrous oxide emissions. For FeMn-steel production, CH4 and nitrous oxide emissions are described to be insignificant and therefore not further included in the estimation. More information w.r.t. the calculation of the emission factor can be found in appendix A6 GHG emission indicator EU steel production.

2.6 Estimated turbine energy yield

In order to compare the emission investment with avoided emissions through OWT renewable electricity production, the energy yield of each reference turbine is assessed. The annual energy yield is the electricity produced by an OWT in a reference year. The cumulative energy yield of an OWT over its lifetime depends on many factors. The most influential factors are a turbine's rated power and their respective power curve, the local wind resource, downtime due to maintenance and defects, inter and intra wake losses between turbines and wind farms and the serviceable lifetime (Jarquin Laguna, 2019). For this research, a simple energy yield estimate based on transmission efficiency (η), turbine rated power (P, in Watt) and capacity factor (CF) for each reference turbine is added and calculated using the following formula:

$$(12) \quad Annual\ OWT\ energy\ yield = P_{turbine,rated} * CF * \sum \eta * t$$

In this equation, t is the number of seconds in a year. To estimate the total energy produced by an OWT, a wind farm lifetime of 20 years is applied.

2.6.1 OWT capacity factor

The capacity factor depends largely on local wind speed, power curve and hub height of an OWT and is therefore susceptible to significant variation. Through an online free-to-use tool – available at: renewables.ninja – capacity factors for various turbines and locations in the North Sea were assessed. Varying available turbine models up to 10MW, hub height and location presented upper and lower bound capacity factors in the range of 0.50-0.65 [-]. Recently, General Electric has announced that their 12MW Haliade-X turbine operates at a capacity factor of 62% and is currently leading in that aspect (General Electric, 2020). Taking this into account, the aforementioned range is assumed to adequately represent North Sea conditions for the purpose of illustrating the estimated energy yield.

2.6.2 Transmission losses

Energy losses occur through voltage conversion between inter-array cabling and the export cable, the export cable and the main electricity grid, in some cases through alternating and direct current conversion and cable resistance losses (Ummels, 2019a). Converter and cable optimization make for a whole area of research in itself. Hence taking all of these factors into account in detail goes beyond the scope of this estimation. For this estimation, cumulative voltage conversion and cable losses are assumed to negate 5% of annual output power. Inter and intra wind farm wake losses are not included in the energy yield estimation, as these are dependant on the local wind resource and overall wind farm layout, which fall outside the scope of this research.

2.7 Sensitivity of model parameters

With respect to the model accuracy, design dimensions and masses for several design combinations were compared with reference literature. For monopiles, results provided by the model showed to be similar to reference literature and the mass error for tower and monopile segments was found under 10%. For jackets, the model shows to overestimate total support structure mass requirements up to 50% compared to reference values. Individual component mass, like that of a TP or foundation pile, shows larger variation in some cases up to 100% mass difference, and is mostly due to variation in overall design conditions. Upon further analysis it is found that the mass allocated to the jackets is

similar to that provided by Pontow et al. (2017), but that the mass allocated to transition pieces is overestimated significantly by 100-150%. A more accurate mass estimate can be obtained if the transition piece is modelled to be less massive, or alternatively the TP mass provided can be reduced by 50%. This would increase the overall model accuracy to an estimated error of approximately 30% for jacket support structures**.** Jacket support structure mass values presented in this research are based on the unadjusted mass values.

Considering the dimensioning, the interface height proved to be most influential. For monopile support structure typologies, diameter over thickness ratios for tower and monopile, the soil strength and the value of the target natural frequencies influenced final monopile support structure masses most. For jacket support structure typologies, the batter angle, upper bay width and foundation pile length showed to be most influential. For the material making GHG emission estimate, Lubetsky et al. (2006) elaborate that the value of the emission indicator has an approximate error of 10%.

Besides modelling uncertainty, there is uncertainty in model input parameters like the wave height and soil bearing capacity. For these, it should be understood that in this research values are applied that characterise environmental conditions of three North Sea regions and not for any specific location in particular. With respect to the estimated energy yield, it should be noted that the estimation is based on a simple calculation and not on actual measurements. The values provided are considered sufficiently accurate to reflect an average energy output over the lifetime of an OWT in the North Sea region.

3. Results

In this chapter, results of the literature review process and mass estimation model are presented. First present and future support structure typologies are discussed and elaborated that followed from existing literature. Second, the development of the OWT rated power within the temporal scope is discussed. Next, the development of the water depth in development areas within the North Sea is presented. These parameters are then used as input parameters for the dimensioning and mass estimation model, followed by the obtained results.

3.1 OWT support and substructure typologies

For offshore wind turbine support structures, a general division can be made between bottom founded and floating structures, of which the former is the focus of this research. An OWT support structure can be divided into multiple components, as described in the definitions in the Methods section. Various typologies for bottom founded substructures are elaborated that followed from literature review. A visual overview of these is presented in Figure 7. Additionally, a general overview of floating substructure typologies is included and visualised in Figure 8.

3.1.1 Present bottom founded substructures

By far the most well known and used OWT substructure is the monopile. The monopile is a single large cylindrical shaped structure connecting the tower to the ocean floor. The monopile performs both as substructure and foundation and is fabricated by welding multiple segments of similar diameters and wall thickness into one large tube. Monopile dimensions vary based on the requirements of individual OWTs and their location. Currently the maximum monopile manufacturing length, diameter and thickness are 120 and 11 meter and 250 mm respectively, indicated by Sif Group which is a leading manufacturer of steel tubular sections in the EU (Sif, 2018). However, the maximum manufacturing capabilities have shown to increase with time. Up to 2020, 4258 offshore monopiles have been installed within the EU of which 153 were installed in 2019 (Wind Europe, 2019; Wind Europe, 2020). Monopiles have been installed up to water depths of 37 meter, as is the case for the Gemini Wind Farm in the Dutch part of the North Sea, but are claimed to be feasible in water depths up to 60 meter (Igwemezie et al., 2019; Higgins & Foley, 2014; Daubney, 2013). Conceptual variations of the monopile substructure typology include guyed designs - where the monopile is supported by submerged guys, buoyant designs – where the monopile is outfitted with a submerged caisson and articulated buoyant designs – where the monopile is outfitted with a submerged caisson and hinged foundation connection (Watson et al., 2019).

The second most used bottom founded substructure is the jacket structure. A jacket structure is a lattice type structure connecting a OWT tower - via a transition piece - to the ocean floor. Jacket dimensions vary based on functional requirements, but can be extremely large. For example, one of the largest jacket type structures ever constructed is the Bullwinkle fixed steel oil platform, with a total height of 529 meter weighing 50,000 tons. Jackets used in OWT designs are known to be constructed in water depths up to 55 meters, as the case for the Beatrice wind farm in the United Kingdom, but are considered suitable for water depths up to 80 meters (Perez-Collazo, Greaves & Iglesias, 2015). Jacket structures are commonly fixed to the seabed with steel foundation piles, but alternative designs, like suction buckets, are known to exist which were used in the EOWDC wind farm near Aberdeen in the United Kingdom (Wang, Zeng & Li et al., 2018; Wind Europe 2019). Up to and including 2019, 468 jacket structures for OWTs are installed within the EU, of which 65 were installed in 2019 (Wind Europe, 2019; Wind Europe, 2020). Variations of the jacket substructure designs are mostly found in the number of legs – commonly 3, 4 or 6 - and the layout of the trusses – namely x-braces or k-braces.

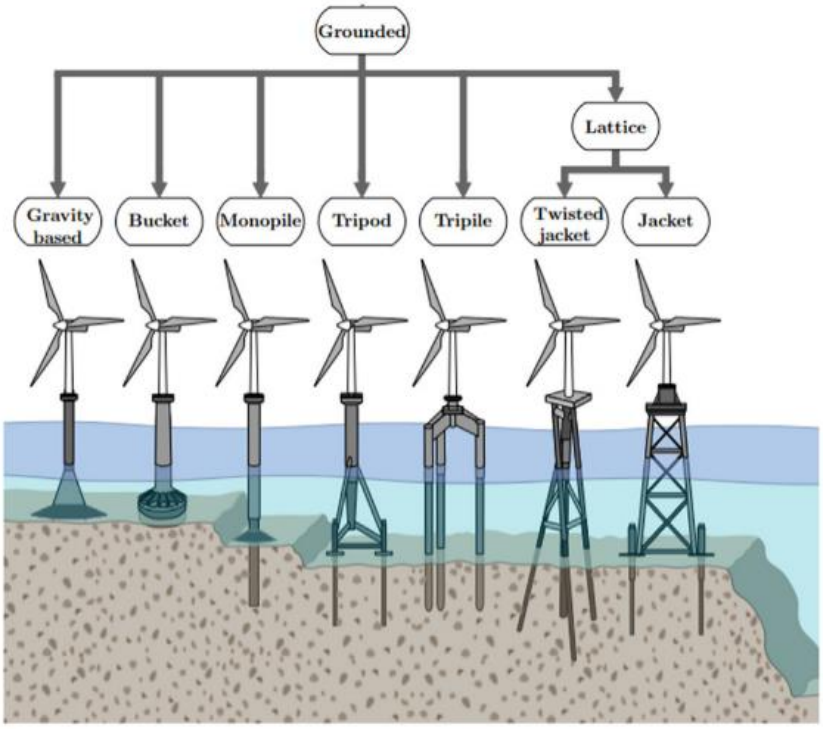

Figure 7: Overview of existing bottom founded offshore wind turbine support structures. Obtained from Igwemezie et al. (2018).

The next most common substructure typology is the gravity base design, of which 301 units are installed in the EU up to 2020 (Wind Europe, 2020). This type of structure is suitable for shallow water turbines, most commonly around 10 meter but up to 30 meter of water depth. This typology is not applied often recently, as only a single installation took place in 2019 and before that it was last applied at the Thornton Bank wind farm in Belgium in 2009 (Wind Europe, 2019; Wang et al., 2018). As the name of the structure implies, the gravity base structure relies on a large base mass for stability. An advantage of the gravity base structure is the fact that no hammering of pile driving is required during installation. Known drawbacks are the mass requirements and associated installation and capital cost.

Last to be considered are tripod and tri-pile structures, which are essentially variations of the monopile structure using three foundation piles instead of one. Up to 2020, respectively 126 and 80 units are installed in the EU (Wind Europe, 2020). Most recent installations were at the Global Tech 1 and Trianel Windpark Borkum 1 wind farms in Germany in 2015, at water depths of 30 and 40 meter respectively (Wang et al, 2018).

In summary, monopile and jacket typology structures are currently the most dominant support structure typologies applied, forming 90**%** of the currently installed OWTs. Alternative typologies, like gravity base, tripod and tri-pile structures are applied in lesser numbers.

3.1.2 Support structure development until 2050

Considering development of the offshore wind industry towards 2050, it is expected that offshore wind will continue to grow and play a major role in the overall development of renewable energy. A studies performed by Watson et al. (2019) shows an estimate of the technology readiness level (TRL) for a range of wind power concept technologies, which range from airborne wind generation – e.g. with the use of planes and kites - to multi-rotor systems and alternative support structure typologies as covered in the previous paragraph. Most of these technological concepts are in conceptual or early

stage of development and not considered likely to gain market share within the temporal scope of this research. Examples of these are airborne wind generation at a TRL between 1 and 3 and multi-rotor systems at a TRL of 2 to 6. Conceptual variations to the traditional monopile design, like guyed and semi-buoyant designs, are considered to have a low TRL in the range of 1 to 3.

Jacket typology development

An alternative design variation to the jacket substructure is the full-lattice tower structure. In this typology, the conical tower is excluded and the full support structure – from seabed to NRA – is constructed as a lattice structure. This design variant could be interesting for very large OWTs to avoid structural frequency response problems and would make the currently required tower-to-jacket transition piece obsolete (Watson et al., 2019). Drawbacks of the lattice type structure are an increased risk of weld failure, increased manufacturing time and cost and limitations considering turbine accessibility. The latter argument could potentially in time become irrelevant, as the latest turbine designs are outfitted with helicopter access points near the nacelle. A proposed variation to this concept is the self-rising tower, which mostly differs in the manor of installation. The tower is constructed by raising each tower subsection from the prior lower tower section, reducing the need for large scale cranes. Examples of these concepts are the EU funded HyperTower and SHOWTIME design concepts, albeit these designs are until now focused on the onshore wind turbine market (Stavirdou, Koltsakis & Baniotopoulos, 2019; Shah Mohammadi et al., 2018). The lattice type structures and self-rising variations are deemed to have TRL in the range of 8 to 9 and 2 to 5 respectively (Watson et al., 2019). It should be noted that the self-rising tower variant focuses on onshore towers currently, but that the technology shows potential for offshore development as well, hence the lower TRL.

Floating support structure typologies

Although out of the research scope, a relatively new and upcoming substructure typology is the floating OWT structure. Three main concepts have so far been proposed, which are the tension-leg, semi-submersible and spar buoy structures. Floating OWTs are considered most interesting for areas with relatively steep continental shelves as it is expected that this typology will greatly expand the deployment area for offshore wind (Watson et al., 2019). This is the case for, for example, the West coast of the United States, Japan and Portugal. Current barriers to the full deployment of floating wind are mostly related to proof of concepts and cost reduction. However, within the last three years ten floating wind projects have been realized or are expected to be deployed this year worldwide (Igwemezie et al, 2019).

The first successfully commissioned large scale (>5MW) floating OWT was the Hywind Scotland in 2017. This project uses the spar buoy design concept and consists of five 6MW SWT-6.0-154 turbines supplied by Siemens. That same year the Fukushima Phase 1&2 (5MW) started operation in Japan also using a spar type buoy, followed by the Windfloat Atlantic (25MW) project in Portugal consisting of three 8.4 MW turbines mounted on semi-submersible platforms (JWPA, 2017; Energias de Portugal, 2018). Next year, the 30MW EolMed wind farm project in France is expected to start operation using three V164-10.0MW turbines mounted on floating barges (4Coffshore, 2020). From these examples it can be seen that development in offshore floating wind is going in a rapid pace and that the current proof-of-concept phase might soon develop into full scale deployment.

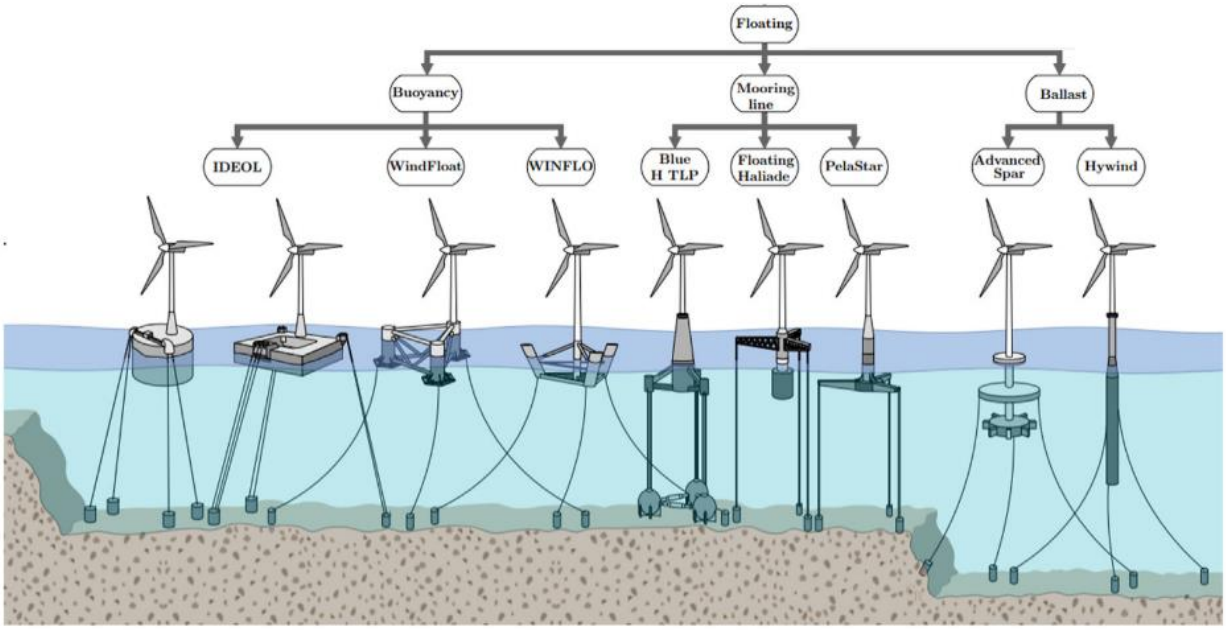

Figure 8: Existing floating support structure typologies for offshore wind turbines. Obtained from Igwemezie et al. (2018).

3.2 OWT rated power

OWT rated capacity has been increasing throughout the years, allowing the offshore wind parks to enlarge their power nameplate without proportionally increasing the number of turbines. Not only do the rated power of individual turbines increase, the number of turbines constructed per wind park is also increasing (Rodrigues et al, 2015).

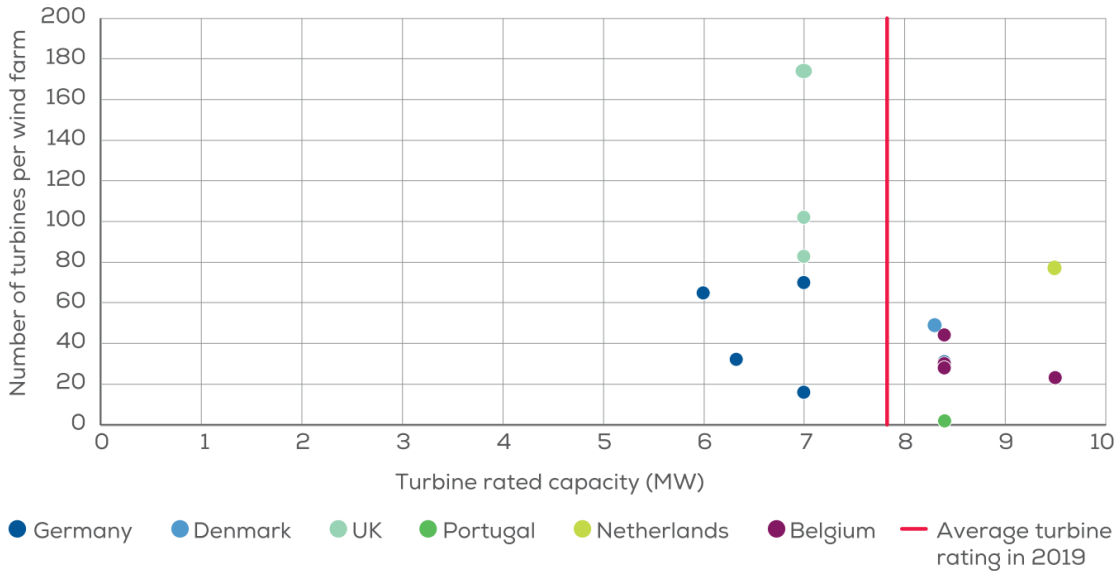

Figure 9: Average turbine rated capacity and number of turbines at wind farms under construction in 2019. This image is obtained from Wind Europe (2019).

Starting off with turbine sizes in the order of magnitude of 500 kW in 1990, by the year 2000 multi-MW turbines were being installed. In the first 10 years of the new millennium, annual and cumulative installed capacity increased massively, from 50MW/y annual additions in 2000 to almost 900 MW/y in 2010 and maximum turbine sizes doubling from 2 to 4 MW (EWEA, 2013). Average turbine size,

however, stayed relatively constant at 4 MW between 2010 and 2015, but has been steadily increasing with almost 1 MW per year between 2015 and 2019. Average rated turbine capacity in 2019 was 7.8 MW, see Figure 9, with the largest turbines under construction having rated capacities of 9.5 MW (Wind Europe, 2019). General Electric has recently installed one unit of the Haliade-X 12 MW turbine in Rotterdam in the Netherlands (General Electric, 2020). The turbine is expected to be commercially available in 2021.

3.2.1 Development of turbine rated capacity until 2050

McKenna et al. (2016) state that there is little consensus about future development of large wind turbines in the next 10 to 15 years, but that experts suggest a rated power in the range of 3-10 MW, with a tower height of 120-200 meters and rotor diameters between 120-180 meters. At this point in time, turbines at the higher end of that range are already the standard for newly constructed wind farms. To keep the lead in competition and achieve high design efficiencies, the offshore wind industry is making effort to upscale OWTs to the 10-12 MW range which are expected to be commercially available by 2021 (Igwemezie et al., 2019). Due to the larger rotor radius of higher capacity wind turbines, the rated capacity is reached at lower wind speeds (General Electric, 2020). Reaching rated capacity at lower wind speed in turn increases the capacity factor of these larger turbines. The capacity factor provides an indication for the time of operation within a given reference period. The capacity factor is defined as actual power produced divided by the maximum power a wind turbine could have produced at continuous full power operation, and is expressed as a percentage. For Europe, given the high quality wind resource and leading technological development, average capacity factor are rising rapidly. Where in 2018 the average capacity factor was 43%, in 2040 this is expected to be near 60% (Wind Europe, 2019). The Haliade-X for example reports a capacity factor of 60-64%, which is 5 to 7 percent point higher than the current average (General Electric, 2020).

Looking further ahead, even bigger turbines are expected. A good indication of turbine sizes is often given by the development of reference turbines. Reference turbines are created and used by researchers and developing industries to provide insight in the next generation wind turbine models. Detailed reference turbines have been created for 5 MW – created by the National Renewable Energy Laboratory (NREL) and Danish Technical University (DTU) in 2009, 8 MW – proposed by Desmond et al. in 2016, 10 MW and most recently 15 MW (Jonkman, Butterfield & Musial et al., 2009; Desmond, Murphy & Blonk et al., 2016; Bak, Zahle & Bitsche et al., 2013; Gaertner, Rinker & Sethuraman et al., 2020). Initial estimates are provided for a 20 MW reference turbine, but this has not been developed to the same level of detail as the first four (Jensen, Chaviaropoulos & Naterjan et al., 2017; Pontow, Kaufer & Shirzahdeh et al., 2017).

A report from the INNWIND.EU delivery package 5 series shows a road map discussing TRLs for 10-20 MW reference turbines (Dobbin, Mast & Echavarria et al., 2017). Here an estimate is made that the next generation reference turbine at 20 MW rated capacity could see first commercial application somewhere around 2030, with the nacelle components to be available a couple years before and bottom founded structures available shortly after. Watson et al. (2019) give an indication that bottom fixed wind turbines could to be scaled up to roughly 30 MW rated capacity, based on current rotor technology and lattice type support structures. They do not, however, provide an estimate time for commercial application or TRL for this size of NRA but just consider this to be a maximum. They do indicate that NRAs of this magnitude will behave much more dynamically than their 10-20 MW counterparts.

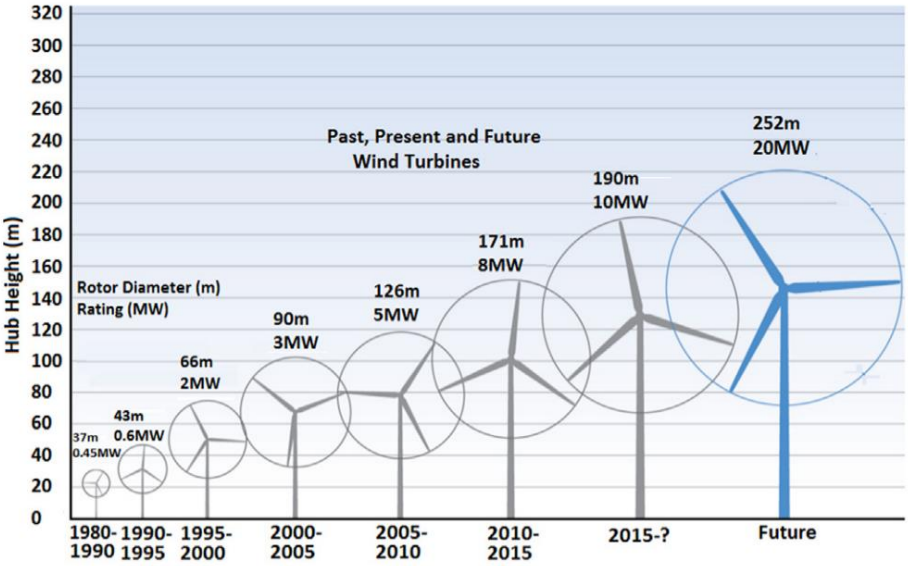

Figure 10: Growth in maximum size and power of horizontal axis offshore wind turbines. This images is obtained from Igwemezie et al. (2019).

3.3 OWT water depth development

So far, offshore wind turbines have been largely constructed in water depths up to 50 meters (Igwemezie, 2019). An example of this can be seen in a figure presented by Wind Europe, see Figure 12, that shows water depth and distance to shore for offshore wind farms under construction for the EU28 in 2019 (Wind Europe, 2020). The average water depth of the EU's offshore wind turbines was 33 meters in 2019, see Figure 12, which is a slight increase compared to the 30 meter average water depth of 2018 and 25 meter depth in 2015 (Wind Europe, 2020; Rodriguez et al., 2015). However, in comparison to the early offshore wind turbines constructed in the 1990's at water depths of 4 to 10 meters, see Figure 11, the trend of exploiting deeper waters for wind energy becomes clear.

The water depth at which offshore wind turbines will be constructed is likely to be much larger than is current practice, as floating OWTs are passed the proof-of-concept phase and widely experimented with. An interesting question, however, is until what water depth bottom founded structures will be considered. Hermans & Peeringa (2016, pg5) state that: "Not long ago, water depth more than 25 meters or 5+ MW class turbines were considered the tipping point towards jackets or other alternative support structures. Nowadays, 'XL monpiles' of over 1000 tons are produced with diameters up to 8 meters for water depths up to 30-35 meters". In their report, Hermans & Peeringa (2016) provide an initial design for a monopile structure supporting a 10 MW turbine at 50 water depth. Other authors mention that monopiles are reported to be dominant for water depths up to 30 meter, but kept under consideration for water depths up to 60 meter depending on site conditions (Perez-Collazo et al., 2015; Daubney, 2013). A similar conclusion applies to jacket structures, which are reported optimal for 30-60 meter water depth, but their maximum deployment range suitable for OWTs is mentioned up to 80 meter (Wang et al., 2018; Perez-Collazo, 2018). Higgins & Foley (2014) consider floating designs for >60 meter water depth. Igwemezie et al. (2019) make a deep water distinction at >30 meter and group jackets and floating in the same category in this regard. However, the lowest operational water depth found for floating OWTs in papers analysed during this research is 85 meter depth for the Windfloat project.

Water depth ranges in the North Sea vary per area, see Figure 13. In the Southern Bight– at latitudes 51-54°N, e.g. the area in between France, Belgium, The Netherlands and the UK – water depth reaches up to 50 meters. In the Central North Sea – latitudes 54-57°N, e.g. the area West of Denmark and East

of the UK – the depth commonly varies between 40 and 100 meters, with an exception to shallower areas near the Dogger Bank and the Danish coast. In the Northern part of the North Sea – latitude >57°N, e.g. North of Denmark, South and West of Norway – water depths up to 200 meters can be found, with even deeper waters of 500-700 meter in the Norwegian Channel (Alfred Wegener Institute, 2009, p23).

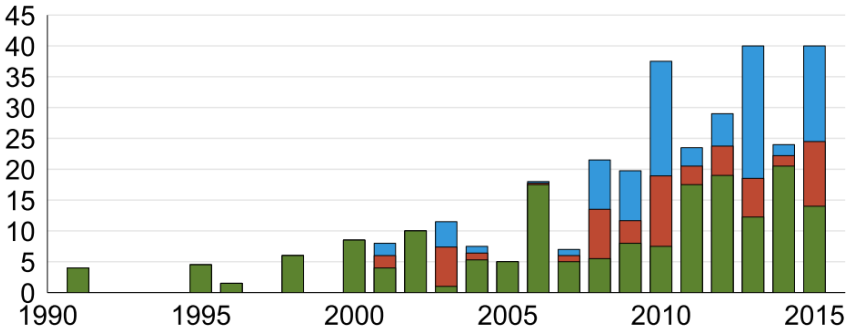

Figure 11: Minimum (green), mean (red) and maximum (blue) water depth in meters plotted versus commission year, based on yearly statistics of commissioned and under construction EU28 offshore wind parks consisting of >5 turbines. Image obtained from Rodrigues et al. (2015).

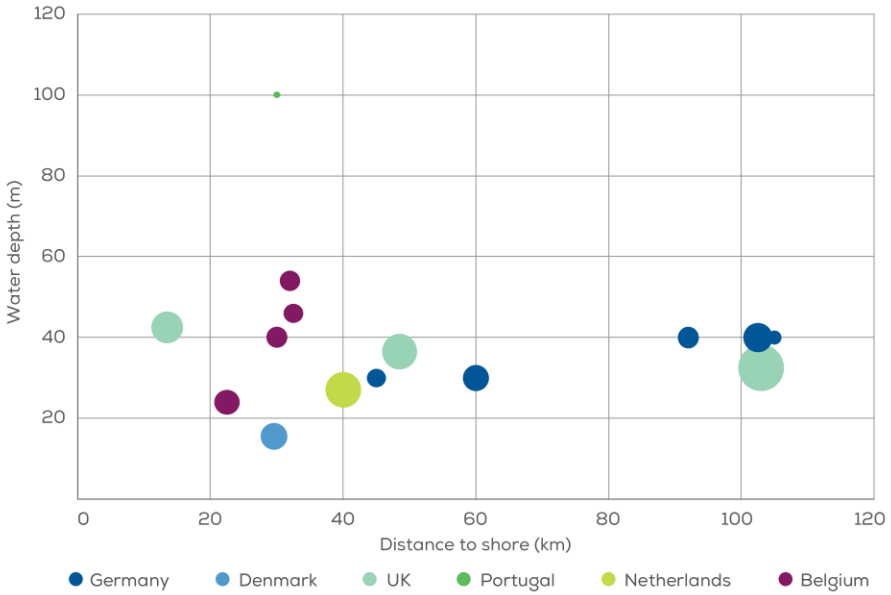

Figure 12: Average water depth and distance to shore of offshore wind farms under construction in 2019. Bubble size indicates wind farm cumulative capacity. This image is obtained from Wind Europe (2019).

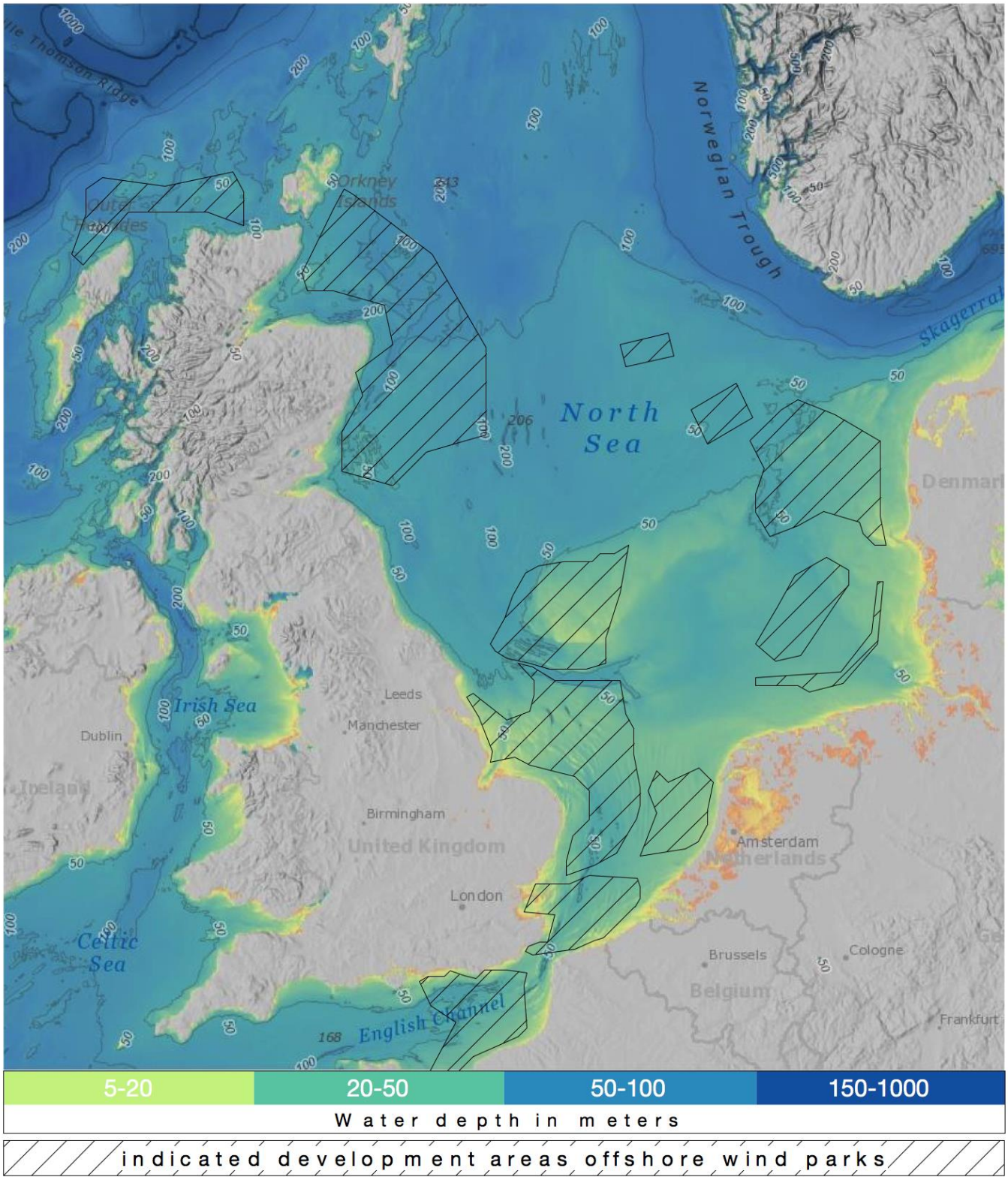

Figure 13: Planned wind parks on North Sea bathymetry. Bathymetry base map obtained from NOAA (2020) available at: https://maps.ngdc.noaa.gov/viewers/bathymetry/. Wind park development zones obtained from the 4Coffshore website available at: 4Coffshore.com/offshorewind.

3.4 Dimensioning model results

In the following, the dimensioning model results are presented for both monopile and jacket support structures. In assessing the steel demand for the offshore support structures, it is important to understand that the net steel demand is equal to the difference between upfront steel requirements and the quantity of retrievable steel available after decommissioning. Steel that is recovered at an OWT's end-of-life can be recycled and remains available for later use. Steel that is not recovered can be considered lost to the environment and is no longer available for later use. The distinction between these two steel quantities is important, as they have a different effect on the amount of GHG emissions associated with the support structure over its lifecycle.

First the most important environmental parameters are shortly discussed that were used in the dimensioning process. Then, the mass estimates of monopile and jacket support structures are visually presented and elaborated. After that, the retrievable support structure mass and the support structure steel mass for a 500 MW wind farm are compared at three water depths. Finally, the estimation of GHG emissions associated with support structure steel are discussed.

3.4.1 North sea environment analysis

Several environmental aspects are important for the design of OWT support structures. Therefore, an environmental analysis for the North Sea region is carried out in order to formulate input parameters for the dimensioning model. In this analysis, information is gathered with respect to water depth, wave characteristics, currents and soil composition. Of these aspects, water depth and wave characteristics are discussed below. With respect to water currents, astronomical tides are taken into account for the various development regions. Two soil types are included in the model, being soft-medium and medium-dense sandy soils, as these are most dominantly present in the North Sea region. An elaborate overview of applied methods and environmental parameters is included in appendix A5 Technical design and modelling details.

Water depth in OWT development zones

The water depth is an important parameter for the dimensioning of OWT substructures, as it largely determines the minimal required height of a support structure. The website 4Coffshore (4Coffshore, 2020) keeps track of available development zones for offshore wind parks. On the previous page, an illustration is shown indicating aggregated available wind park development zones – as available in November 2020 – projected on the North Sea bathymetry. The bathymetry base map is obtained from the National Oceanic and Atmospheric Administration (2020) website and shows a digital elevation model (DEM) with colour shaded relief. From this illustration it can be seen that in the Southern Bight many zones are made available for offshore wind parks in shallow areas with water depth up to 50 meter. In the Central North Sea, near the Danish coast and the Dogger Bank, some development areas are also available in shallow water regions but overall the water is deeper, reaching up to 50 meter in German territorial waters and even up to 70 meter in Danish waters. In the Northern North Sea, most developing zones are located near the UK accompanied by two Norwegian development zones, being the squares furthest out the coast of Denmark. The UK zones in this part of the North Sea vary between 50 and 120 meter water depth, with some areas reaching water depths up to 200 meter. The Norwegian development zones both have water depths between 60 and 80 meters.

Wave characteristics in the North Sea

Wave characteristics are important to assess, as they affect the minimal required height of the support structure. Furthermore, waves interact with, and hence apply forces onto, the support structure influencing the required member thickness for members located in the splash zone. The splash zone is the range of height in which waves interact with the support structure.

Another important phenomenon is the possibility of structural resonance. As waves and wind interact with the support structure, they can induce vibrations. From a structural integrity perspective, it is important to make sure that the eigenfrequency of the support structure does not overlap with the wind and wave excitation frequencies, as resonance can then occur. Resonance can lead to amplification of forces acting on the support structure and can potentially lead to structural failure. To account for this, the spectral energy density of waves occurring in the North Sea is assessed by fitting the JONSWAP curve to the significant wave periods. Then, a target eigenfrequency is determined outside the frequency range of the rotor (1P-range) and passing rotor blades (3P-range) and minimized for waves for each combination of water depth and wave period. As the rotor speed can vary, the 1P and 3P frequencies are visualised as a range, see the purple boxes in Figure 14. The target natural frequency is chosen to be in between the 1P and 3P ranges with a 10% margin from the 1P range upper boundary.

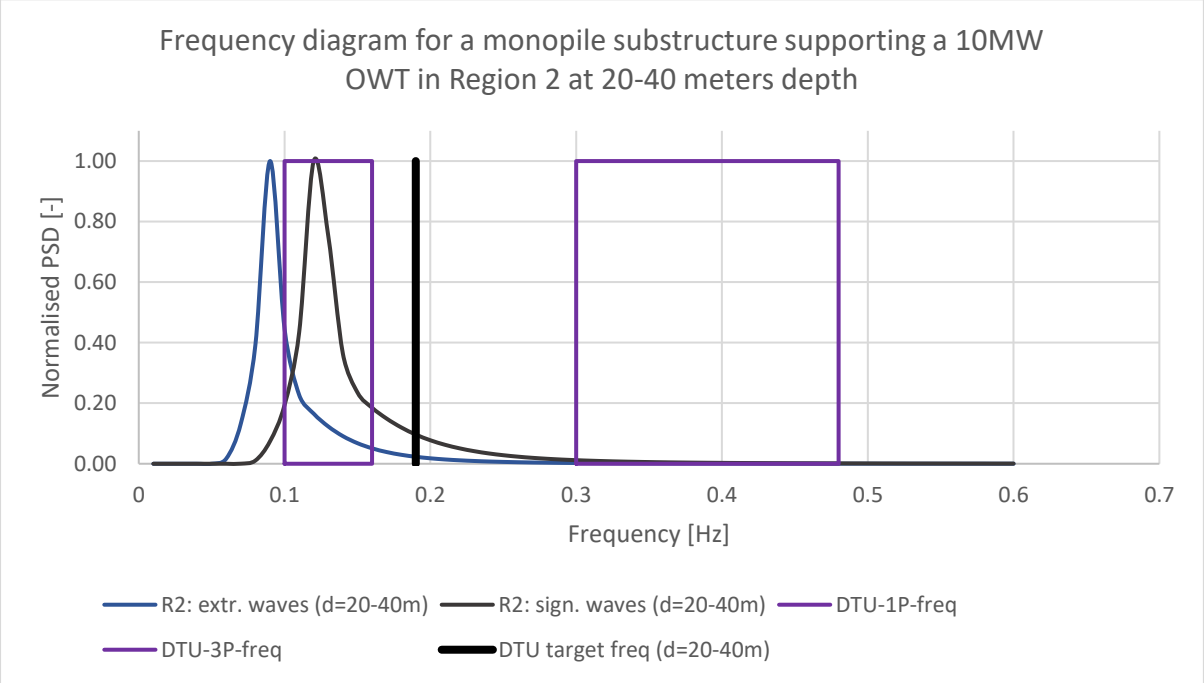

Figure 14: Frequency diagram for DTU-10MW at 20-40m water depth in Region 2. On the vertical axis, normalised energy variance density in m2/Hz. Rotor frequency range (1P-range) and blade passing frequency range (3P-range) are shown respectively as the left and right purple boxes. Target eigenfrequency for the monopile substructure is shown as the vertical black line.

Generally, a lower target eigenfrequency – or natural frequency – leads to more slender monopile designs, reducing the steel requirements for this type of support structure. Therefore, the location of the natural frequency is used as the design driver for the dimensioning of the monopile support structures. In practice, other design criteria like the Ultimate Limit State and Fatigue Limit state should also be checked. However, considering that goal of this research, these are not considered in this work.

Monopiles are characterised by large pile diameters, resulting in a large area obstructing passing waves. In contrast, due to the more 'open' nature of jacket structures and smaller member dimensions, waves are less obstructed and transfer much less of their energy to the substructure. In general, jacket structures are much more rigid than monopile structures, which makes that eigenfrequencies for jacket substructures are generally higher than for their monopile counterparts and outside of the wave induced resonance range. Therefore, in the dimensioning model, the

frequency assessment is used in monopile substructure dimensioning, but not for jacket substructures. As an example, a visual representation of the wind and wave frequency range and the target eigenfrequency for a monopile substructure is shown in Figure 14.

3.4.2 Results considering up-front monopile support structure steel demand

Considering monopiles, dimensions were obtained for 130 combinations of water depth, soil conditions and turbine rated capacity. However, due to exceeding one or more manufacturing constraints only 35 combinations resulted in viable designs. The monopile design constraints are a maximum monopile length at 130 meter, maximum diameter of 12 meter and maximum monopile mass of 2500 tons. Of these, the maximum length and mass constraints were most often superseded, see Figure 15. With respect to the rated power of OWTs, viable MP designs are obtained for 5, 8 and 10 MW rated power turbines. For 5 MW turbines, all combinations of water depth and soil conditions proved viable. For 8 and 10 MW turbines, soil conditions proved a dominant factor influencing design viability, favouring medium-dense soil conditions.

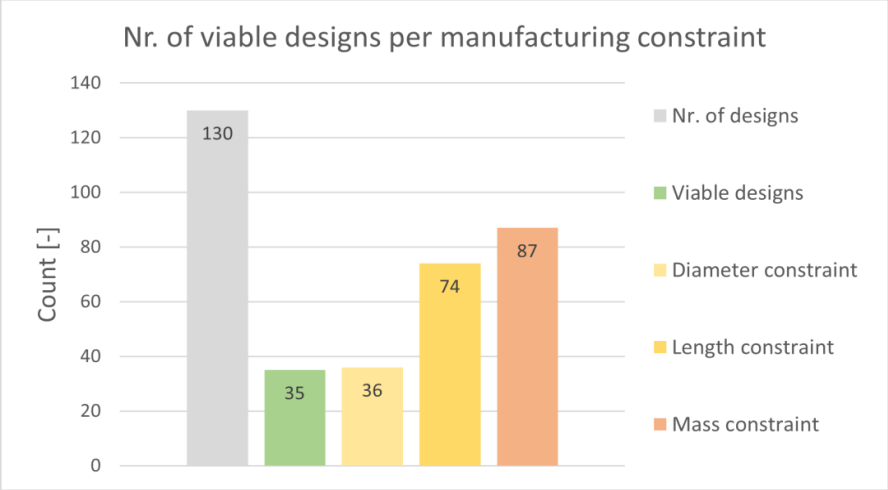

Figure 15: Number of viable MP design combinations and manufacturing constraints.

The development of monopile support structure mass with respect to water depth is shown in Figure 16 for 5, 8 and 10 MW turbines. For the designs obtained, a linear regression is fitted for each turbine size. A general formula and fitted linear parameters for these turbine sizes are included in Table 2. No viable combinations supporting 15 and 20 MW designs are found, as for each combination the maximum monopile mass constraint is superseded.

Monopile and tower mass estimates for manufacturable designs are shown in Figure 17. Monopile and tower support structure mass for viable designs are found to be in a range of 997-2966 ton for NREL-5MW, LW-8MW and DTU-10MW reference turbines at water depth of 20 to 60 meter. From this figure, it can be seen that consistently the majority of steel is embedded in the monopile (dark blue) compared to the tower (light blue).

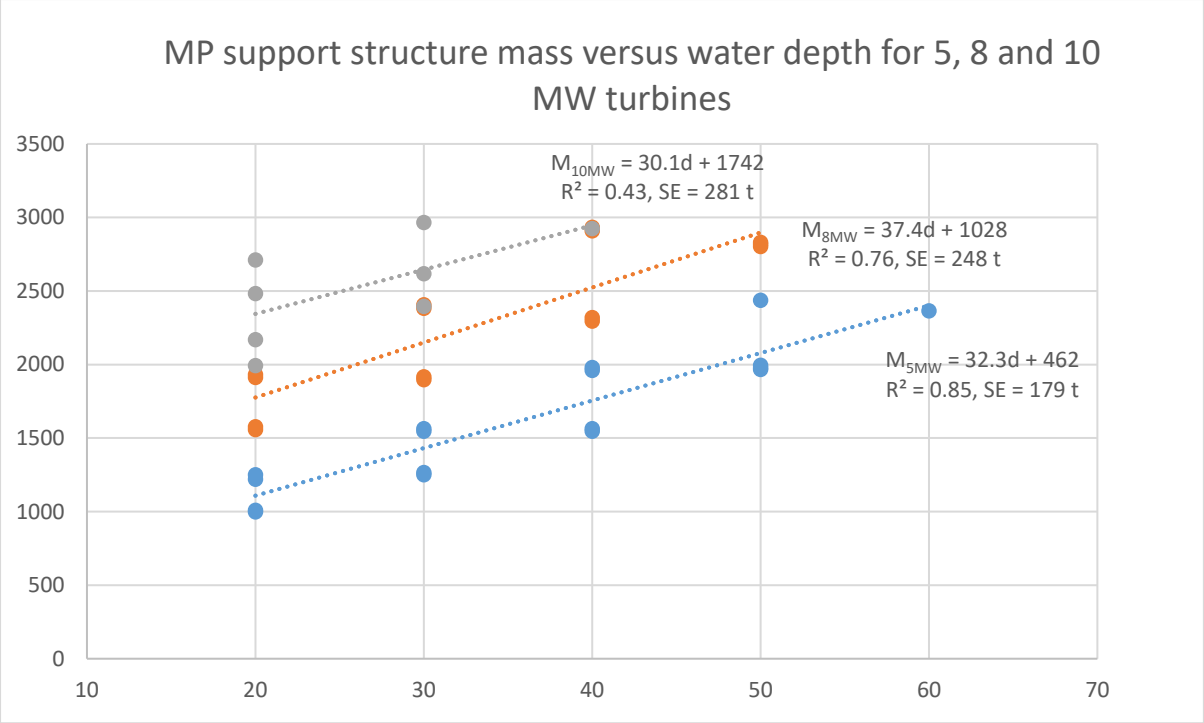

Figure 16: Monopile support structure mass for 5, 8 and 10 MW OWTs versus water depth. For each turbine size, a linear regression has been fitted to the modelled support structure masses. For each regression, the goodness of fit parameter R^2 and the standard error are included.

Initially, a higher-power relation was expected for the development of support structure mass with increasing water depth. However, a linear regression seems to fit with near equal accuracy and the mass difference with respect to a linear relation proves to be relatively small (<10%) for this range of water depth. The overall goodness of fit for the linearisation for the 5 and 8 MW turbine is considered acceptable, at R^2 of 0.85 and 0.76 respectively. See Figure 16. The accuracy for the 10 MW turbine is lower, at R^2 of 0.43. This is a direct result from the low number of viable designs obtained for this turbine size. Considering the accuracy of the obtained model results and the small difference between the two estimation methods, the development of steel requirements over water depth can indeed be assessed using a linear relation, supporting the approach of Topham et al. (2019) and Shammugam et al. (2019).

Table 2: Linear parameters fitted to monopile support structure mass (M, in tons) development w.r.t. water depth (d, in meter) for turbines of varying rated power.

P [MW]	**a**	**b**	General formula	Water depth range [m]
5	32.3	462	$M_{support\ structure}(d) = \boldsymbol{a} * d + \boldsymbol{b}$	20-60
8	37.4	1028		20-50
10	30.1	1742		20-40

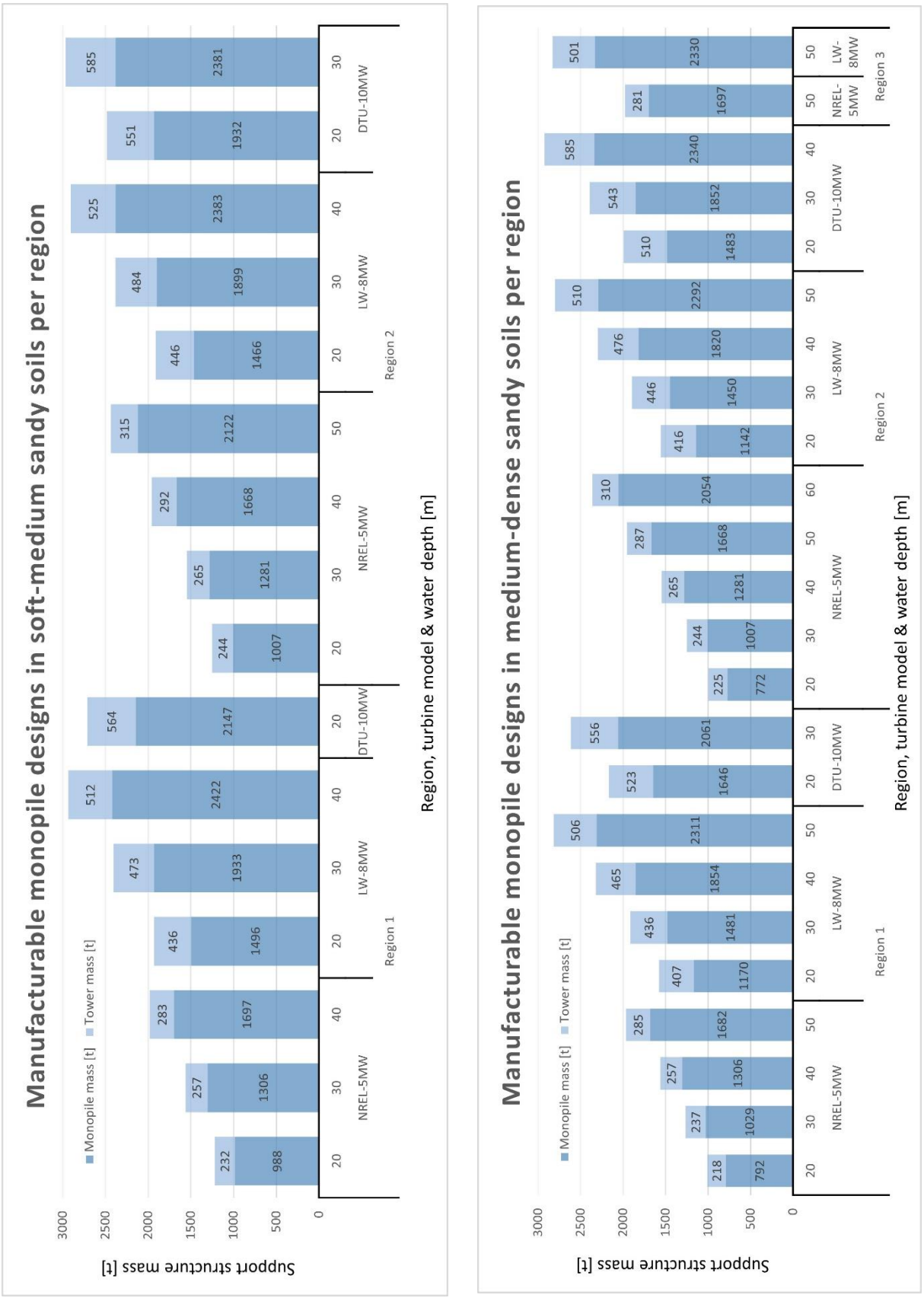

Figure 17: Overview of monopile and tower support structure mass in tons per turbine model, region and water depth. All designs shown meet manufacturing constraints. More designs proved possible in dense soils, as soft soils required larger monopile dimensions. Monopile mass shown in dark blue, tower mass shown in lighter blue. No monopile designs proved viable for the IEA-15MW and IW-20MW turbines mostly due to the maximum mass constraint.

3.4.3 Results considering up-front jacket support structure steel demand

Considering jackets, dimensions were obtained for 170 combinations of water depth, soil conditions and turbine rated capacity. The design driver for the modelling of the jacket substructure is member slenderness. Due to stability and deformation requirements, member diameters are determined based on slenderness (Hoving, 2017). The slenderness of a structural member depends on its cross-sectional dimensions, namely its diameter and thickness compared to its length.

With respect to design constraints for the modelling of the jacket structures, a maximum component mass constraint of 2500 tons applies. This constraint, associated with marine vessel crane lifting capacity, was violated for all jacket designs in water depths larger than 70 meters and for the 20 MW turbine at depths larger than 60 meters. In total, 44 out of the 170 combinations showed to have a jacket substructure mass greater than 2500 tons. Cumulative jacket support structure typology mass for viable designs are found to be in a range of 630-6480 ton steel, considering the five assessed reference turbines at water depths between 20 and 70 meters. A detailed breakdown of the estimated component and cumulative jacket support structure mass for turbines situated in region 2 is shown in Figure 19. Similar visualisations for the other assessed regions are included in appendix A5 Technical design and modelling details.

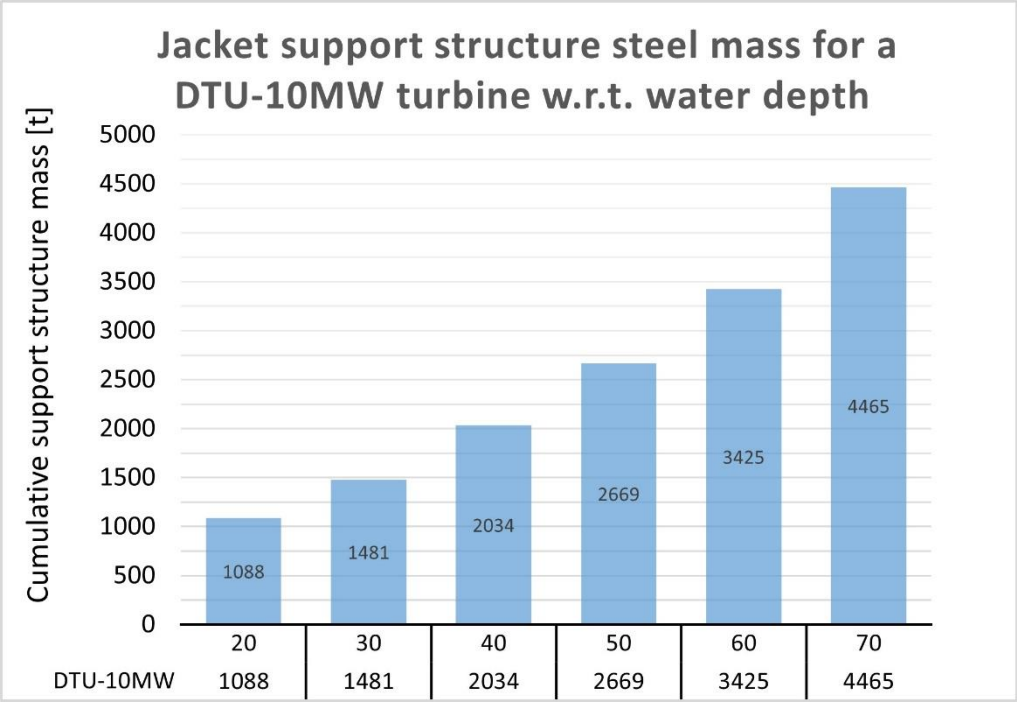

Figure 18 Cumulative jacket support structure steel mass (in tons) for a 10MW OWT at various water depths (in meter)

In Figure 18 the development of support structure mass per water depth is shown for a 10 MW reference turbine. Important to note from this figure, is the large influence of the water depth on the total steel demand. Figure 21 shows a visual impression of this difference. It should be kept in mind that both turbines are hosting the same tower at roughly 120 meters height, and that visually only minimal difference can be observed between a turbine installed at 30 or 60 meters depth. However, considering the quantity of construction material, this difference is much more significant. Where the installation of a single 10 MW wind turbine at 30 meters depth would require approximately 1500 tons of construction steel, the same turbine would require almost 3500 tons of steel if it were to be placed at 60 meters depth.

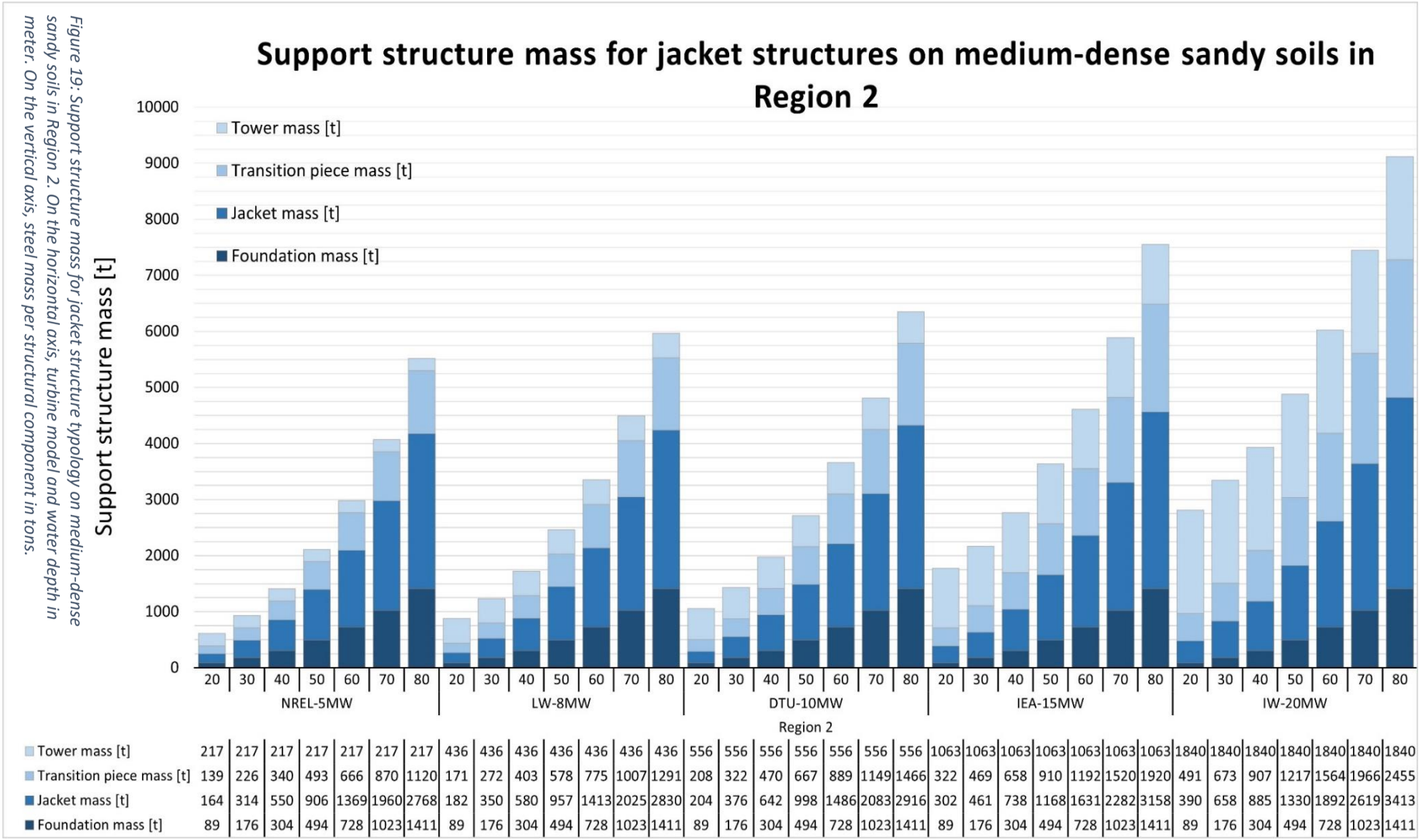

Tower mass [t]	217	217	217	217	217	217	217	436	436	436	436	436	436	436	556	556	556	556	556	556	556	1063	1063	1063	1063	1063	1063	1063	1840	1840	1840	1840	1840	1840	1840
Transition piece mass [t]	139	226	340	493	666	870	1120	171	272	403	578	775	1007	1291	208	322	470	667	889	1149	1466	322	469	658	910	1192	1520	1920	491	673	907	1217	1564	1966	2455
Jacket mass [t]	164	314	550	906	1369	1960	2768	182	350	580	957	1413	2025	2830	204	376	642	998	1486	2083	2916	302	461	738	1168	1631	2282	3158	390	658	885	1330	1892	2619	3413
Foundation mass [t]	89	176	304	494	728	1023	1411	89	176	304	494	728	1023	1411	89	176	304	494	728	1023	1411	89	176	304	494	728	1023	1411	89	176	304	494	728	1023	1411

Figure 19: Support structure mass for jacket structure typology on medium-dense sandy soils in Region 2. On the horizontal axis, turbine model and water depth in meter. On the vertical axis, steel mass per structural component in tons.

For the cumulative jacket support structure mass a 2th power increase can be observed with respect to water depth, see Figure 20 and Table 3. For each turbine size assessed, the general formula and parameters fitted to the mass development with respect to water depth are shown. These parameters can be used to find an initial estimate of jacket support structure mass for a combination of a turbine rated power and water depth. When multiplied with the number of turbines present in a given wind farm, an initial estimate of the wind farm's overall OWT support structure steel requirements can be obtained.

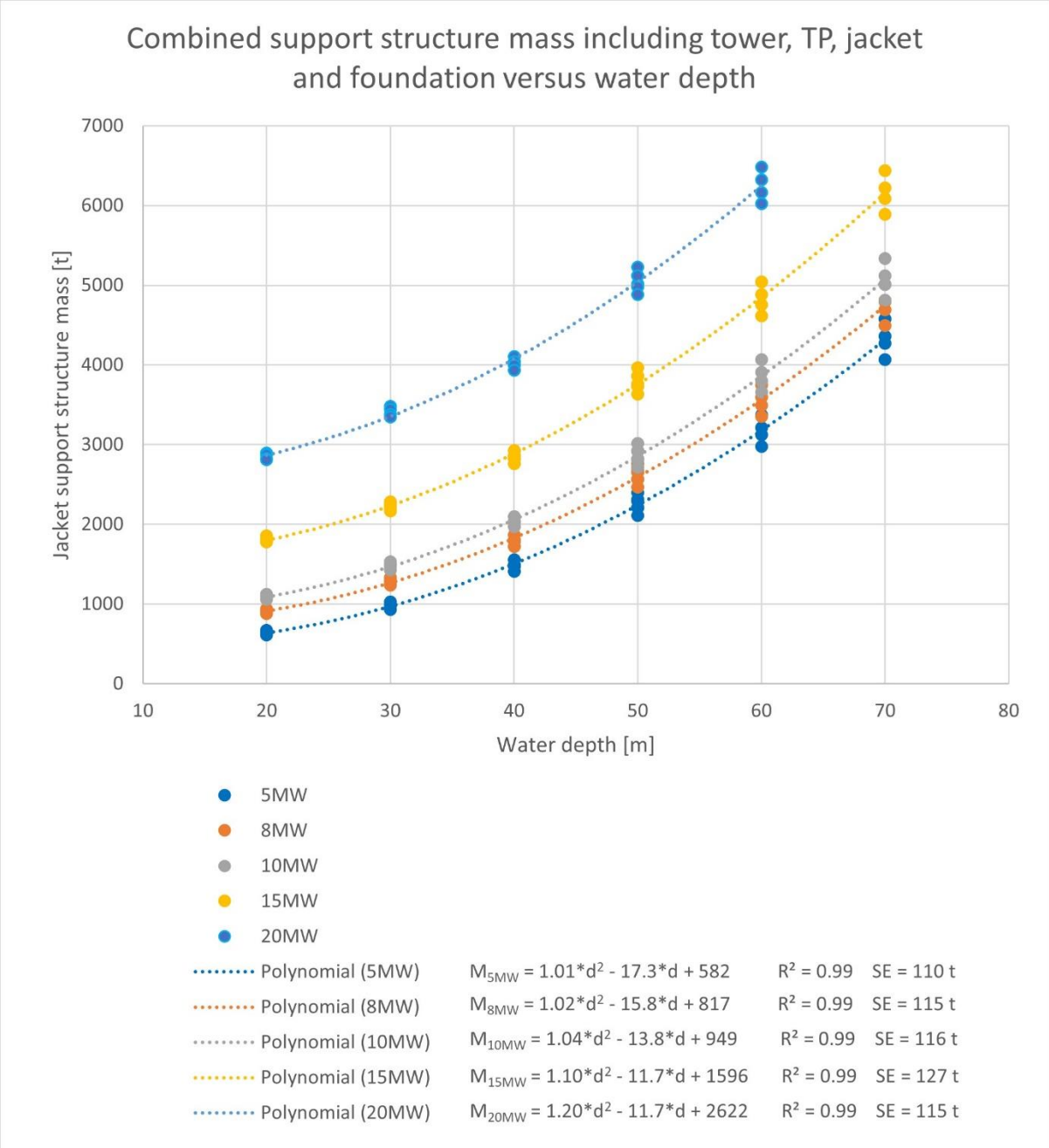

Figure 20: Combined tower, TP, jacket and foundation mass for 5, 8, 10, 15 and 20 MW OWTs versus water depth. For each turbine size, a polynomial regression has been fitted to the modelled support structure masses. For each regression, the goodness of fit parameter R^2 and the standard error are included.

Table 3: Polynomial parameters fitted to jacket support structure mass (M, in tons) development w.r.t. water depth (d, in meter) for turbines of varying rated power.

Turbine rated power [MW]	a	b	c	General formula	Water depth range [m]
5	1.01	-17.3	582	$M_{support\ structure}(d) = \boldsymbol{a} * d^2 + \boldsymbol{b} * d + \boldsymbol{c}$	20-70
8	1.02	-15.8	817		20-70
10	1.04	-13.8	949		20-70
15	1.10	-11.7	1596		20-70
20	1.20	-11.7	2622		20-60

With respect to the turbine rated capacity, a similar higher-power trend of increasing support structure mass can be observed, see Figure 23. For example, doubling the rated power from 5 to 10 MW for an OWT at 50 meter water depth increases the support structure steel mass from approximately 2100 to 2700 tons. Doubling this again to 20 MW rated capacity, increases the cumulative support structure mass from 2700 to 4850 tons. An illustration of this can be seen in Figure 22. The difference between these two times 'doubling' the rated power illustrates the significance of an OWT's rated power on its steel demand. This effect, however, is less significant than that observed with respect to water depth. In other words, within the presented range of water depth and rated power, a doubling of the water depth is more impactful for construction material requirements than a doubling of the rated power.

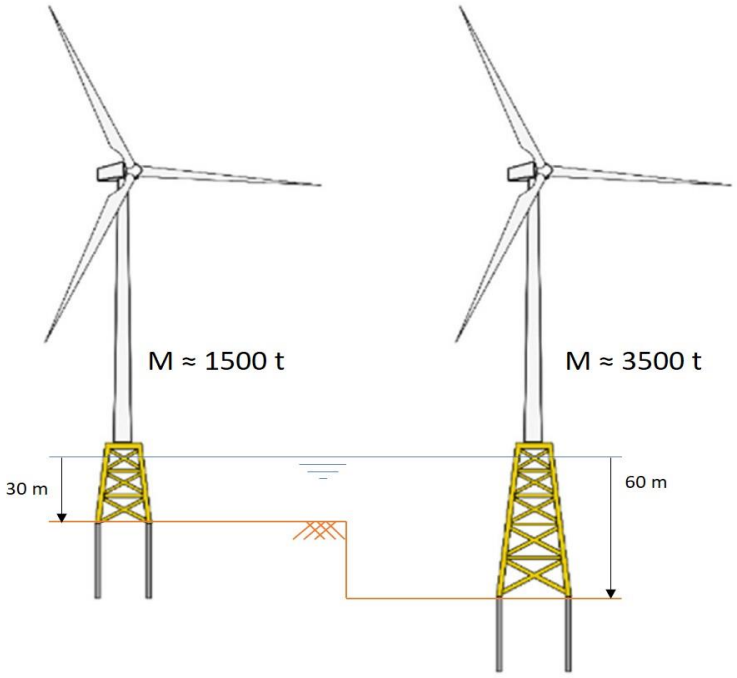

Figure 21: Illustration emphasizing the influence of water depth on cumulative support structure mass. For two similar 10 MW offshore wind turbines, one at 30 meters depth and one at 60 meters depth, the required steel mass increases from approximately 1500 tons to approximately 3500 tons.

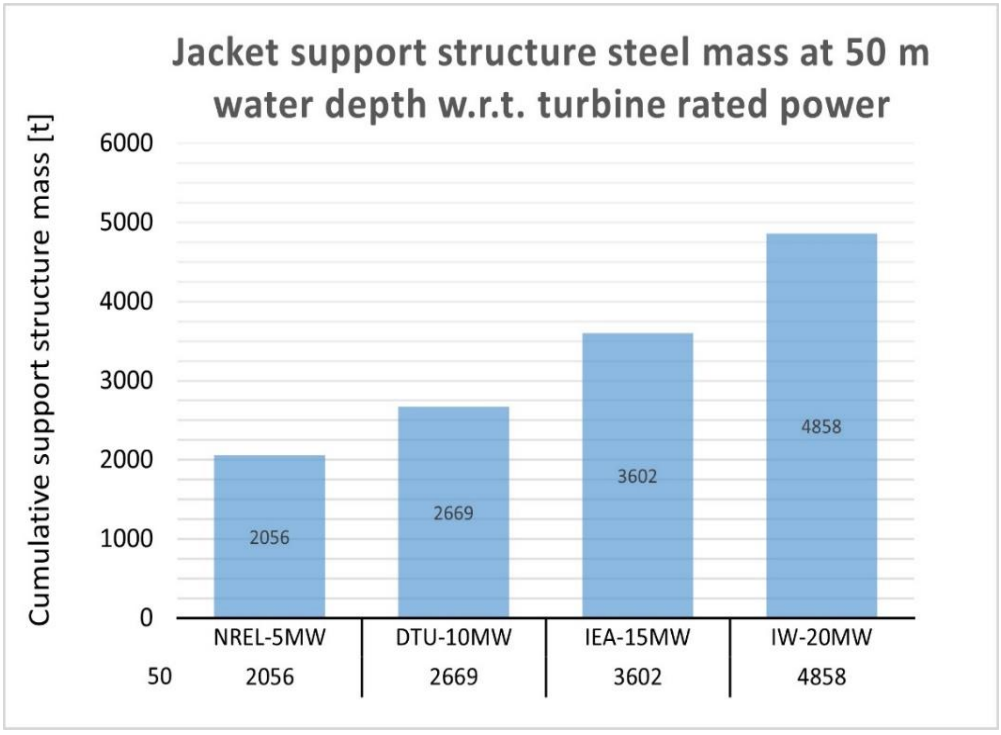

Figure 23: Cumulative jacket support structure steel mass (in tons) for a 5, 10, 15 and 20 MW OWT at 50 meter water depth.

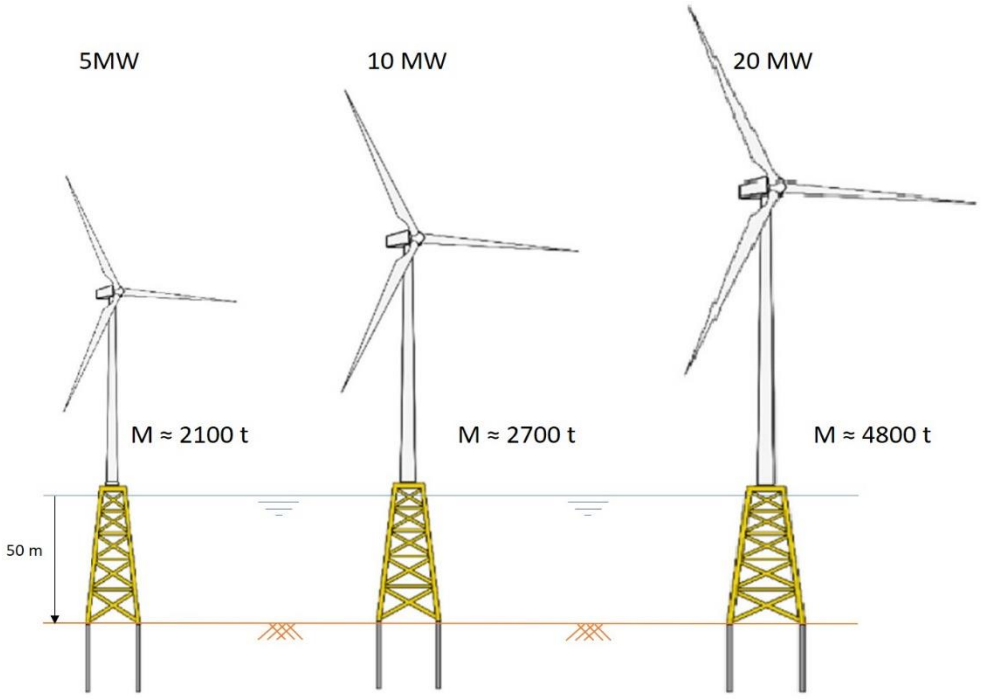

Figure 22: Illustration emphasizing the effect of increased turbine rated capacity on the cumulative support structure steel demand. For equal water depths, support structure mass increases from 2100 to 2700 and 4800 tons for 5, 10 and 20 MW rated capacity turbines respectively.

The model results contradict earlier findings by Topham et al. (2019), who found that a single 4 MW turbine requires more construction steel than two 2 MW turbines. The findings of this research suggest that within the range of water depth assessed, for both monopile and jacket support structures two turbines of a given rated power require more construction material than a single turbine at double that power. The opposing outcomes can be due to a variety of reasons, such as the difference in modelling approach, but further study is recommended.

3.4.4 Retrievable steel mass at decommissioning stage

The net steel use of an OWT's support structure over its lifetime is determined by the initial steel requirements and the quantity of steel that can be recovered at end-of-life. Important to understand is that an OWT's foundation piles are driven and fixed into the seabed during installation to guarantee the OWT's stability. So far, it has not been economically feasible to withdraw these foundations when an OWT is decommissioned (Lourens, 2019b). On the other hand, leaving the complete substructure out at sea is not favourable either, as this would bring safety concerns for amongst other things marine transport. Current practice dictates that at the decommissioning stage, the NRA, tower and substructure are retrieved from sea, while the foundation is (mostly) left behind. The foundation needs to be removed up to 2 meter below the mudline, such that the remaining stumps do not become exposed over time (Topham et al., 2019; Smith, Garrett & Gibberd, 2015).

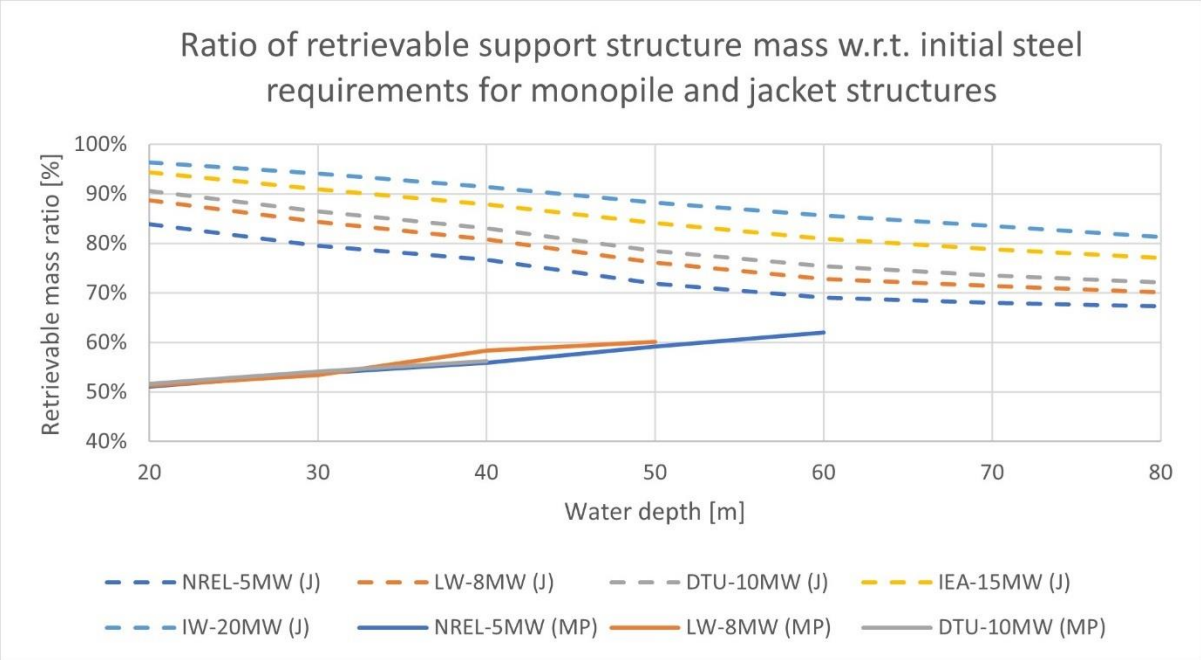

Figure 24: Influence of water depth on relative retrievable support structure mass.

The recoverable steel quantity is calculated for all combinations of turbine rated power, water depth and soil conditions. With respect to water depth it can be seen that the amount of recoverable steel increases linearly for monopile substructures and quadratically for jacket substructures, see the foundation mass in Figure 17 and Figure 19.

Interestingly, the relative retrievable mass – the ratio between recoverable and initial steel demand – increases with water depth for monopile structures, see Figure 24. In other words, this implies that for monopile substructures every ton of steel added above the seabed requires less than a ton of foundation steel below the seabed. For jacket structures, the opposite seems to be the case. Every ton of steel added above the seabed, requires more than a ton of foundation steel below the seabed. In Figure 24 this can be seen as that the retrievable mass ratio declines with increasing water depth.

This effect can be a result of the modelling method applied and it would be interesting to see if alternative modelling methods lead to the same outcome. With respect to this research, this observed effect has little influence, as the quantity of initial and recoverable steel are the focus of this research. For monopiles, the ratio of retrievable support structure steel mass varies in a range of approximately 50-60%, depending on the water depth. The rated turbine capacity does not influence the retrievable mass ratio. For jackets, this ratio varies in a range of approximately 70-95% depending on both water depth and turbine rated capacity.

3.4.5 Estimated steel requirements of a 500 MW wind farm

Besides the development of support structure mass per turbine model and water depth the obtained results allow to compare the steel needs of a wind farm at a specific water depth. A wind farm of 500 MW is used as the basis for this comparative scenario, at 20, 40 and 60 meters water depth. Here, the variable parameter is the cumulative steel quantity for the full wind farm. The results are presented in Figure 25 on the next page.

The comparison shows the trade-off between a wind farm consisting of a high number of low-power turbines and a wind farm consisting of a lower number of high-power turbines. For example, a hundred 5 MW turbines compared to twenty-five 20 MW turbines which both combine to 500 MW total installed capacity. Furthermore, it illustrates the large relative difference between monopile and jacket substructures in terms of upfront and recoverable steel quantities. In all cases, monopiles require more steel upfront and lose much more steel in the decommissioning phase. To illustrate this point, the following example: the total steel requirement of a 500 MW wind farm at 20 meters depth consisting of 10 MW turbines supported on jacket structures is smaller than the losses of steel associated with the decommissioning of a similar wind farm consisting of 5 MW monopile-supported turbines.

As the wind farm is placed in deeper water, the favourable turbine rated capacity increases. At 20 m depth, 10 MW turbines supported by jacket support structures require the lowest quantity of steel at 54,000 tons, closely followed by 8 MW turbines at 57,000 tons. For a 500 MW wind farm, this results in an average steel intensity of approximately 110 ton steel per MW installed capacity. In this configuration, the steel losses amount to approximately 8,000 tons. Next, at 40 m depth, 15 MW turbines supported by jacket support structures require the lowest quantity of steel at 95,000 tons. Steel losses amount to approximately 16,000 tons and the average steel use per MW installed capacity is approximately 190 t steel/MW in this configuration. At 60 m depth, 15 and 20 MW turbines supported by jacket support structures require similar steel quantities, namely 145,000 tons and 146,000 tons respectively. Steel losses differ for these turbine sizes, where the 20 MW turbines show a slightly lower steel loss at 27,000 tons compared to the 15 MW turbines of which the steel losses amount to 33,000 tons. Given this relatively small difference, both turbine sizes are considered favourable at this water depth. The steel use per MW installed capacity for both turbines is approximately 290 t steel/MW installed capacity.

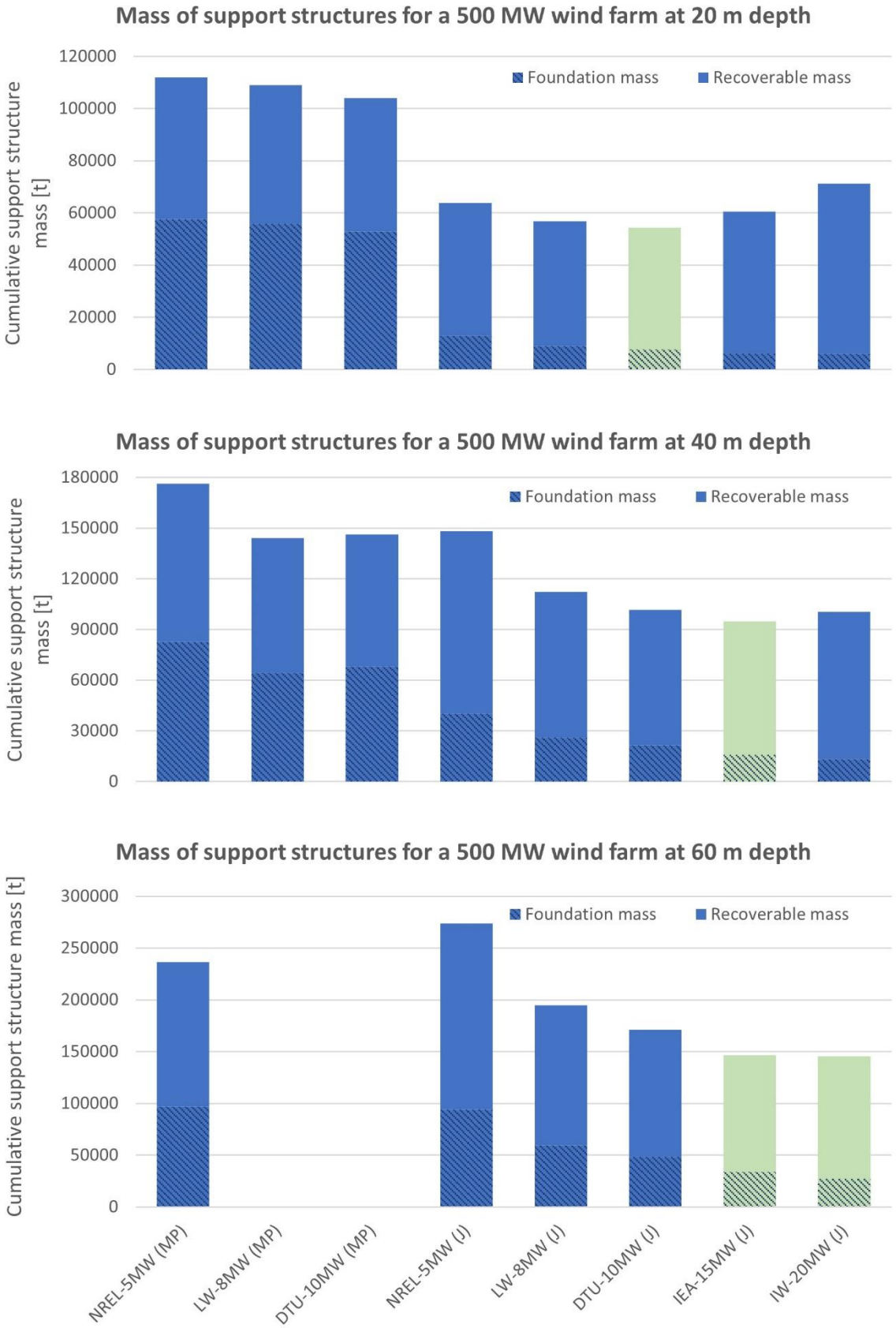

Figure 25: Comparison of support structure mass requirements for wind turbines of varying capacity. A wind farm of 500 MW cumulative capacity is assessed at 20, 40 and 60 meters depth. Columns in green show configurations with minimum steel requirements. Abbreviations: MP = monopile support structure, J = jacket support structure.

3.5 GHG emissions for support structure steel and emission payback time

With initial and recoverable steel quantities known, an estimate is made of the GHG emissions associated with OWT support structure steel. The GHG emissions related to steelmaking and recycling practices, e.g. lifecycle stages 3 and 9, are determined by the introduction of an emission factor for support structure steel, following the IPCC Guidelines for National Greenhouse Gas Inventories by Lubetsky et al. (2006). Lubestky et al. (2006) mention that this indicator is 1.5 tCO2-eq/t steel, taking into account average global production but that this indicator should be adapted towards the applicable geographic location. This is due to the fact that a variety of steel production methods is globally available and that these are associated with different GHG emissions. The GHG emission factor applied per ton steel required is 1.22 tCO2-eq/t support structure steel, under the assumption that OWT support structure steel production is well reflected by the EU's steel mix and production methods. The emission factor presented includes emissions of lifecycle stages 3 and 9, which form the majority of emissions from a material perspective. More information w.r.t. the emission indicator can be found in appendix A6 GHG emission indicator EU steel production.

3.5.1 GHG emissions per turbine and water depth

An overview of the steel production GHG emissions per turbine rated power and water depth is depicted in the Table 4. It can be seen that the emissions for monopile support structures is consistently higher than that for jacket support structures. For example, an 8 MW OWT supported on a monopile support structure in 30 meters water depth would require a similar emission investment as a 15 MW OWT supported on jacket support structures. See the green highlights in Table 4. With a similar emission quantity, almost double the installed power capacity can be realised. Similarly, an 8 MW monopile-supported OWT at 20 meters depth would require approximately the same emission investment as an 8 MW jacket-supported OWT at 40 meters depth. See the orange highlights in Table 4. Here too a wind farm could be constructed at double the water depth with similar emission quantities invested by changing the support structure typology from monopiles to jacket structures.

Table 4: Upfront GHG emissions related to steel making for OWT support structures of various turbine-water depth combinations. Values are obtained through multiplication of the upfront required steel mass and steel emission factor elaborated above. Abbreviations: MP = monopile, J = jacket.

Upfront emissions associated to steelmaking for OWT support structures in ton CO2-eq								
Turbine	Typology	Water depth [m]						
		20	30	40	50	60	70	80
NREL-5MW	MP	1366	1716	2150	2543	2884	-	-
LW-8MW	MP	2129	2624	2815	3436	-	-	-
DTU-10MW	MP	2539	3057	3569	-	-	-	-
NREL-5MW	J	778	1195	1809	2508	3339	4532	6205
LW-8MW	J	1107	1565	2191	2948	3799	5052	6766
DTU-10MW	J	1327	1806	2481	3257	4179	5447	7242
IEA-15MW	J	2212	2712	3470	4395	5355	6777	8739
IW-20MW	J	3477	4162	4905	5927	7095	8704	10674

After decommissioning, the retrievable support structure steel can be offered for recycling as scrap metal. Recycling steel is approximately six times less emission intensive than the refining of steel from iron ore (Yang, 2019). Therefore, offering the support structure steel scrap to recycling services can potentially reduce the need for future steelmaking from iron ore, consequently saving approximately 0.9 tCO2-eq/t recovered steel scrap. The end-of-life stage could lead to GHG emission savings as depicted in Table 5, which is why they are displayed as negative emissions. For monopiles, a potential

emission reduction of 35-45% can be achieved compared to the upfront emissions released in steel making. For jackets, this reduction is higher and in a range of 50-70%.

Table 5: Potential emission saving associated with OWT supports structure steel recycling after decommissioning in ton CO2-eq per turbine. Emission quantities are negative, as they have the potential to reduce the support structure steel net GHG emissions if the support structure steel is properly recycled.

Emissions associated to steel recycling for retrievable OWT support structure steel in ton CO2-eq								
Turbine	Typology	Water depth [m]						
		20	30	40	50	60	70	80
NREL-5MW	MP	-505	-668	-870	-1090	-1295		
LW-8MW	MP	-790	-1015	-1190	-1496			
DTU-10MW	MP	-950	-1198	-1453				
NREL-5MW	J	-473	-688	-1005	-1305	-1669	-2231	-3026
LW-8MW	J	-711	-956	-1282	-1625	-2004	-2612	-3436
DTU-10MW	J	-870	-1130	-1492	-1850	-2281	-2900	-3784
IEA-15MW	J	-1511	-1786	-2208	-2677	-3137	-3868	-4874
IW-20MW	J	-2427	-2836	-3248	-3787	-4399	-5267	-6280

3.5.2 Estimated annual energy yield per turbine model

Albeit that Table 4 and Table 5 provide insight into the net emission investment associated with the two substructures typologies, it does not yet provide insight into the emissions compared to the OWTs' electricity yield. The energy yield of each turbine needs to be determined, so that one is able to compare the invested emissions with the electricity produced per turbine model. An estimated energy yield for each turbine is included in Table 6. A lower and upper bound of the estimated annual energy yield is given, as site specific conditions have a large influence on a turbine's power production. The energy yield as presented in Table 6 is derived as the multiplication of a turbine's rated power, capacity factor and transmission losses. A capacity factor range of 0.50-0.65 [-] is applied.

Table 6: Estimated annual electricity yield in GWh per turbine, based on a capacity factor range of 0.50-0.65 [-] and 5% transmission losses.

Turbine	Estimated annual energy yield [GWh/(turbine*year)] (lower and upper bound)
NREL-5MW	20.8 - 27.0
LW-8MW	33.3 - 43.3
DTU-10MW	41.6 - 54.1
IEA-15MW	62.4 - 81.1
IW-20MW	83.2 - 108.2

3.5.3 Emission payback time

The emissions invested into the creation of the OWT are compared to the emissions saved during the OWT's operational time and the 'emission payback time of support structures' is determined. This is defined as the amount of time required for an OWT to be operational in order to equal the emissions associated with the making and refining of its embedded steel. In this comparison, the GHG emission intensity of electricity generation is applied, which is 275 tCO2-eq/GWh for the year 2019 and expected to reduce over time, see Figure 26 (European Environment Agency, 2020). An overview of the emission payback time for support structures in included in Table 7. It can be seen that the emission payback time is in the order of magnitude of months.

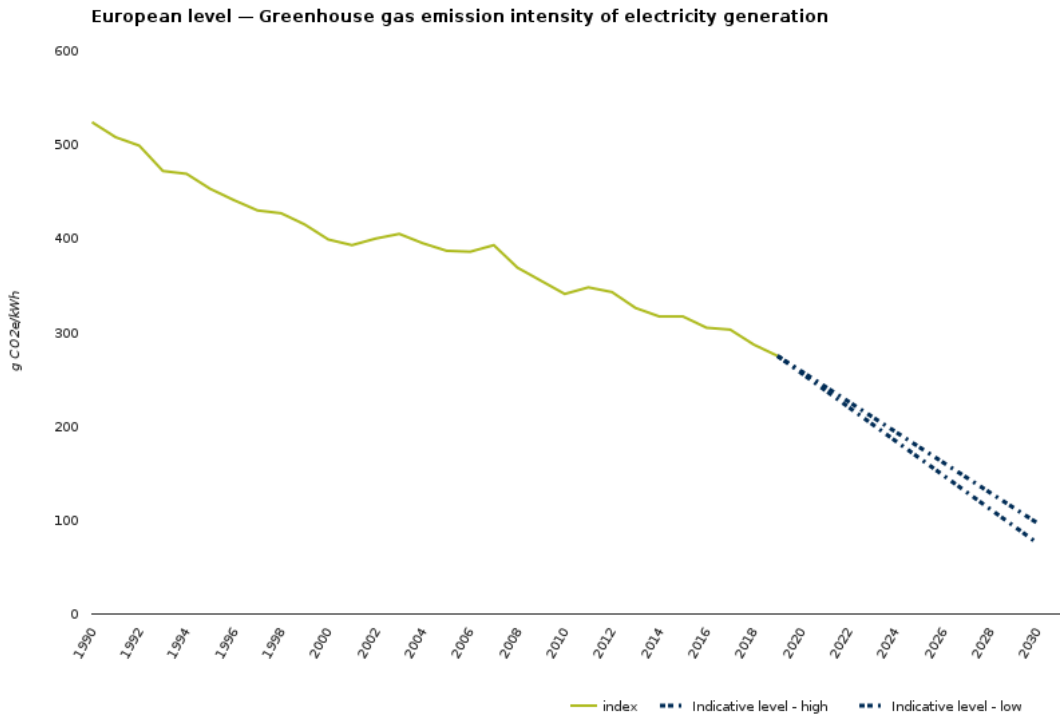

Figure 26: European average Greenhouse gas emission intensity of electricity generation over time. In 2019, this was 275 gCO2-eq/kWh and is expected reduce further towards 2030. Image obtained from European Environment Agency (2020).

Table 7: Approximate payback time of emissions associated for support structure steelmaking with respect to the 2019 average GHG emission intensity of Europe's electricity generation at 275 g CO2-eq/kWh.

Approximate payback time of support structure steelmaking emissions per turbine-water depth combination [months]								
Turbine	Typology	Water depth [m]						
		20	30	40	50	60	70	80
NREL-5MW	MP	4	5	6	8	9	-	-
LW-8MW	MP	4	5	5	6	-	-	-
DTU-10MW	MP	4	5	5	-	-	-	-
NREL-5MW	J	2	4	5	7	10	14	19
LW-8MW	J	2	3	4	5	7	9	13
DTU-10MW	J	2	3	4	5	6	8	11
IEA-15MW	J	2	3	3	4	5	7	9
IW-20MW	J	3	3	4	4	5	6	8

For monopile support structures, the payback time ranges between 4-9 months, depending on turbine rated capacity and water depth. Logically, larger turbines situated in shallow water have a lower payback time than small turbines situated in deeper waters. Compared to the total operational time of the OWT, the obtained payback times are relatively low. This is positive with respect to the goal of reducing emissions of electricity generation. With respect to water depth, the payback time increases similarly to that of steel demand.

For jacket support structures, the payback time is generally somewhat lower. The payback time for jackets ranges between 2-19 months considering the five assessed turbines at water depths of 20-80 meters. However, this includes unfavourable – and less likely – combinations of turbine size and water depth. More optimal combinations result in emission payback times of 2-9 months, where higher

rated power turbines show to be less affected by the changes in water depth than smaller turbines. Increase in turbine rated power dampens the variation in emission payback time.

As the European electricity's emission intensity reduces over time, the support structure steel emission payback time increases. This can be as much as three times by 2030 compared 2019, if no alternative non-fossil steel production methods become available in this period of time. In the case of zero-emission electricity, as is the European Commission's goal for 2050, the emission payback time becomes infinite. This phenomenon is further discussed in section 4.1.4, in the discussion of this research.

3.5.3.1 Energy payback time

Additionally, next to the payback time of invested emissions, one can also consider the payback time of invested energy. For each combination of turbine and water depth, the energy required to produce the steel mass embedded in its support structure is compared to the electrical energy generation of the OWT. For this comparison, similar ratios of BF-BOF (59.8%) and EAF (40.1%) steelmaking processes are taken into account as applied for the emission payback time. The energy intensity of BF-BOF and EAF steelmaking are 22.4 GJ/t steel and 11 GJ/t steel respectively (Pardo, Moya & Vatopoulos, 2015). Combined, the energy intensity of an average European ton of steel is found as 17.8 GJ/t steel. The energy payback time for each turbine-water depth combination is shown in Table 8. For monopiles, the energy payback time varies between 3-6 months. For jackets, the energy payback time varies between 1-5 months for more optimal combinations of turbine rated power and water depth.

Table 8: Approximate energy payback time associated with OWT support structure steelmaking and electricity generation.

Turbine	Typology	Approximate payback time of energy invested in support structure steelmaking [months] Water depth [m]						
		20	30	40	50	60	70	80
NREL-5MW	MP	3	3	4	5	6	-	-
LW-8MW	MP	3	3	4	4	-	-	-
DTU-10MW	MP	3	3	4	-	-	-	-
NREL-5MW	J	2	2	4	5	7	9	13
LW-8MW	J	1	2	3	4	5	6	9
DTU-10MW	J	1	2	3	3	4	6	7
IEA-15MW	J	1	2	2	3	4	5	6
IW-20MW	J	2	2	2	3	4	4	5

When comparing the emission and energy payback time, see Table 7 and Table 8, it can be seen that the time to repay the energy invested in steelmaking is less than the time to repay the invested GHG emissions. This can be partly explained by the high carbon intensity of the energy that is invested in the steelmaking process. More carbon intensive at least than the average European electricity generation, by which the emission payback time is estimated. Therefore, to repay the invested carbon emissions a wind turbine has to generate electricity for a longer period of time.

3.5.4 The contribution of a support structure to an OWT's climate change potential

To assess the emission quantities in perspective of a fully operation wind turbine, the calculated mass and emission values are compared to the findings of Bonou et al.'s (2016) LCA study. In this study, a lifecycle assessment is performed for an offshore wind farm situated approximately 40 km out of the coast at a water depth of 20 meter. The study assesses 4 and 6 MW OWTs supported on monopile foundations, which compare well to the 5 MW monopile supported OWTs assessed in this research. With respect to support structure mass, Bonou et al.'s study finds an average steel use of

approximately 1200 ton steel per turbine. For similar conditions, the dimensioning model derived for this research estimates a monopile support structure mass of 1120 ton steel per turbine and a jacket support structure mass of 640 ton per turbine. Bonou et al. (2016) find the contribution of support structure steel, at 3.2 g CO2-eq/kWh, to be approximately 33% of the OWT's total contribution to climate change. Similarly, the dimensioning model results would lead to support structure contribution of 3.0 and 1.7 g CO2-eq/kWh for the monopile and jacket support structure respectively, which are approximately 32% and 21% of the total climate change contribution. At 20 meter water depth, the OWTs produce electricity at 9.4 and 8.1 g CO2-eq/kWh. The application of the jacket support structure reduces the support structure's contribution with approximately 1.3 g CO2-eq/kWh, leading to a 15% reduction of the total climate change potential.

At a water depth of 40 meters, the total contribution increases to 11.2 and 8.9 g CO2-eq/kWh. The contribution of the support structures then respectively increases up to 42% and 28% for monopile and jacket structures. At 60 meters depth, the total contribution increases to 12.8 and 10.2 g CO2-eq/kWh, where monopile and jacket support structure share increase to 50% and 37% of the total climate change contribution. At both 40 and 60 meters depth, jacket structures result in a 20% reduction of the full OWT's climate change potential compared to monopile typologies.

Overall, the emissions for 5 MW monopile founded OWTs' electricity generation vary between 9.4-12.8 g CO2-eq/kWh at water depths of 20-60 meter. For 5 MW jacket founded OWTs, this range is 8.1-10.2 g CO2/kWh. As a comparison, an average coal-fired power plants generates electricity at approximately 1057 g CO2-eq/kWh and an average gas-fired power plant at 583 g CO2-eq/kWh (Treyer & Bauer, 2016). The GHG emission intensity of European electricity is currently 275 g CO2/kWh (European Environment Agency, 2020).

Table 9: Contribution of monopile and jacket support structure steelmaking to an OWTs climate change potential for a 5 MW OWT at 20, 40 and 60 meters water depth.

	d=20m				d=40m				d=60m			
	MP		J		MP		J		MP		J	
OWT component:	kg CO2-eq/kwh				kg CO2-eq/kwh				kg CO2-eq/kwh			
Support structure	**3.0**	***32%***	**1.7**	***21%***	**4.7**	***42%***	**2.5**	***28%***	**6.4**	***50%***	**3.8**	***37%***
Grid cables	1.2	*13%*	1.2	*15%*	1.2	*11%*	1.2	*14%*	1.2	*9%*	1.2	*12%*
NRA equipment	1.9	*20%*	1.9	*24%*	1.9	*17%*	1.9	*22%*	1.9	*15%*	1.9	*19%*
Substation	0.5	*5%*	0.5	*6%*	0.5	*4%*	0.5	*5%*	0.5	*4%*	0.5	*5%*
Subtotal material making contribution	6.6	*70%*	5.3	*66%*	8.4	*75%*	6.1	*69%*	10.0	*78%*	7.4	*72%*
Contribution of installation, manufacturing, transport and decommissioning	2.8	*30%*	2.8	*34%*	2.8	*25%*	2.8	*31%*	2.8	*22%*	2.8	*28%*
Total contribution to CC potential	**9.4**		**8.1**		**11.2**		**8.9**		**12.8**		**10.2**	

4. Discussion and interpretation of results

The goal of the research was to provide insight in the development of steel requirements associated with bottom-founded support structures of offshore wind turbines of various sizes at various water depths. The second goal was to fill the knowledge gap regarding growing OWT support structure dimensions and their associated environmental impact in terms of climate change potential. By applying qualitive and quantitative research methods, a model is created to determine steel requirements of monopile and jacket support structures for varying water depths and turbine sizes based on initial dimension estimates. Modelling results are used to derive parameters to estimate upfront and recoverable jacket support structure steel mass and associated steelmaking emissions. Furthermore, a comparison is made showing the steel requirements of a 500 MW wind farm and the effect of applying many lower rated power turbines versus a lesser number of high rated power turbines. In this chapter, a discussion with respect to the obtained results is presented.

4.1 Discussion of modelling results

Considering the trend of mass development with respect to water depth and turbine rated power, water depths shows to influence overall steel demand more significantly than turbine rated power. Monopile modelling results, albeit being limited in number, suggest a linear increase of support structure steel mass with respect to water depth. For jackets, modelling results suggest a second order polynomial increase of jacket steel mass with respect to water depth. The general formula and turbine specific parameters derived in section 3.4 can be used to determine an initial estimate of embedded support structure mass in existing wind farms and help estimate the steel mass requirements of future offshore wind farms that apply turbine sizes which are currently not yet in production. When combined with Figure 24, an estimate of recyclable steel quantities available after decommissioning can be obtained. An estimate of the GHG emissions that emerge in steelmaking are depicted in Table 4. Table 5 shows the GHG emissions that can be avoided if the OWT support structure steel is properly recycled and the need for future BF-BOF steel is reduced.

4.1.1 Monopile modelling results compared to reference literature

It should be noted that some combinations of water depth and turbine rated power did not result in viable monopile designs following the method applied in this research. This is for example the case for monopile substructures for 10 MW turbines at 50 meters depth. In this research, the 10 MW turbine was found to be viable in water depths up to 30 and 40 meter, depending on soil conditions. In reference literature, attempts have been made to verify monopile designs for 10 MW rated power turbines in water depth conditions of 50 meter. For example, Hermans & Peeringa (2016) show a basic monopile and tower design in these environmental conditions but indicate that their design pushes for the current maximum manufacturable capabilities. Furthermore, considering 15 MW OWTs, this research finds no monopile designs within current manufacturing limits. Gaertner et al. (2020) do include an initial monopile design for a 15 MW turbine at a water depth of 30 meter in their report. A significant difference, however, can be found in environmental operating conditions, as Gaertner et al. (2020) situate their OWT in an area with a much less energetic wave climate. This allows them to reduce the support structure's natural frequency to 0.13 Hz, where in the North Sea this would not be possible. Taking this into account, it should be noted that the modelling approach and design constraints applied might underestimate the viability of monopile designs for 8 and 10 MW turbines in the water depth range between 30 and 50 meter. Within the scope of this research, the obtained results provide a useful insight into the development of support structure steel demand, but should not be interpreted as a study towards maximum viable monopile designs.

Results provided by the model showed to be similar to reference literature and the mass error for tower and monopile segments combined was found <10%. With respect to 20 MW turbines, no monopile designs were found in analysed reference literature. Considering the goodness of fit for the linear regressions, for 5 and 8 MW turbines an R^2 of 0.85 and 0.76 is found which means that the linear regression fits the results reasonably well. For the 10 MW turbine R^2 is much lower and found as 0.43, which is probably caused by the limited number of results and larger differences in mass values per water depth. The standard error was found to be 179, 248 and 281 ton for the 5, 8 and 10 MW turbines respectively which is approximately 10-15% of the mass of the monopile support structures assessed.

4.1.2 Jacket modelling results compared to reference literature

Considering validation of the jacket modelling results with reference literature, it is found that significant variations occur. This can be largely attributed to the fact that environmental conditions differ significantly for any given location and so also the mass of support structures. Therefore, the dimensioning model was checked with parameters as suggested by Pontow et al. (2017) for two jackets supporting a 10 and 20 MW OWT at 50 meters depth and by Sandal et al. (2018) for a jacket supporting a 10 MW OWT at 50 meters depth. The combined jacket and TP masses provided by Pontow et al. (2017) are 900-1100 tons and 1600-1700 tons for the 10 and 20 MW designs, whereas the model presents 1660 tons and 2550 tons respectively. This suggests that the model overestimates the mass of the jacket support structures, roughly 50% in both cases. From further analysis it is found that the mass allocated to the jackets is similar to that provided by Pontow et al. (2017), but that the mass allocated to the transition pieces is overestimated significantly at 100-150%. Similarly, Sandal et al. (2018) provide a jacket and TP combined mass as 870 tons, which also indicates that the mass estimation model derived in this research overestimates the cumulative jacket support structure mass. This indicates that the transition piece design as suggested by Lee et al. (2017) are less suitable for larger jacket structures. A more accurate jacket support structure mass estimate could be obtained if the TP was modelled to be less massive. Alternatively the TP mass can be reduced by 50%. This adjustment would decrease the model error towards an accuracy of approximately 30%. Support structure mass estimates provided in this report are based on the unadjusted TP dimensions.

Considering the goodness of fit for the polynomial regression, an R^2 of 0.99 was found for the support structure mass results of each reference turbine. This indicates that the polynomial regression fits the results very well. The standard error was found to be in a range of 110-127 ton which is approximately 2-15% of the mass of the assessed jacket support structures, depending on the water depth at which the support structure mass and standard error are compared.

4.1.3 Manufacturability and crane lifting constraints

With respect to manufacturing constraints, some combinations of turbine rated power, water depth and soil conditions lead to large dimensions and turned out not to be manufacturable. For monopiles, 35 out of the 130 combinations of water depth, turbine size and soil conditions lead to manufacturable designs. For jacket structures, 44 out of 170 combinations of water depth, turbine size and soil conditions lead to designs surpassing manufacturing constraints. From the obtained results it was found that jackets are able to support higher rated-power turbines to greater water depths.

Hermans & Peeringa (2016) describe an initial design for a 10 MW OWT supported on a monopile substructure at 50 meters water depth, whereas the method applied in this research obtained viable designs up to 30 meters depth. In the North Sea's wave climate, which consists of relatively energetic waves, monopiles are limited to more shallow water to avoid the occurrence of resonance between environmental loads and the support structure. Hermans & Peeringa (2016) obtained their design for an area with a less energetic wave climate. This allowed them to design a structure with lower natural

frequency, reducing its overall dimensions and mass to be just within manufacturing constraints. The modelling approach applied in this research provides more conservative monopile dimensions and subsequent mass estimates, fitting to a more active wave climate as present in the North Sea.

Increased manufacturing capabilities could make designs possible that extend the water depth range of the monopile typology. However, considering the high upfront steel requirements of this typology in combination with the lower mass returns during decommissioning, this might not be preferable. Instead, from a material demand and GHG emission perspective it is more favourable to push for increased uptake of jacket support structures, especially considering the large number of turbines that need to be installed to achieve the energy transition as envisioned by the European Commission (2018).

Considering the crane lifting capacity constraint, a maximum value of 2500 tons is taken into account. This is based on suggestions by Van de Brug (2019) and considers the installation vessels of Van Oord. Van de Brug (2019) mentions that development of the crane lifting capacity of installation vessels depends on demand. To illustrate this example, in 2002 crane lifting capacity was 230 tons, in 2014 this increased to 900 tons and by 2018 the crane lifting capacity reached 1600 tons. Vessels with 2500 ton crane lifting capacity can be expected to be operational by 2030. The crane lifting constraint affects the number of viable monopile and jacket designs considered in this research. For monopiles, the maximum lifting capacity was superseded most often, closely followed by the maximum diameter constraint. Therefore, increasing the crane lifting capacity would not necessarily lead to an increase in the number of viable monopile designs. For jackets, increasing the crane lifting capacity would allow the construction of larger support structures and therefore increase the maximum depth at which jacket designs could be considered. However, a more in-depth technical assessment focussed on structural analysis would be required to confirm this statement as this research is solely based on initial estimated dimensions.

4.1.4 Retrievable support structure mass for monopile and jacket structures

From the model results it becomes clear that jacket support structures have lower initial steel requirements than monopile support structures. Furthermore, the ratio of retrievable steel mass at end-of-life is significantly higher for jacket structures. Combined this indicates that for the jacket support structure typology a lesser amount of steel is required to initially construct an OWT's support structure and that relatively more steel can be recovered during decommissioning. Steel in itself is not considered to be a critical material. However, some alloying elements that are present in steel for offshore application, like vanadium, titanium, silicon and niobium are currently on the European list of critical raw materials. Niobium is associated with the highest criticality within the EU, combining the highest supply risk and economical dependency of these four critical materials (European Commission, 2020c). Losses of these critical elements should therefore be avoided.

The concentration of niobium in support structure steel is approximately 0.022 wt% (Igwemezie et al., 2019). For a 500 MW wind farm consisting of 8 MW turbines at a water depth of 40 meter, steel losses for monopile and jacket support structures were found to be 62.000 ton and 28.000 ton respectively, see Figure 25 in 3.4.5. The loss of niobium in this case amounts to 1350 ton for monopile structures and 620 ton for jacket support structures. Considering that the global niobium production was 74.000 ton in 2019 (USGS, 2020), the importance of these losses becomes more apparent. Approximately 730 ton of niobium loss could be avoided by applying jacket structures over monopile structures, which is almost 1% of annual global niobium production. At this water depth, 15 MW OWTs supported on jacket structures showed to require the lowest amount of support structure steel. Steel loss in this configuration would amount to approximately 16.000 ton. Associated niobium losses would be 350

ton in this case, which is 75% less compared to a similar sized wind farm consisting of 8 MW monopile-supported OWTs.

Considering the replaceability of niobium in the steel composition, niobium is specifically added to steels for offshore application as it positively affects grain size formation and corrosion resistance. The addition of niobium to a steel mix guarantees a sufficiently small grain size, especially for thick steel plates. This smaller grain size is necessary for the level of crack and fatigue resistance required in this type of structural application. A known substitute for niobium is titanium, but this is already present in offshore steel and a critical raw material itself. For monopile support structures, very thick steel plates are required which makes niobium hard to substitute. For jackets, the required plate thickness is generally smaller which might reduce the need for alloying elements that facilitate small grain size formation or allow for other steel types to be used. This can be interesting for future research. More information about alloying elements and their effect on steel properties can be found in appendix A3 Steel composition and element criticality.

4.1.5 Discussion of the comparative scenario

A notable effect observed from the comparative scenario in 3.6, is that a configuration consisting of a high number of medium capacity turbines in shallow water (≤20 m) conditions results in the most favourable steel requirements. In contrast, for deeper water conditions at 60 m water depth, a configuration containing a lesser number of high capacity turbines results in the lowest steel requirements. This suggests that an optimal configuration is affected by all three parameters, which are water depth, number of turbines installed and turbine rated power. This opposes earlier findings by Topham et al. (2019), who showed an increase of steel intensity per MW installed capacity for higher rated power turbines under, assumingly, similar water depth conditions. The results presented in Figure 25, however, suggest that this is not exclusively so. For the statement of Topham et al. (2019) to hold true, the optimum configuration should favour the application of many 5 MW turbines over a lesser number of higher power turbines. This is not the case, as for the three water depth conditions assessed the favourable turbine rated power is consistently not the lowest rated power available. Even more so, favourable turbine rated power increases as the water depth increases.

A practical implication of this finding considers currently installed wind farms that will soon reach end-of-life and are to be replaced. In this situation, one can consider applying increased rated power turbines with jacket support structures as this would minimize overall steel requirements and inherent GHG emissions associated with the construction of the new wind farm. In some cases, steel that is recovered during decommissioning of older turbines would already cover the steel need of a new wind farm, significantly limiting the overall need for new iron and alloying elements required to produce the offshore steel. In practice, the choice of turbine rated power depends on many considerations, like for example the prevailing wind speed on site or the cost of individual turbines. Choosing a turbine size close to the suggested configurations presented in Figure 25, however, can help to reduce the steel intensity of any new wind farm.

The overall steel intensity per MW installed capacity increases rapidly for deeper water development areas. Also, the variation in cumulative mass between the various turbine sizes increases for larger water depths. For example, where at 20 meters depth the various jacket-supported turbines differ up to approximately 20% in cumulative support structure mass, at 60 meters depth this difference increases to almost 100%. This indicates that for increasing water depths, the choice of turbine rated capacity and support structure typology rapidly gains importance. In the case that multiple developing areas are available, choosing a site with more shallow water can significantly reduce the quantity of steel required for the construction of the wind farm.

It was found that no single turbine size is exclusively most beneficial for all water depths, but that the configuration with minimal steel requirements is a combination of water depth, the number of installed turbines and turbine rated power. Choosing a turbine rated power and support typology similar to the suggestions in Figure 25 helps to reduce a wind farm's steel intensity and inherent GHG emission payback time.

4.1.6 Discussion of support structure GHG emissions

With respect to the emissions embedded in support structure steel, it is found that these are of significantly lesser magnitude than the emissions avoided through an OWT's electricity generation. Emission payback time of the support structure steel was found to be in a range of months compared to a design-lifetime of approximately 20 years. This means that all assessed OWTs placed in water depths up to 70 meter generate electricity at lower GHG emissions than the current average kilowatt of electricity produced within the EU. Due to the better performance of OWTs compared to traditional fossil fuel based electricity, the absolute differences between monopile and jacket steel GHG emissions may seem small. In contrast, the relative differences between monopiles and jackets are quite significant, up to a 100% difference in favour of the jacket substructure typology.

For 5 MW monopile supported turbines situated at 20, 40 and 60 meter water depth, the share of support structure steel emissions ranges between 32-50%. Similarly, for jackets this share ranges between 21-37%. Overall, the application of jacket support structures reduces an OWT's total climate change potential with 15-20%. This shows the significance of a support structure's contribution to the overall climate change contribution of OWTs and stretches the importance of minimizing steel requirements of these structures. It would be interesting to see how these contributions change for the higher power turbines. For these turbines, no breakdown of climate change contribution per component as presented by Bonou et al. (2016) was found in assessed literature. Given the large assumptions required to create such a breakdown, this is not included in this report and suggested for future research.

Given the relatively high share of EAFs in the EU's steelmaking mix, the value derived for the GHG emission indicator can appear to be low when compared with individual steelmaking companies or other geographic regions than the EU. This should be taken into account if the modelling results of this report are compared to GHG emission estimates for other regions. Within the region, the GHG emission indicator value compares well to reference reports. For example, in a 2019 sustainability report of a large steel manufacturer (U.S. Steel, 2019), a GHG emission indicator of 2.11 kg CO2-eq/t steel is reported for BF-BOF processes. For this research, a value of 1.84 kg CO2-eq/t steel was derived for this steelmaking process. The difference in emissions could be caused by the type and amount of coal and cokes used, the iron content of the iron-ore and the amount of scrap fed to the melt. Considering that the indicator used for this research is based on average statistics for EU steelmaking plants, the difference of 15% is considered acceptable.

Considering the GHG emission indicator over time, its value could be reduced if alternative iron-ore reduction technologies are implemented. A recent report by Roland Berger consultants (2020) describes that significant financial investments are required to set-up large scale alternative primary steel production methods, like for example hydrogen-based direct reduction, but that this is not considered likely to happen before 2030. Therefore, the GHG emission indicator of 1.22 tCO2-eq/t support structure steel can be considered constant up to 2030. Carbon capture and storage is mentioned as an intermediate solution, as this can be reasonably easy integrated with existing infrastructure. However, public acceptance, suitable storage locations and logistics slow the uptake of this technical adaptation**.** The findings of Berger's report are confirmed by steelmaking companies'

sustainability reports. For example, U.S. Steel – a large steelmaking company responsible for approximately 5% of the EU's steel production – has recently committed to reduce the emission intensity of their global footprint with 20% by 2030 (U.S. Steel, 2020). Of itself, this is a good commitment. However, this is mainly achieved by increasing efficiency of current practices and by the implementation of an additional EAF production facility. Considering alternatives for primary iron-ore reduction, the report states that 'there are currently no viable technological alternatives for the reduction of iron ore' (U.S. Steel, 2019, p39), that their engineers 'are at the forefront of investigating breakthroughs associated with circular carbon technologies and the use of hydrogen as a reductant' and that as a company they 'are prepared to invest and capitalize on the these developments'. However, no concrete plans or targets with respect to primary iron-ore reduction after 2030 are given, while this is the most emission intensive process. For U.S. Steel, the 2030 reduction of emission intensity goal is achieved by upscaling secondary, scrap-based steel production and increased product throughput.

Considering development after 2030, the Berger consultant's report indicates that the European steel industry is expected to present a strategy to achieve carbon neutrality by 2050 before the end of the decade. Similar to U.S. Steel, Berger's report refers to the introduction of hydrogen as a reductant. In traditional BF-BOF steelmaking practices carbon is used as the reductant. In the future, carbon might be exchanged with hydrogen which has two advantages. Firstly hydrogen can be produced from liquid water via electrolysis, which uses electricity as its energy source. This electricity can be obtained from renewable energy sources like offshore wind. Secondly, when applied as a reductant hydrogen is converted back to water vapour in the steelmaking process. This severely reduces the GHG emission intensity of the steel production process.

The implementation of hydrogen-based steelmaking will require the creation of a sufficiently large hydrogen producing industry, hydrogen distribution infrastructure and the replacement of current blast furnaces with hydrogen reduction furnaces. The rate-of-change required to achieve net-zero steelmaking by 2050 will require a strong commitment by the steelmaking industry, hydrogen production industry, policy makers and end-consumer. The feasibility of achieving these alternatives by 2050 largely influences the value of the GHG emission indicator. For example, if by 2050 half of the iron-ore would be processed using hydrogen rather than traditional cokes and coal, the emission intensity of steelmaking would decrease from 1.22 tCO2-eq/t steel to approximately 0.71 tCO2-eq/t steel. Similarly, if by 2050 all iron-ore would be processed using hydrogen, the emission intensity of steelmaking would decrease to approximately 0.27 tCO2-eq/t steel. The emission intensity of hydrogen reduced iron-ore in this example is 0.39 tCO2-eq/t steel and is derived using the following assumptions:

1) Per ton of steel approximately 3.5 MWh electricity is consumed for the production of green hydrogen and the efficiency of hydrogen production based on water electrolysis is within a range of 60-80% (Kumar & Himabindu, 2019; Vogl, Åhman & Nilsson, 2018)
2) Green hydrogen is produced using renewable electricity sources at an emission intensity of 36 gCO2-eq/MJ hydrogen (CertifHy, 2016).
3) The ratio between BF-BOF and EAF steel production remains 59.8% and 40.1% respectively.
4) Electricity used in EAF steel production is well reflected by the average EU electricity emission intensity of 100 gCO2-eq/kWh by 2030 (European Environment Agency, 2020).

EAF steelmaking is a suitable technology for recycling steel, but is not suited for converting iron-ore. EAF steelmaking relies on the availability of steel scrap. In EAF steelmaking, electricity is used to melt steel scrap in which only limited chemical reactions occur, hence the emission intensity of EAF steelmaking is much lower than that of BF-BOF steelmaking processes.

4.1.7 Discussion of emission and energy payback time

Considering the emission payback time, it is found that as average emissions associated to electricity generation decrease, the payback time increases. This increase is considered to become significant on a short term. If average electricity emissions decrease as predicted by the European Environment Agency (2020), environmental payback time can increase threefold by 2030. Current emission payback time lies within a range of months, but this can increase to one or several years if the GHG emissions of steelmaking do not decrease similar to that of average European electricity generation. A limitation of the emission payback time indicator emerges when the GHG emissions of EU electricity become zero, as the emission payback time would then become infinite. To avoid this, the emission intensity of steelmaking processes should reduce in a similar rate as the emission intensity of electricity generation. This signifies the importance for fast implementation of alternative low-emission steelmaking processes. Especially considering the high steel intensity of the offshore wind energy industry.

The energy payback time is found to be shorter than the emission payback time. This is due to the fact that the energy invested in steelmaking is more emission intensive than an average kilowatt of European electricity is. An advantage of the energy payback time is that, in contrast to the emission payback time, the energy payback time does not change much as electricity generation is decarbonized. The energy payback time, however, does not provide direct insight into the quantity of GHG emissions associated with the production or consumption of the energy. Also, it does not take into account in what form the energy is available, being chemically, electricity or heat. When assessed alongside each other the indicators provide the most useful insight. As both the actual energy requirements and the emission intensity of the energy used are then accounted for.

4.2 Limitations of the research

Considering the limitations of the research, it should be kept in mind that exclusively the OWT's support structures are assessed. Steel embedded in secondary infrastructure, like stairs and boat landings, substations and their support structures, inter-array cables and export cables are not included in the provided estimations. The overall contribution of these components to a wind farm's total steel requirements, however, are much smaller than the steel embedded in the OWT support structures.

Next, this research contributes to overall insight into the development of offshore wind turbines with higher rated power and increased water depth, but does not touch upon the development of critical metals present in generator equipment. Insight into the resource needs of higher rated power turbine NRAs and the effect of upscaling turbine rated power on their material demand can complement this research.

Another important aspect to keep in mind is that the steel mass values derived in the modelling of this research are based on design rules-of-thumb and not obtained from measurements. Individual cases can deviate significantly from the obtained results depending on the environmental circumstances of any specific project. The results do showcase the importance of a support structure's typology on the overall steel requirements of an offshore wind farm. As larger turbines and development zones located in deeper water are exploited, data can be gathered to further improve or validate the model and subsequent steel demand estimations.

Considering the OWTs annual energy production, the method applied in this research is used to provide an estimate range of electricity production. Both the emission and energy payback time are directly related to the annual energy production. A better annual energy production estimate can be obtained if site specific wind conditions are combined with the power curve of each OWT. The method

applied in this research fits the more general nature of the research aim, but should not be considered to reflect wind farm conditions on a specific location. Furthermore, the estimation takes 5% transmission losses into account, but does not consider inter and intra-array wake effects or repair and maintenance downtime.

Next, the GHG emissions emerging throughout lifecycle stage 4-8 - being component manufacturing, component transportation, turbine construction, turbine operation and decommissioning processes – are not included in the modelling. The extraction and transport of iron-ore, cokes and coal – e.g. lifecycle stage 1 and 2 – are also not included in the provided GHG emission estimates. Bonou et al. (2016) show that for OWTs of 4-6 MW rated power, the GHG emissions emerging in these lifecycle stages combine to approximately 22% of the total contribution to climate change compared to approximately 70% spend on materials production. How these ratios will change for larger turbines and support structures could not be determined from this research, but could be considered in future studies.

With respect to the calculated GHG emissions, methane and nitrous gas emissions are excluded from calculations following the guidelines presented by Lubetsky et al. (2006). These emissions, albeit of lesser significance than the carbon-dioxide emissions emerging from steelmaking processes, might be more relevant in the assessment of other environmental indicators than climate change potential. For this research, the applied method is considered to sufficiently reflect the overall contribution of support structure steelmaking in terms of their climate change potential.

The cost difference between jacket and monopile typologies has not been studied in this research. Overall, jacket support structures align better with the European Commission's goal of reducing GHG emissions in power generating industries. Furthermore, lower steel losses inherently translate to lower losses of critical raw materials that are used as alloying elements in steel for offshore application. A cost-benefit analysis can help to determine the added value of reducing steel demand and increasing steel recovery potential related to choosing jackets over monopile support structures and compare this to any additional financial cost involved.

4.3 Future research suggestions

Future studies can be dedicated to how the steel mass requirements of floating turbines evolve compared to that of bottom-fixed structures. Especially, to find out if there is a water depth at which a tipping point occurs from which floating support structures become more material efficient than bottom-fixed structures. Second, the support structure mass development formulas derived in this research can be used to further study the use of critical raw materials in the offshore wind industry. A mass flow analysis for niobium or titanium can be performed to gain more detailed understanding into stock formation and critical raw material losses that emerge throughout the lifecycle of an OWT. Next, a cost-benefit analysis can provide insight into the financial differences between monopile, jacket and perhaps even floating support structures. Lastly, a study considering the resource needs of higher rated power turbine NRAs and the effect of upscaling turbine rated power on their critical raw material demand can complement this research.

5. Conclusion

This research revolves around the development of support structure mass and associated GHG emissions for bottom-fixed OWTs related to the trend of increasing turbine rated power and depth of exploitation. To answer the main research question, two sub-questions were determined and two additional questions were formulated in support of the first and second research sub-questions. Combined these provide an answer to the main research question. In the following the sub-questions will be answered. The main research question of this research was:

How do support structure steel demand and associated environmental impact evolve for offshore wind turbines in the North Sea until 2050, following trends of exploitation at increasing water depth and turbine rated power?

The first additional question considers support structure typologies available for wide-spread implementation. The second additional question considers historical and future water depth of exploitation and turbine rated power. The additional questions were formulated as follows:

1. *Which bottom-fixed support structure technologies will be available for offshore wind turbines at various water depths in the North Sea until 2050?*
2. *How have water depth and rated power of wind turbines in the North Sea evolved over time and what is expected until 2050?*

From literature analysis follows that for bottom-founded structures, monopile and jacket support structures are currently most applied. This trend can be expected to continue in the following thirty years. Monopiles are traditionally applied in water depths up to 35 meter, but are claimed to be suitable up to 60 meters depth. Jackets are traditionally applied in water depth between 30-60 meter, but considered economically viable up to 80 meters depth. Together, these two support structure typologies make up for 90% of the installed number of turbines. The share of jacket structures can be expected to increase as turbine rated power increases and deeper waters are exploited.

The average water depth has continuously increased up to this point in time, being 5-10 meters in the 1990's and 33 meters in 2019. Available OWT development zones are found in three distinguishable regions with varying water depth ranges. The first region, the Southern Bight, is characterised by a water depth range of 20-50 meters. In the second region, the Central North Sea near the coast of Denmark, water depth largely varies between 40-100 meters. The third region hosts the largest water depths, with a minimum of 50 meters and up to 200 meters. Overall, the water depth in the North Sea region can be said to vary between 20 and 200 meters. Development areas have so far been restricted to areas with water depths up to 50 meters. However, given the plans to expand the North Sea wind sector and high availability wind farm development areas in depths up to 100 meters, it can be expected that the average and maximum depth of exploitation will continue to increase within this range. Based on the availability of development sites it can be expected that the average water depth of exploitation for bottom founded OWTs will develop to be in a range of 40-70 meters, as these are the most commonly found water depths in region 1 and 2. The average turbine rated power has increased over time, reaching 7.8 MW in 2019. Maximum turbine rated power also increases over time, with the highest rated power turbine installed being 9.5 MW in 2019. Considering development up to 2050, the maximum turbine rated power available for large scale implementation is expected to increase to 20 MW rated power.

The first sub-question considers material requirements for support structures and reads as follows:

SQ1:How does the material demand for main support structure technologies change with increasing water depth and rated power?

A support structure mass estimation model was created following design rules-of-thumb for both monopile and jacket support structures. Ultimate, serviceable and fatigue limit state checks were not included in the model, as the model is based on geometric estimations. Five reference turbines in a range of 5-20 MW rated capacity were used in the model. Environmental parameters, like water depth, wave height and soil conditions, were collected for three regions in the North Sea to account for varying operating conditions. Wind conditions were found to be similar in the three regions.

Monopile support structure mass is found to increase following a linear relation between combined monopile and tower mass and water depth. Applicable water depth range and parameters for the linearization are shown below. A visual overview of the results can be found in Figure 16.

P [MW]	**a**	**b**	General formula	Water depth range [m]	R^2 / SE
5	32.3	462	$M_{support\ structure}(d) = \boldsymbol{a} * d + \boldsymbol{b}$	20-60	0.85 [-] / 179 [t]
8	37.4	1028		20-50	0.76 [-] / 248 [t]
10	30.1	1742		20-40	0.43 [-] / 281 [t]

In total, 35 feasible monopile designs are obtained for 5, 8 and 10 MW rated power turbines out of the original 130 design combinations. For 5 MW turbines, all combinations of water depth and soil conditions proved viable. For 8 and 10 MW turbines, soil conditions proved a dominant factor influencing design viability, favouring medium-dense soil conditions. Monopile and tower support structure mass for feasible designs are found to be in a range of 1120-2930 ton for NREL-5MW, LW-8MW and DTU-10MW reference turbines at water depth of 20 to 60 meter. No viable combinations supporting 15 and 20 MW designs are found using this dimensioning approach, as for each combination of turbine size and water depth the maximum monopile mass constraint of 2500 ton is superseded. Support structure mass that could be retrieved at end-of-life is found to be approximately 50-60% of the initial monopile and tower mass depending on water depth.

Jacket support structure mass is found to increase following a second order polynomial between cumulative component mass and water depth. These components include the tower, transition piece, jacket and foundation piles. Parameters for the polynomial regression are shown below. A visual overview of the obtained results and regression can be found in Figure 20.

Turbine rated power [MW]	**a**	**b**	**c**	General formula	Water depth range [m]	R^2 / SE
5	0.92	-20.4	735	$M_{support\ structure}(d) = \boldsymbol{a} * d^2 + \boldsymbol{b} * d + \boldsymbol{c}$	20-70	0.99 [-] / 110 [t]
8	0.94	-18.9	970		20-70	0.99 [-] / 115 [t]
10	0.96	-17.8	1118		20-70	0.99 [-] / 116 [t]
15	1.04	-17.8	1803		20-70	0.99 [-] / 127 [t]
20	1.08	-11.6	2716		20-60	0.99 [-] / 115 [t]

In total, 126 out of the original 170 design combinations resulted in jacket support structure designs with dimensions within crane lifting constraints. The crane lifting constraint was violated for all jacket designs in water depths larger than 70 meters. For the 20 MW turbine no design was found in water depths larger than 60 meters. Cumulative jacket support structure typology mass for viable designs are found to be in a range of 630-6480 ton steel. Support structure mass available for retrieval at end-of-life is found to be in a range 75-95%, depending on turbine rated power and water depth.

The lower steel intensity per electricity generating capacity and higher ratios of retrievable steel mass for jacket structures can help reduce the loss of critical raw materials that are used for alloying elements in offshore steel. Especially the loss of niobium is important to consider, as the EU heavily relies on import for its supply. Niobium losses for a 500 MW wind farm are in the order of several hundred tons, which is significant considering that global niobium production amounts to approximately 74.000 tons per year.

The second sub-question considers the GHG emissions that emerge during the steelmaking process:

SQ2: What is the environmental impact in terms of climate change potential related to the steel requirements of assessed OWT support structures and what is the environmental payback time?

An emission factor of 1.22 tCO2/t support structure steel is applied to convert the support structure steel masses to emission quantities. The GHG emissions for monopile support structures vary between 1366-3569 ton CO2-eq per structure, depending on the combination of turbine rated power and water depth. Taking recycling of the monopile support structure steel into account, a potential reduction in climate change potential of 35-45% can be achieved. For jackets, the GHG emissions vary between 778-7095 ton CO2-eq per structure. Recycling of initial jacket structure steel at end-of-life can lead to a 50-70% reduction in climate change potential.

The emission payback time for both monopile and jacket structures is found to be in a range of 2-14 months when compared to average electricity emission for the EU in 2019. All combination of water depth and turbine rated power lead to emission payback times that are less than the turbine lifetime, indicating that every assessed turbine is able to produce electricity at more favourable emissions than the current average electricity produced in the EU. However, a reduction of the EU's average electricity emissions results in increased payback times. This can be as much as three times longer by 2030 compared 2019, if no alternative non-fossil steel production methods become available in this period of time. A limitation of the emission payback time indicator emerges when average electricity GHG emissions reduce to near zero. In this case, the emission payback time indicator becomes near infinite and is no longer able to distinguish low-carbon investments from high-carbon investments. This emphasizes the relation between steelmaking emission intensity and the emission intensity of offshore wind electricity generation. Infinite emission payback times can be avoided if steelmaking emissions reduce similarly to those of electricity generation. The energy payback time is not affected by this phenomenon and proves to be a more stable indicator when electricity generation approaches zero GHG emissions. The energy payback time indicator by itself, however, is less insightful in the assessment of invested and avoided GHG emissions. When assessed in conjunction, the indicators provide the most insight in the environmental payback time of offshore wind electricity generation.

The combination of water depth and turbine rated power with minimal emission payback time shifts towards higher rated power turbines as water depth increases. At 20 meters depth, most favourable combination is a wind farm consisting of 10 MW jacket supported OWTs. This results in an average steel intensity of approximately 110 ton steel per MW installed capacity. For a wind farm situated at 40 and 60 meter water depth, the application of 15 and 20 MW turbines show to be most favourable. The support structure steel intensity at 40 and 60 meters depth then are 190 and 290 ton steel per MW installed capacity respectively.

Limitation of the research are that exclusively primary steel infrastructure is included in the estimations and that only steel as a construction material is assessed. The support structure mass estimates are based on initial dimensions, other design criteria like Ultimate Limit State (ULS) or Fatigue Limit State (FLS) are not considered in this work. GHG emissions from steelmaking and recycling are

included, but emissions emerging during extraction and transport of raw materials, component manufacturing and transportation, turbine construction, operation and decommissioning processes are not included.

In answer to the main research question, the choice of turbine, support structure and water depth all influence the development of support structure steel requirements and associated GHG emissions. Mass development for monopile support structures varies for each turbine size assessed and is described by linear regressions. Mass development for jacket support structures also vary per turbine rated power and are described by a second-order polynomial function. Initial required support structure mass is lower and the steel recovery potential is higher for jacket support structures than for monopile support structures. Considering the influence of water depth on the total climate change potential of OWTs, for 5 MW OWTs it is found that the application of jacket structures reduces an OWT's total climate change potential with 15-20% compared to monopile structures. For 5 MW turbines at 20 meters depth, the emission intensity of electricity generation is found to be 9.4 and 8.1 g CO2-eq/kWh for monopile and jacket founded OWTs. At this depth, the support structures contribute 32% and 21% respectively to the OWT's total climate change potential. At 60 meters depth the emission intensity of electricity generation increases to 12.8 and 10.2 g CO2-eq/kWh for monopiles and jackets respectively and the relative support structure share increases to be 50% and 37%.

Bibliography

4Coffshore (2020). EolMed Offshore Wind Farm. Accessible at: https://www.4coffshore.com/windfarms/france/eolmed-france-fr64.html

Alfred Wegener Institute (2009). Digital Atlas of the North Sea – An overview about geo-information considering the sea floor and the bottom water column, p23&71. Retrieved from: https://epic.awi.de/22497/1/Sch2009bi.pdf

American Welding Society (2009). Effect of chemical elements in steel. Retrieved from: https://www.steeltank.com/Portals/0/Articles/Effect%20of%20Chemical%20Elements%20in%20Steel.pdf?ver=2009-05-31-010753-797

API (2005). Recommended Practice for Planning, Designing and Constructing Fixed Offshore Platforms—Working Stress Design. 68–71.

Arany, L., Bhattacharya, S., Macdonald, J., & Hogan, S. J. (2017). Design of monopiles for offshore wind turbines in 10 steps. *Soil Dynamics and Earthquake Engineering*, *92*, 126–152. https://doi.org/10.1016/j.soildyn.2016.09.024

Bak, C. (Author), Zahle, F. (Author), Bitsche, R. (Author), Kim, T. (Author), Yde, A. (Author), Henriksen, L. C. (Author), ... Natarajan, A. (Author). (2013). The DTU 10-MW Reference Wind Turbine. Sound/Visual production (digital)

Björkman, B. & Samuelsson, C. (2014). Chapter 6 - Recycling of Steel. In Worrell, E. & Reuter, A.M., *Handbook of Recycling* (pp. 65-83). Amsterdam, The Netherlands: Elsevier.

BMT Cordah Limited (2011). Management of marine growth during decommissioning. Retrieved from: https://oilandgasuk.co.uk/wp-content/uploads/2019/07/The-Management-of-Marine-Growth-during-Decommissioning.pdf

Bureau of International Recycling (2018). World steel recycling in figures 2013-2017 – Steel scrap: a raw material for steelmaking. Retrieved from: https://www.bdsv.org/fileadmin/user_upload/180222-Ferrous-report-2017-V07.pdf

Bonou, A., Laurent, A., & Olsen, S.I. (2016). Life cycle assessment of onshore and offshore wind energy-from theory to application. Applied Energy, 180, 327–337. Retrieved from: https://doi.org/10.1016/j.apenergy.2016.07.058

Hoving, J.S. (2017). *Lecture 2&3: Substructure Design, Geometry & Configuration* [PowerPoint slides]. Retrieved from TU Delft Bottom Founded Offshore Structures OE44095 site.

Bottom Founded Offshore Structures (2017). Introduction to substructure design and configuration. Course code: OE44095, lecture 2&3.

CertifHy (2016). Developing a European guarantee of origin scheme for green hydrogen – Definition of green hydrogen [PowerPoint slides]. Retrieved from: https://www.certifhy.eu/images/media/files/CertifHy_Presentation_19_10_2016_final_Definition_of_Premium_Hydrogen.pdf

Dähne, M. Gilles, A. Lucke, K. et al. (2013). Effects of pile-driving on harbour porpoises (Phocoena phocoena) at the first offshore wind farm in Germany. Environmental Research Letters, 8(2): p.025002. DOI: 10.1088/1748- 9326/8/2/025002.

Daubney, K. (2013). In depth: Cost imperative drives monopiles to new depths. Wind Power Offshore. Retrieved from: https://www.windpowermonthly.com/article/1210058/depth-cost-imperative-drives-monopiles-new-depths

Deltares (June 15th, 2016). Costs offshore wind further down to 7 eurocent/kWh by 2030. Retrieved from: https://www.deltares.nl/en/news/costs-offshore-wind-further-down-to-7-eurocentkwh-by-2030/

Desmond, C., Murphy, J., Blonk, L., Haans, W. (2016). Description of an 8 MW reference wind turbine. *Journal of Physics: Conference series: 753 092013.* Doi: 10.1088/1742-6596/753/9/092013

DNV-GL (2016). Standard – Support structures for wind turbines. Retrieved from: http://rules.dnvgl.com/docs/pdf/dnvgl/ST/2016-04/DNVGL-ST-0126.pdf

DTU Wind (2013). Design Report - Reference Jacket. Deliverable 4.3.1. [online] DTU Wind, pp.29-62. Available at: http://www.innwind.eu/-/media/Sites/innwind/Publications/Deliverables/DeliverableD4-31_20131030_INNWIND-EU.ashx?la=da&hash=A29780A9EA7462E24017D68F3BE7E7CE753DAEBB [Accessed 1 June 2020].

El-Faramawy, H.S., Ghali, S.N. & Eissa, M.M. (2012). Effect of Titanium addition on behaviour of medium carbon steel. Retrieved from: https://www.scirp.org/pdf/JMMCE20121100008_97677514.pdf#:~:text=Titanium%20content%20has%20great%20influence,of%20grain%20refinement%20of%20titanium.

Energias de Portugal (2018). Innovation at EDP – WindFloat Atlantic. Accessible at: https://www.edp.com/en/innovation/windfloat

Equinor (2020). How Hywind works. Accessible at: https://www.equinor.com/en/what-we-do/floating-wind.html

EuroFer (2019). European steel in figures. Retrieved from: https://www.eurofer.eu/assets/Uploads/European-Steel-in-Figures-2019-Final-v2.pdf

European Commission (2017). Critical raw materials and the circular economy – Background report. Retrieved from: https://www.researchgate.net/profile/Bernd_Gawlik/publication/321998000_Critical_raw_materials_and_the_circular_economy/links/5a3ce345458515f7ea5416c0/Critical-raw-materials-and-the-circular-economy.pdf

European Commission (2018). A Clean Planet for all: A European Long-Term Strategic Vision for a Prospectus, Modern, Competitive and Climate Neutral Economy. European Commission, Brussels. Accessible at: https://eur-lex.europa.eu/legal-content/EN/TXT/?uri=CELEX:52018DC0773

European Commission (2020). An EU strategy to harness the potential of offshore renewable energy for a climate neutral future. European Commission, Brussels. Accessible at: https://ec.europa.eu/energy/sites/ener/files/offshore_renewable_energy_strategy.pdf

European Commission (2020b). SETIS - Energy efficiency in the iron and steel industry. Retrieved from: https://setis.ec.europa.eu/technologies/energy-intensive-industries/energy-efficiency-and-co2-reduction-iron-steel-industry/info

European Commission (2020c). Critical raw materials resilience: Charting a path towards greater security and sustainability. Retrieved from: https://eur-lex.europa.eu/legal-content/EN/TXT/PDF/?uri=CELEX:52020DC0474&from=EN

European Environment Agency (2020). Greenhouse gas emission intensity of electricity generation. Retrieved from: https://www.eea.europa.eu/data-and-maps/indicators/overview-of-the-electricity-production-3/assessment

Gaertner, E., Rinker, J., Sethuraman, L., Zahle, F., Anderson, B., Barter, G., Abbas, N., Meng, F., Bortolotti, P., Skrzypinski, W., Scott, G., Feil, R., Bredmose, H., Dykes, K., Shields, M., Allen, C. & Viselli, A. (2020). Definition of the IEA 15-Megawatt Offshore Reference Wind. Golden, CO: National Renewable Energy Laboratory. NREL/TP-5000-75698. Retrieved from: https://www.nrel.gov/docs/fy20osti/75698.pdf

General Electric (2020). Haliade-X offshore wind turbine. Accessible at: https://www.ge.com/renewableenergy/wind-energy/offshore-wind/haliade-x-offshore-turbine

Globe Metal (Feb, 2020). Significant opportunities to recycle Niobium. [Online source] Available at: https://globemetal.com/niobium-recycling/#:~:text=The%20typical%20recycling%20process%20of,lost%20in%20the%20slag%20phase

Higgins, P., & Foley, A. (2014). The evolution of offshore wind power in the united kingdom. Renewable and Sustainable Energy Reviews, Vol. 37, pp. 599–612. Retrieved from: https://doi.org/10.1016/j.rser.2014.05.058

Holthuijsen, L., (2009). Waves In Oceanic And Coastal Waters. *Cambridge University Press*, pp.150-162, 2009 edition. Cambridge.

Igwemezie, V., Mehmanparast, A., & Kolios, A. (2019). Current trend in offshore wind energy sector and material requirements for fatigue resistance improvement in large wind turbine support structures – A review. Renewable and Sustainable Energy Reviews, 101(October 2018), 181–196. https://doi.org/10.1016/j.rser.2018.11.002

International Energy Agency (2019). Offshore wind outlook 2019: World energy outlook special report. *International Energy Association.* Retrieved from: https://webstore.iea.org/download/direct/2886?fileName=Offshore_Wind_Outlook_2019.pdf

Jalbi, S., Nikitas, G., Bhattacharya, S., & Alexander, N. (2019). Dynamic design considerations for offshore wind turbine jackets supported on multiple foundations. *Marine Structures*, *67*(May), 102631. https://doi.org/10.1016/j.marstruc.2019.05.009

Jamieson, P. & Branney, M. (2012). Multi-rotors; a solution to 20 MW and beyond? Energy Procedia 24 (2012) pp.52-59. Doi: 10.1016/j.egypro.2012.06.086. Retrieved from: https://www.sciencedirect.com/science/article/pii/S1876610212011265/pdfft?isDTMRedir=true&download=true

Jarquin Laguna, A. (2019). *Lecture 3b: Turbine selection* [PowerPoint slides]. Retrieved from TU Delft Offshore Wind Farm Design OE44120 site.

Jensen, P.H., Chaviaropoulos, T. & Natarajan, A. (2017). LCEO reduction for the next generation offshore wind turbines – Outcomes from the INNWIND.EU project. Retrieved from: https://www.academia.edu/attachments/61373810/download_file?st=MTYwNjIyNTYxNywyMTMuMTI3LjMyLjEw&s=swp-splash-header

JWPA (2017). Offshore Wind Power Development in Japan. Retrieved from: http://jwpa.jp/pdf/20170302_OffshoreWindPower_inJapan_forTWTIA.pdf

Kumar, S. & Himabindu, V. (2019). Hydrogen production by PEM water electrolysis – A review. *Materials Science for Energy Technologies, Volume 2, Issue 3, Pages 442-454, ISSN 2589-2991*. https://doi.org/10.1016/j.mset.2019.03.002

Kumar, Y., Ringenberg, J., Depuru, S. S., Devabhaktuni, V. K., Lee, J. W., Nikolaidis, E., … Afjeh, A. (2016). Wind energy: Trends and enabling technologies. Renewable and Sustainable Energy Reviews. https://doi.org/10.1016/j.rser.2015.07.200

Lee, Y. S., González, J. A., Lee, J. H., Kim, Y. Il, Park, K. C., & Han, S. (2016). Structural topology optimization of the transition piece for an offshore wind turbine with jacket foundation. *Renewable Energy*. https://doi.org/10.1016/j.renene.2015.07.052

Lourens, E. (2019a). *Lecture 1: Introduction to offshore engineering* [PowerPoint slides]. Retrieved from TU Delft Offshore Wind Farm Design OE44120 site.

Lourens, E. (2019b). *Lecture 6: Support structure design* [PowerPoint slides]. Retrieved from TU Delft Offshore Wind Farm Design OE44120 site.

Lubetsky, J.S., Steiner, B.A., Faerden, T., Lindstad, T., Olsen, S.E. & Tranell, G. (2006). IPCC Guidelines for National Greenhouse Gas Inventories - Volume 3: Industrial Processes and Product Use – Chapter 4. Retrieved from: https://www.ipcc-nggip.iges.or.jp/public/2006gl/pdf/3_Volume3/V3_4_Ch4_Metal_Industry.pdf

Meteorological Service of New Zealand Ltd (2020). Metoceanview Hindcast. Available at: https://app.metoceanview.com/hindcast/

Natarajan, A., Stolpe, M., & Njomo Wandji, W. (2019). Structural optimization based design of jacket type sub-structures for 10 MW offshore wind turbines. *Ocean Engineering*, *172*(December 2018), 629–640. https://doi.org/10.1016/j.oceaneng.2018.12.023

National Oceanic and Atmospheric Administration (2020). Bathymetry maps. Available at: https://maps.ngdc.noaa.gov/viewers/bathymetry/

NSWPH (2019). The challenge. Retrieved from: https://northseawindpowerhub.eu/wp-content/uploads/2019/07/Concept_Paper_1-TheChallenge.pdf

Pardo, N., Moya, J.A. & Vatopoulos, K. (2015). Prospective Scenario on Energy Efficiency and CO2 Emissions in the EU Iron & Steel Industry (Re-edition). *JRC Scientific and Policy Reports – European Commission*. Retrieved from: https://publications.jrc.ec.europa.eu/repository/bitstream/JRC74811/ld1a25543enn.pdf

Pontow, S., Kaufer, D., Shirzahdeh, R. & Kuhn, M. (2017). Design Solution for a Support Structure Concept for future 20 MW. Deliverable 4.36. [online] DTU Wind, pp.66-93. Available at: http://www.innwind.eu/-/media/Sites/innwind/Publications/Deliverables/INNWIND-Deliverable-D4-36.ashx?la=da&hash=28B5C257A99CDB83C035BD53FD5150007400E69C [Accessed 1 September 2020].

Pérez-Collazo, C., Greaves, D., & Iglesias, G. (2015). A review of combined wave and offshore wind energy. Renewable and Sustainable Energy Reviews, 42, 141–153. DOI: https://doi.org/10.1016/j.rser.2014.09.032

Ritchie, H., Roser, M. (2019). CO_2 and other Greenhouse Gas Emissions. Published online at OurWorldInData.org. Retrieved from: 'https://ourworldindata.org/co2-and-other-greenhouse-gas-emissions' [Online Resource]

Rodrigues, S., Restrepo, C., Kontos, E., Teixeira Pinto, R., & Bauer, P. (2015). Trends of offshore wind projects. Renewable and Sustainable Energy Reviews, Vol. 49, pp. 1114–1135. DOI: https://doi.org/10.1016/j.rser.2015.04.092

Roland Berger GMBH (2020). The future of steelmaking – How the European steel industry can achieve carbon neutrality. Retrieved from: https://www.rolandberger.com/publications/publication_pdf/rroland_berger_future_of_steelmaking.pdf

Sandal, K., Verbart, A. & Stolpe M (2018). Conceptual jacket design by structural optimization. *Wind Energy*. 21:1423–1434. DOI: https://doi.org/10.1002/we.2264

Satyendra (Feb, 2020). Vanadium in steels. [Online source] Available at: https://www.ispatguru.com/vanadium-in-steels/

Schobert, H. & Schobert, N. (2015). Comparative carbon footprints of metallurgical coke and anthracite for blast furnace and electric arc furnace use. Retrieved from: http://www.blaschakcoal.com/wp-content/uploads/Carbon-Footprint-Archival-Report-v-4-September-20151.pdf

Senvion Wind (2016). Power curve & Sound power level – [MM92/2050kW/50Hz]. Retrieved from: http://www.windparkferrum.nl/files/dec2016/Bijlage_2-2_Specificaties_Turbines_5.pdf

Shah Mohammadi, M.R., Richter, C., Pak, D., Rebelo, C. & Feldmann, M. (2018). Steel hybrid onshore wind towers installed with minimal effort: Development of lifting process. Wind Engineering. 42. 335-352. DOI: 10.1177/0309524X18777331

Shammugam, S., Gervais, E., Schlegl, T. & Rathgeber, A. (2019). Raw metal needs and supply risks for the development of wind energy in Germany until 2050. *Journal of Cleaner Production*, *221*, 738–752. https://doi.org/10.1016/j.jclepro.2019.02.223

Sicong, G. (2020). Re-manufacturing for reuse of steel structures. Retrieved from: https://www.theseus.fi/bitstream/handle/10024/348976/Sicong_GE.pdf?sequence=2&isAllowed=y

Sif Group (2017). Offshore foundations for wind turbines and oil & gas platforms. Retrieved from: https://sif-group.com/en/component/rsfiles/download-file/files?path=media-kit%252Fdocumentation%252F2017DEF-corporate-presentatie.pdf&Itemid=544

Smart, G. (2016). Offshore wind cost reduction – Recent and future trends in the UK and Europe. Retrieved from: https://ore.catapult.org.uk/app/uploads/2017/12/SP00007-Offshore-Wind-Cost-Reduction.pdf

Smith, G., Garrett, C. & Gibberd, G. (2015). Logistics and cost reduction of decommissioning offshore wind farms. Retrieved from: https://production.presstogo.com/fileroot7/gallery/DNVGL/files/original/41811dc2ccce40b3adc4d73b475c70f6.pdf

Stavirdou, N., Koltsakis, E., Baniotopoulos, C. (2019). Structural analysis and optimal design of steel lattice wind turbine towers. *Proceedings of the Institution of Civil Engineers – Structures and Buildings*, 172(8), 564-579. DOI: 10.1680/jstbu.18.00074

Stolpe, M., Njomo Wandji, W., Natarajan, A., Shirzadeh, R. & Kuhn, M. (2017). Innovative design of a 10MW steel-type jacket. Deliverable D4.34. [online] DTU Wind. Available at: http://www.innwind.eu/-

/media/Sites/innwind/Publications/Deliverables/230117/DeliverableD434_Innovative-Design-of-a-10MW_steel-jacket_Rev10_FINAL.ashx?la=da&hash=7C8A2092EDA6136855819AE3025CC53D3A65B5F1

Takeda, O. & Okabe, T.H. (2019). Current status of titanium recycling and related technologies. *JOM, 71(6), 2019*. https://doi.org/10.1007/s11837-018-3278-1

Topham, E. & McMillan, D. (2016). Sustainable decommissioning of an offshore wind farm. Renewable Energy, 102(2017), 470-480. https://doi.org/10.1016/j.renene.2016.10.066

Topham, E., McMillan, D., Bradley, S., & Hart, E. (2019). Recycling offshore wind farms at decommissioning stage. Energy Policy, 129(September 2018), 698–709. https://doi.org/10.1016/j.enpol.2019.01.072

Treyer, K. & Bauer, C. (2016). Life cycle inventories of electricity generation and power supply in version 3 of the ecoinvent database—part I: electricity generation. *Int J Life Cycle Assess* 21, 1236–1254. https://doi.org/10.1007/s11367-013-0665-2

Ummels, B. (2019a). *Lecture 7: Electrical Infrastructure* [PowerPoint slides]. Retrieved from TU Delft Offshore Wind Farm Design OE44120 site.

Ummels, B. (2019b). *Lecture 12: Development and planning* [Powerpoint slides]. Retrieved from TU Delft Offshore Wind Farm Design OE44120 site.

U.S. Steel (2019). Sustainability Report 2019. Retrieved from: https://www.ussteel.com/documents/40705/43725/U.+S.+Steel+2019+Sustainability+Report_web.pdf/52f7fb7e-a2aa-c80b-7d72-202afc5ab5ff?t=1603766679756

U.S. Steel (April 21st, 2020). *United States Steel Corporation Announces Goal to Achieve Carbon Neutrality by 2050* [Online article] Businesswire. Accessible at: https://www.businesswire.com/news/home/20210421005580/en/

Van Borstel, T. (2013). INNWIND.EU Design report – Reference jacket. Deliverable D4.3.1. [Online] DTU Wind. Available at: http://www.innwind.eu/-/media/Sites/innwind/Publications/Deliverables/DeliverableD4-31_20131030_INNWIND-EU.ashx?la=da&hash=A29780A9EA7462E24017D68F3BE7E7CE753DAEBB

Van de Brug, E. (2019). *Lecture 13: Offshore wind – lessons learned: or the practical approach* [PowerPoint slides]. Retrieved from TU Delft Offshore Wind Farm Design OE44120 site.

Van der Laan, M., Andersen, S., Ramos García, N., Angelou, N., Pirrung, G., Ott, S., Sjöholm, M., Sørensen, K., Vianna Neto, J., Kelly, M., Mikkelsen, T. and Larsen, G. (2019). Power curve and wake analyses of the Vestas multi-rotor demonstrator. *Wind Energy Science*, 4(2), pp.251-271.Wind Europe (2019). Wind energy is the cheapest source of electricity generation. Retrieved from: https://windeurope.org/policy/topics/economics/

Veum, K., Cameron, L., Hernando, D.H. & Korpas, M. (2011)

Vogl, V., Åhman, M. & Nilsson, L.J. (2018). Assessment of hydrogen direct reduction for fossil-free steelmaking. Retrieved from: https://doi.org/10.1016/j.jclepro.2018.08.279

Vos, P.C. (2015). Origin of the Dutch landscape - Long-term landscape evolution of the Netherlands during the Holocene, described in visualized in national, regional and local palaeogeographical map series. Barkhuis (Groningen): p359.

Wang, X., Zeng, X., Li, J., Yang, X., & Wang, H. (2018). A review on recent advancements of substructures for offshore wind turbines. Energy Conversion and Management, 158 (September 2017), 103–119. https://doi.org/10.1016/j.enconman.2017.12.061

Wind Europe (2019). Offshore wind in Europe - Key trends and statistics 2018. Retrieved from: https://windeurope.org/wp-content/uploads/files/about-wind/statistics/WindEurope-Annual-Offshore-Statistics-2018.pdf

Wind Europe (2020). Offshore wind in Europe – Key trend and statistics 2019. Retrieved from: https://windeurope.org/wp-content/uploads/files/about-wind/statistics/WindEurope-Annual-Offshore-Statistics-2019.pdf

World Steel Association (2016). Raw materials used in iron making. [Online source] Available at: https://www.worldsteel.org/steel-by-topic/raw-materials.html

World Steel Association (2018). Steel Statistical Yearbook 2018. Retrieved from: https://www.worldsteel.org/en/dam/jcr:e5a8eda5-4b46-4892-856b-00908b5ab492/SSY_2018.pdf

World Steel Association (2019). Steel facts - 2018. Retrieved from: https://www.worldsteel.org/en/dam/jcr:ab8be93e-1d2f-4215-9143-4eba6808bf03/20190207_steelFacts.pdf

Yang, Y. (2019). Recycling Engineering Materials - Lecture 8_Metals Recycling I: Steel recycling. Retrieved from: https://brightspace.tudelft.nl/d2l/le/content/194802/viewContent/1360699/View

Zaaijer, M. (2019). *Lecture 2: Wind Turbine Technology* [PowerPoint slides]. Retrieved from TU Delft Offshore Wind Farm Design OE44120 site.

Appendices

List of appendices:

A1 Literature review process
A2 Background information wind industry
A3 Steel composition and element criticality
A4 Steelmaking and the steel recycling process
A5 Technical design and modelling details
A6 GHG emission indicator EU steel production

A1: Literature review process

As primary information source, a literature review is performed to get familiarized with the historical trends and state-of-the-art of offshore wind power technology in academic literature. The primary search engine used is Scopus, but in a later stage Google Scholar was used to find specific follow-up references from in Scopus obtained articles. Besides academic literature, grey literature like annual industry reports and policy documents were consulted. A concise description of the search method is presented in the following paragraph.

First, focus was put on current trends within the offshore industry energy market covered in academic articles. Therefore, keywords used were 'offshore wind', 'energy' and 'trend' but this lead to large amount of articles (>4000) and the search had to be narrowed down. Multiple combinations of keywords and limitations were tried and eventually the number of search results was narrowed down, see Table 10. From these articles, follow-up references were obtained that link to special or annual industry and policy reports. Much used examples of these are the 'World Energy Outlook Special Report' (International Energy Agency, 2019), annual offshore wind trends and statistics in Europe (Wind Europe, 2019; Wind Europe 2020) and 'A clean planet for all' (European Commission, 2018).

Table 10: Overview of keywords and search limitations used to obtain initial scientific articles considering trends in the offshore industry.

Phase 1 (a) Goal: Familiarize with trends in European offshore industry	Keywords and search limitations: ("offshore wind" AND ("turbines" OR "farm" OR "park")) AND "renewable energy" AND TITLE-ABS("trend" OR "evolution") AND (LIMIT-TO(DOCTYPE, "re")) AND (LIMIT-TO(EXACTSRCTITLE, "Renewable And Sustainable Energy Reviews"))		
Title	Author(s)	Year	Journal
Current trend in offshore wind energy sector and material requirements for fatigue resistance improvement in large wind turbine support structures – A review	Igwemezie, V., Mehmanparast, A. and Kolios, A.	2019	Renewable and Sustainable Energy Reviews
Future emerging technologies in the wind power sector: A European perspective	Watson, S., Moro, A. & Reis, V. et al.	2019	Renewable and Sustainable Energy Reviews
Wind energy: Trends and enabling technologies	Kumar, Y., Ringenberg, J. & Depuru, S. et al.	2016	Renewable and Sustainable Energy Reviews
Key challenges and prospects for large wind turbines	McKenna, R., Ostman, P. & Fichtner, W.	2016	Renewable and Sustainable Energy Reviews
Trends of offshore wind projects	Rodrigues, S., Restrepo, C. & Kontos, E. et al.	2015	Renewable and Sustainable Energy Reviews
A review of combined wave and offshore wind energy	Pérez-Collazo, C., Greaves, D., & Iglesias, G.	2015	Renewable and Sustainable Energy Reviews
The evolution of offshore wind power in the united kingdom	Higgins, P. & Foley, A.	2014	Renewable and Sustainable Energy Reviews

It should be noted that the exit of the United Kingdom from the European Union presented some challenges in the comparability of the statements made in consulted reports. Often, references in shown statistics covered 'Europe' or 'the European Union' and it was left to the reader to interpret these terms as EU28 or EU27 based on the date of publication. This, amongst reasons, contributed to the decision to set the geographic boundaries of this thesis to the North Sea region rather than political boundaries within continental Europe.

Academic literature was searched regarding technical components within offshore wind structures, again initially using the Scopus search engine with follow-up through Google Scholar. Many results were shown and a first scan based on title, followed by a second scan based on the articles' summaries, was performed. An overview of this is presented in Table 11. Main typologies were identified and, when necessary, complementary searches were executed to add on the information obtained, to fill in remaining gaps in the authors knowledge or clarify confusing definitions and statements found in literature. Furthermore, detailed support structure designs were studied to get a feel for structure dimensions and orders of magnitude. Much was learned from studying a series of reference design reports created by the Danish Technical University (DTU, 2013) and the technical drawings they included in their works. Also the step-by-step guide to monopile design provided by Arany, Bhattacharya & MacDonald et al (2017) proved very useful. Lastly, study material provided in the lectures of the 'Offshore Wind Farm Design' (OWFD) course is often referred to, as well as to personal communication with the professors presenting this course.

Table 11: Overview of keywords used to obtain initial scientific articles considering support structures for OWTs.

Phase 1 (b) Goal: Familiarize with technical components in European offshore industry		Keywords and search limitations: Monopile OR Jacket AND offshore AND material AND design	
Title	Author(s)	Year	Journal / published in
Structural optimization based design of jacket type sub-structures for 10 MW offshore wind turbines	Natarajan, A., Stolpe, M. & Njomo Wandji, W.	2019	Ocean Engineering
Dynamic design considerations for offshore wind turbine jackets supported on multiple foundations	Jalbi, S., Nikitas, G. & Bhattacharya, S. et al.	2019	Marine Structures
Foundations of offshore wind turbines: A review	Wu, X., Hu, Y.;& Li, Y. et al.	2019	Renewable and Sustainable Energy Reviews
Conceptual jacket design by structural optimization	Sandal, K., Verbart, A. & Stolpe, M.	2018	Wind Energy
A review on recent advancements of substructures for offshore wind turbines	Wang, X., Zeng, X. & Li, J. et al.	2018	Energy Conversion and Management
Design of monopiles for offshore wind turbines in 10 steps	Arany, L., Bhattacharya, S. & MacDonald, J. et al.	2017	Soil Dynamics and Earthquake Engineering

In later stages of the research, focus lies on the impact related to the construction material use of the offshore wind sector in the North Sea with the aim of providing perspective for the interpretation of model results and to express model results in terms of environmental impact, specifically climate change potential. The latter to enhance comparability of the support structure with other OWT components and/or other renewable energy technologies. The primary data source for this section is again literature review and the aim is to find academic literature related to the global warming potential of the types of construction steel used in OWT support structures. The primary search engine used is Scopus and after that, when necessary, followed up with Google Scholar. Keywords like 'material' and 'recovery' where used in combination with 'wind energy' and 'North Sea'. From the articles obtained, references of useful information were analyzed and added to literature overview. Most of the secondary articles that proved useful focus on life-cycle assessment specified to offshore wind parks. An overview of the final configuration of keywords and the obtained articles are shown in Table 12.

Table 12: Overview of keywords used to obtain initial scientific articles considering material use, material recovery and climate change potential for OWT support structures.

Phase 3 Goal: Familiarize with material use and recovery in European offshore industry	Keywords and search limitations: "wind energy" AND material AND (recovery OR recycling) AND "North Sea" AND (LIMIT-TO(SUBJAREA, "ENGI") OR LIMIT-TO(SUBJAREA, "ENER"))		
Title	Author(s)	Year	Journal
A comprehensive review and proposed architecture for offshore power system	Itiki, R.; Di Santo, S.G.; Itiki, C. et al.	2019	International Journal of Electrical Power and Energy Systems
Recycling offshore wind farms at decommissioning stage	Topham, E.; Mcmillan, D.; Bradley, S. et al.	2019	Energy Policy
Raw metal needs and supply risks for the development of wind energy in Germany until 2050	Shammugam, S.; Gervais, E.; Schlegl, T. et al.	2019	Journal of Cleaner Production
Relevant articles obtained from analysing references used in above articles:			
Life cycle assessment of onshore and offshore wind energy-from theory to application	Bonou, A.; Laurent, A.; Olsen, S.I. et al.	2016	Applied Energy
Application of hybrid life cycle approaches to emerging energy technologies - The case of wind power in the UK	Wiedmann, T.O.; Suh, S.; Feng, K. et al.	2011	Environmental Science and Technology
Life cycle assessment of a wind farm and related externalities	Schleisner, L.	2000	Renewable Energy

A2: Background information wind industry

In this addendum, focus lies on obtaining a general impression of the current status of offshore wind energy in the European Union and to provide some context and background information of the social-technical system related to this emerging energy sector. Several key trends are highlighted, like historical and future cumulative installed capacity, financial aspects, relevant companies and institutions.

Historical growth of offshore wind power capacity in the North Sea

While initial development was confined to onshore boundaries, from the 1990's a shift towards offshore electricity production has taken place (Kumar, Ringenberg & Depuru et al., 2016). Rodrigues et al. (2015) mention that since 1991 the offshore wind market has grown substantially, with installed capacity annual growth rates of 52% on average, mostly in what can now be considered small projects consisting of a handful of installed turbines. After initial proof of concept, projects became larger – not only in the number of turbines installed, but also in the size of the turbines – with eight more wind farms installed in 2001. Since 2001, the European offshore installed capacity has increased annually by 36% and the 1 GW installed capacity benchmark was achieved in 2007 followed by the 3 GW benchmark already in 2010 (Rodrigues et al., 2015). In 2017, more than 16 GW is readily installed of which 5.8 GW in the UK alone (Igwemezie et al., 2019). At the end of 2019, 22.1 GW of installed capacity has been realised, spread over 5047 turbines and 12 EU member states (Wind Europe, 2020). Interesting to note is that, so far, 99% of the installed offshore capacity is confined to 5 member states, namely – in order of magnitude – the United Kingdom (45%), Germany (34%), Denmark (8%), Belgium (7%) and the Netherlands (5%).

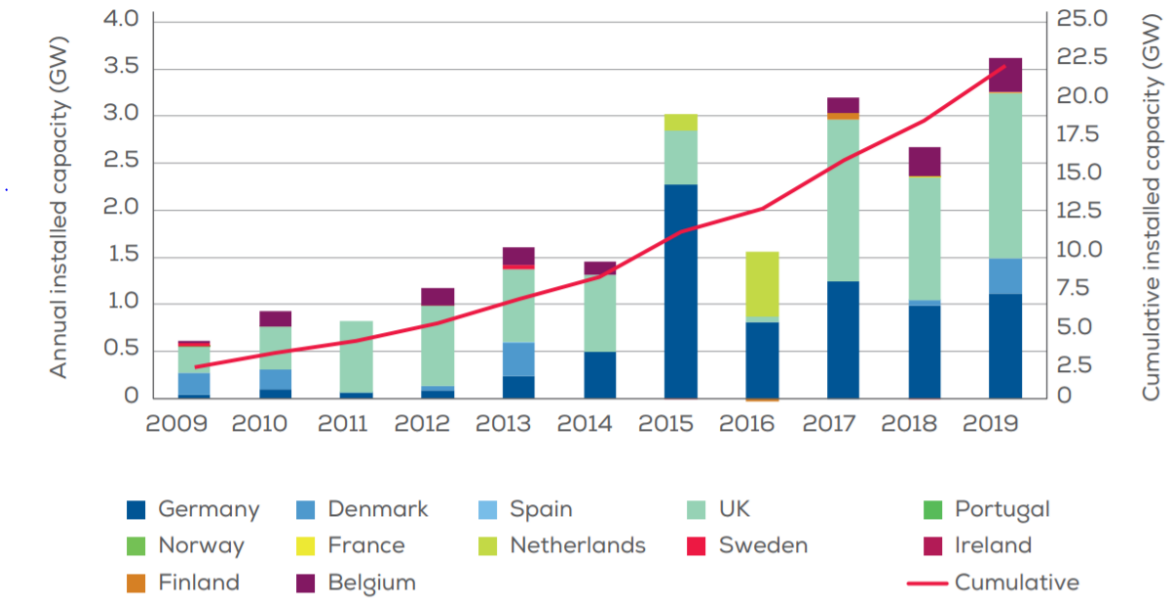

Figure 27: Annual offshore wind installations by country (left axis) and cumulative capacity (right axis) in GW. Image obtained from Wind Europe (2020).

Future outlook for offshore wind power capacity in the North Sea

In 2018, the European Commission presented a report titled 'A clean planet for all' where the commission hints to develop 240-450GW of offshore wind power by 2050 (European Commission, 2018). This range includes all maritime areas, not only the North Sea. Development of offshore wind parks has so far been realised in, amongst others, the North, Baltic and Irish Seas, as these areas

proved suitable and economically feasible to construct wind farms using current technology. However, as technology is constantly advancing – especially keeping in mind that several floating wind turbines have been successfully commissioned vastly increasing potential development area – future development might not be limited to these seas. In 2015, 55% of European offshore wind capacity was confined to the North Sea basin, compared to 25% and 15% for the Baltic and Irish sea respectively (Rodrigues et al., 2015). In 2019, this has changed to 77%, 13% and 10% for the North, Baltic and Irish Seas respectively, indicating an increasing number of installations in the North Sea (Wind Europe, 2020).

In the near future, stated policy targets for the EU member states – United Kingdom included – suggest the aim to increase the total capacity of offshore wind power to 65-85 GW by 2030 and up to 130 GW by 2040, see Figure 28 (International Energy Agency, 2020). An in November by the European Commission released report further elaborates on the potential of offshore renewable energy for a climate neutral future (European Commission, 2020). This is the European Commission's – United Kingdom no longer included – most recent conformation considering the aim to increase offshore cumulative rated capacity to 60 GW by 2030 and 300 GW by 2050. The difference in cumulative installed capacity between the 2018 and 2020 reports is due to the United Kingdom leaving the European Union and not due to a change in future perspective.

Country	Policy	Capacity target	Year set
United Kingdom	UK Offshore Sector Deal	Up to 30 GW by 2030	2019
Germany	The Renewable Energies Act	15-20 GW by 2030	2017
Netherlands	The Offshore Wind Energy Roadmap	11.5 GW by 2030	2017
Denmark	Energy Agreement	5.3 GW by 2030	2019
Poland	Draft National Energy and Climate Plan	Up to 5 GW by 2030	2018
France	Multi-Annual Energy Plan	4.7-5.2 GW by 2028	2019
Belgium	Draft National Energy and Climate Plan	4 GW by 2030	2019
Ireland	Climate Action Plan 2019	3.5 GW by 2030	2019
Italy	Draft National Energy and Climate Plan	0.9 GW by 2030	2018

Figure 28: Stated policy targets for several EU member states and the United Kingdom (International Energy Agency, 2020). These numbers are confirmed in a recent news article by Reuters, published November 6th this year, which was based on an early insight into the NREPs of the EU member states.

Stated policy targets are significantly lower than the scenario presented in the Sustainable Development Scenario (SDS) shown in Figure 29, which is 175 GW installed capacity by 2040, but follow the same order of magnitude. Regardless, these scenarios show that it is likely for offshore wind to heavily expand in the future and that it has an important role in achieving a sustainable energy transition.

The North Sea Wind Power Hub (NSWPH) – a consortium of influential ports and electricity grid managers – assume offshore wind power cumulative capacity to grow to 70-150GW by 2040 and potentially even 180 GW by 2045 (NSWPH, 2019). The consortium indicate interest in creating several hubs, acting as central platforms, that can assist in facilitating the infrastructure required to transfer produced energy – either in the form of electricity or green hydrogen – to shore. This again indicates rapid and substantial growth of offshore wind power in the North Sea region.

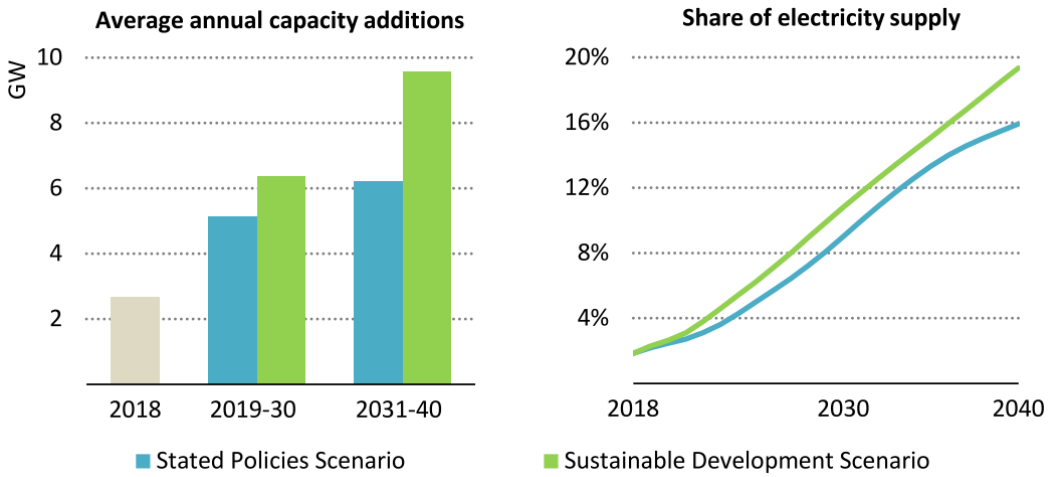

Figure 29: Offshore wind energy capacity additions comparison between European Commission's Sustainable Development Scenario and cumulative policies stated by individual member states for the EU28. Image adapted and retrieved from Wind Europe (2020).

The future can by definition not be predicted, but the fact that multiple influential and powerful institutions, companies and organisation assume this trend to develop does carry weight. For the remainder of this report, the stated policy scenario at 70 GW and 130 GW will be used as an indication of the cumulative installed capacity in the North Sea for 2030 and 2040 respectively. If by 2050 a total installed capacity of 300GW could successfully be commissioned, and one would assume a similar relative distribution of installed capacity for the European seas, a cumulative capacity of 165GW could be allocated to the North Sea basin. This amount is obviously highly speculative, but would be of similar order of magnitude as the NSWPH estimate of maximum 180 GW installed by 2045 and could be used as a ballpark figure, to be used in further analysis.

Financial investments

Regarding overall financial investments up to this point in time, 2016 was the top year. Between 2012 and 2016 financial investments were rising almost exponentially. Then, in 2017, this trend was interrupted. Both total investment and newly financed projects significantly reduced. The year 2018 showed increased financing of new capacity – almost comparable to record year 2016 – and total investments increased. However, 2019 again showed a drop in newly financed offshore wind capacity and total investment decreased towards the level of 2011-2013.

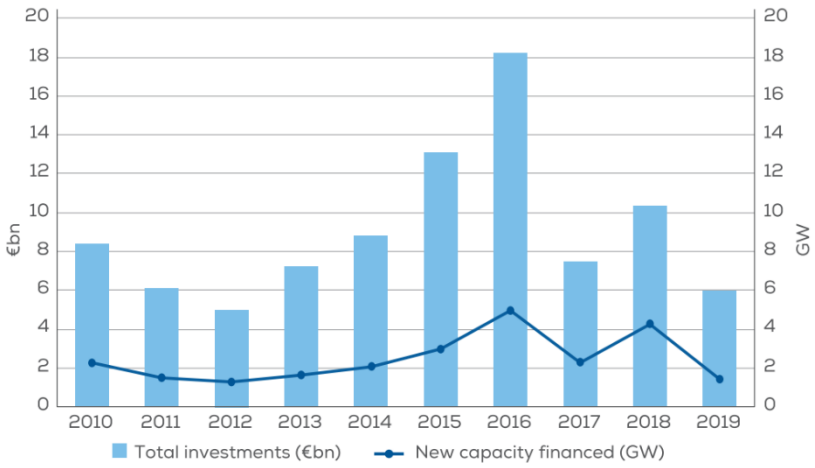

Figure 30: Offshore wind investments and newly financed capacity for EU28. Image obtained from Wind Europe (2020).

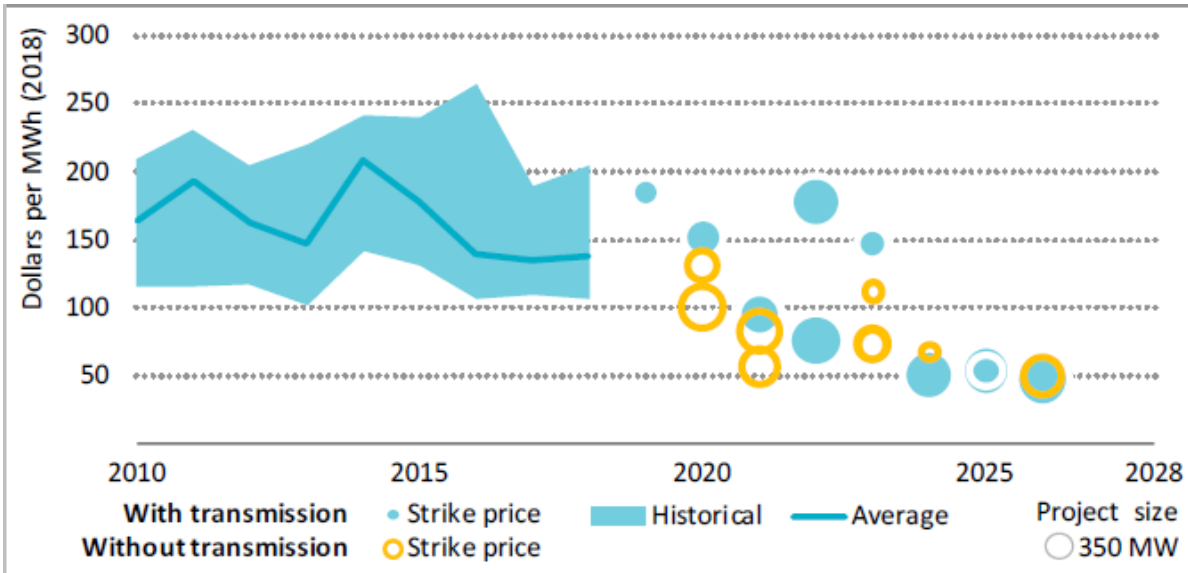

With transmission			Without transmission		
Project	**Strike price ($/MWh)**	**Expected COD**	**Project**	**Strike price ($/MWh)**	**Expected COD**
United Kingdom			**Germany**		
Beatrice	185	2019	Baltic Eagle	74	2023
East Anglia 1	152	2020	Gode wind 3	68	2024
Triton Knoll	95	2021	Gode wind 4	112	2023
Moray East	73	2022	**Netherlands**		
Hornsea 1	178	2022	Borssele I/II	83	2020
Hornsea 2	76	2022	Borssele III/IV	62	2021
Neart na Gaoithe	148	2023	**Denmark**		
Cr. Beck A Dogger Bank	51	2024	Horns Rev 3	118	2020
Cr. Beck B Dogger Bank	54	2025	Kriegers Flak	57	2021
Dogger Bank Teeside A	54	2025	Vesterhav Nord/Syd	73	2023
Seagreen	54	2025	**France**		
Sofia	47	2026	Dunkirk	50	2026

Recent auctions in Europe set the stage for a fall in costs for new projects as the industry moves to deploy higher capacity turbines

Figure 31: Historical LCOE of offshore wind and strike prices in recent auction in Europe. Historical values correspond to LCOEs including transmission. Estimation provided by IEA and based on IRENA (2019). Image adapted from International Energy Association (2020).

Cost competitiveness of wind power

Good indicators of the performance of any energy producing industry are the levelized cost of energy (LCOE) and the strike price. The definition of these to indicators is found as the following: “Strike price is the €/MWh amount paid to an offshore wind generator, usually for a fixed length of time (e.g. 15 years in the UK), for each megawatt hour (MWh) of electricity produced. LCOE is the €/MWh amount the generator must earn for each megawatt hour produced over the full life of the assets, to cover its capital and operating costs and its cost of capital” (Smart, 2016).

So far, the main challenge for the offshore wind industry has been reducing the cost of electricity to make the sector competitive with other energy generating industries. Many factors influence this, not only technological developments but also market developments (monopolies) and the cost of capital. Up to 2010, LCOE prices increased and reached a peak price of 190 €/MWh. This was mostly due to the learning curve that the industry faced. The use of new bigger turbines, exploiting deeper waters, design and installation mistakes and failures all contributed to this fact. In 2011, the Crown Estate – a business created by the UK Act of Parliament – predicted that the LCOE of offshore wind would be reduced to 115 €/MWh by 2020 (Lourens, 2019). In reality this LCOE level was reached much sooner than predicted. This is showcased in Figure 31 by the Borssele 1&2 wind farm setting their LCOE to 87 €/MWh in 2016. The Dutch GROW consortium – a joined research and collaboration program consisting of twenty leading companies and research institutes in offshore wind – dedicated themselves to their motto 'twenty for seven' (Deltares, 2016). Their aim was to reduce the cost of offshore electricity to 7 cents per kWh, or 70 €/MWh, by 2030. Again, this target was met much sooner than predicted and was almost achieved by Borssele 3&4 in 2018. It should be noted that not all wind parks obtain strike prices this low. The fact that the Borssele projects managed to drive down their price this far is considered remarkable and is the result of, amongst other things, favorable interest rates and environmental conditions and good collaboration between public and private parties (Lourens, 2019). What it does show, is the potential for offshore wind to compete well with other energy industries.

In the years to come a decrease in strike prices is expected to continue, leading to 64 €/MWh by 2020 and to drop further to 60 €/MWh by 2025 (Wind Europe, 2019). In a report published by the International Energy Association (IEA, 2020) this estimate is confirmed and shown in Figure 31 on page 71. It can be seen that strike prices continue to go down in the near future.

Actors in the EU's offshore wind market

For the offshore wind industry, the most influential actors can be coarsely divided into turbine, support structure & cable manufacturers, installation & shipping companies, owners & investors and commissioners & policy makers. For each actor category, recent influential actors are depicted in Table 13 on page 73. Interesting to note is that the two largest turbine manufacturers – Siemens Gamesa Renewable Energy and MHI Vestas Offshore Wind – dominate the European market with a combined share 92% total installed capacity (Wind Europe, 2019). For support structures, Sif Group and EEW are the largest monopile manufacturers. Lamprell and Navantia-Windar Consortium were the only two manufacturers delivering jacket structures in 2019. In 2019, Ørsted (16%) and RWE (12%) own the largest shares of EU's cumulative installed wind power capacity. Ørsted (17%) and Global Infrastructure Partners (17%) own the most relative shares of in 2019 added installations. Most relevant policy makers are the EU's individual member states bordering the North Sea and Baltic Sea.

Another set of actors – one frequently consulted regarding trends and data in this thesis, but not displayed in Table 13 – are overarching organisations like Wind Europe and the International Energy Agency. Even though the author is convinced these organisations depict figures and facts fairly and to their best ability, they might have incentive to present their representative industry in an overall positive manor. Despite this remark, the information presented by Wind Europe and the International Energy agency has proven very useful and insightful during the creation of this research.

Table 13: Overview of relevant actors per category.

Turbine manufacturers[a]	Support structure manufacturers[b]	Inter-array & export cable manufacturers	Marine vessel providers[c]	Owners & investors[d]	Commisioners & Policy makers[e]
Siemens Gamesa	Sif Group (MP)	JDR Cable Systems (IA &E)	A2Sea (T)	Ørsted	European Commission
MHI Vestas	EEW (MP & J)	NSW Technology (IA)	Boskalis Subsea (IA)	E. ON	Belgium
Senvion	Lamprell (J)	Prysmian Powerlink (IA & E)	DeepOcean (E)	RWE	Denmark
GE Renewable energy	Navantia-Windar (J)	NKT Group (E)	Fred Olsen Windcarrier (T)	Vattenfall	Germany
		Nexans (IA & E)	Geosea (M)	Macquarie Capital	Netherlands
		Ls Cable & System (E)	Jan de Nul (T & M)	Global Infrastructure Partners	United Kingdom
			Seajacks (M)	Northland Power	
			Seaway 7 (IA)	Innogy	
			Swire Blue Ocean (T)	SSE	
			Tideway (E)	Stadwerke München	
			Van Oord (T, MP, IA & E)	Iberdrola	
			Volstad Maritime AS (F)	Siemens	
				Equinor	

a) Manufacturs that supplied >10 turbines for EU parks in both 2018 and 2019; b) Manufacturers that supplied >10 structures for EU wind parks in both 2018 and 2019; c) Vessel providers for construction of turbines, foundations and cables in 2019, excluding other support services; d) Owners & investors owning >3% EU cumulative capacity in either 2018 or 2019; e) Countries supporting >1% cumulative installed capacity. Sources: this overview is based on Wind Europe (2018, 2019). Abbreviations: E = export cable, F = floating, IA = inter-array cable, J = jackets, MP = monopile, T = turbine

A3: Steel composition and elemental criticality

Steel is an alloy of iron and one or more alloying substances. Alloy management of the steel composition takes place in the secondary steel production process. There are two main groups in steel alloys, namely carbon steel and stainless steel, of which carbon steel is commonly used for, amongst other things, construction purposes. Carbon steel is characterized by being almost pure iron, having a carbon content of 0.1-2% and a few percent of other metallic elements like chromium, niobium, vanadium, manganese and cobalt depending on the steel characteristics required (Yang, 2019). There are over 5000 carbon steel alloys in use, which are mostly combinations of previously mentioned alloying elements and the bulk metal iron.

When it comes to additives in steel alloys, very small quantities of elements can significantly change the material's properties. Material properties important for steel in general – and inherently for offshore use – are yield strength, toughness, ductility, weldability and durability. All of these characteristics in turn influence the financial cost of the steel. Favourable characteristics for steel in offshore use are increased toughness to avoid brittle behaviour, increased ductility to avoid fatigue cracking and good weldability to ease manufacturing (Igwemezie et al., 2019).

Table 14: Overview of material composition in percentages of weight for commonly applied steel in offshore applications. In green: alloying elements enhancing wishful material properties. In dark red: tramp elements enhancing unwanted material properties that cannot be removed from the steel mix. In light red: alloying/tramp elements enhancing either wanted or unwanted material properties depending on required steel characteristics. These elements can be regulated. In blue: dissolved elements related to organic compounds that can be regulated but become harmful at high concentrations.

Material composition in wt% of S355G10+M construction steel for offshore application														
Fe	C	Mn	Si	V	Al	Nb	Ti	Cu	Sn	Cr	Ni	Mo	P	S
97.5	0.06	1.57	0.27	0.001	0.15	0.022	0.003	0.24	0.33	0.006	0.33	0.006	0.013	0.001

For offshore wind, type S355G8+M, S355G10+M, S420G2+M and S460G2+M construction steels are typically applied (Igwemezie et al., 2019). These steel grades have been specifically created to avoid brittle behaviour in offshore use and applied in – amongst other components – pipelines, platforms and OWT structures. For OWT support structures, S355 steel grades are most common, as the cost increases unfavourably for higher steel strengths compared to the material saving they provide (Arany et al., 2017). However, higher grades of steel can offer better structural performance – like strength and buckling resistance – and so lead to lighter structures (Watson et al., 2017). Similarly, Shammugam et al. (2019) mention that higher steel grades in the upper sections of jackets and other lattice type structures can save up to 30% steel for specific components. An overview of the material composition of S355G10+M is obtained from Igwemezie et al. (2019) and is shown in Table 14.

It can be seen that elemental iron forms the bulk of the steel, making up for 97% of the specific weight. Several of the elements shown in Table 14 are purposefully added and called alloying elements, these are shown in green. Alloying elements mainly enhance favourable material characteristics, but in turn can negatively influence other characteristics. For example, elements like manganese, niobium and vanadium are added to increase steel strength, but in turn negatively affect ductility, toughness and weldability. Silicon metal is added to increase strength and hardness. Nickel can be added to increase toughness, but too much makes the steel brittle. Other elements, like copper, tin and phosphorus are not advantageous to have in the steel composition and are called tramp elements. These need be minimized as much as economically possible as they have severe negative influence on steel characteristics. For copper and tin, regulation of the allowable quantities is very important, as these elements cannot be cost effectively removed from the steel mix. Consequentially, any copper or tin that ends up in a steel mix can only be diluted by adding very pure iron but never removed (Yang,

2019). Some elements, like chromium, nickel and molybdenum can either positively or negatively influence material characteristics, depending on application needs, these are shown in light red in Table 14.

It should be mentioned that besides the material composition, other manufacturing properties like rolling technique also influence steel characteristics. A very influential effect on final steel properties is the formation and size of steel grains in the cooling process of hot rolled steel alloys. The steel types suggested for offshore use are all thermo-mechanically rolled, which can be seen by the +M attribute in the steel grade notation. Alloying elements, like niobium, titanium and vanadium are added to improve thermo-mechanically rolling properties. Specific effects of these materials are discussed in following paragraphs.

Critical elements and materials

The increase in steel requirements for larger OWT support structures in combination with reducing retrievable mass quantities the high number of alloying elements present in the steel composition raises questions about the availability of required elements. The European Union has released several lists of critical raw materials (CRMs), the latest of which was released this year in a report regarding European supply resilience, see Table 15 (European Commission, 2020c). In the report, criticality is defined as those raw materials that are most important economically and have a high supply risk. Comparing with Table 14, it can be seen that – although in relatively small quantities – four elements present in steel for offshore application are on the CRMs list. Of these, silicon metal (Si) has the highest concentration in the steel composition at 0.27 wt%. The criticality of the CRMs becomes clear when assessing their production location and associated EU import reliance, see Table 16. Of the four CRMs, only silicon metal is partly produced within the EU but internal production does not cover consumption so inherently supply relies for 63% on imports.

Table 15: Overview of critical raw materials for the EU in 2020. In red: elements present in the steel composition for offshore application. In blue: raw material required in the blast furnace production process for primary steel making. This list is obtained from the European Commission (2020c).

Critical Raw Materials list for the EU in 2020		
Antimony	Hafnium	Phosphorus
Baryte	Heavy REEs	Scandium
Beryllium	Light REEs	Silicon metal
Bismuth	Indium	Tantalum
Borate	Magnesium	Tungsten
Cobalt	Natural Graphite	Vanadium
Coking Coal	Natural Rubber	Bauxite
Fluorspar	Niobium	Lithium
Gallium	PGMs	Titanium
Germanium	Phosphate rock	Strontium

Niobium is associated with the highest criticality within the EU, combining the highest supply risk and economical dependency of the four CRMs (European Commission, 2020c). The majority of niobium – 75% of global consumption – is applied in steel alloys. Besides steel, niobium is used for high-tech applications like the electronics, aerospace, automotive and defence industry and in health care. Niobium is added to low-carbon steel alloys to increase yield strength and toughness as it positively affects the grain size and formation in the cooling of hot rolled steel. However, much niobium is lost through dilution of high strength steel scrap with lower quality steel scrap or trapped steel slags in primary production (Globe Metal, 2020). Currently, no niobium recycling systems are in place, which results in a recycling input rate of 0%.

Table 16: Production source and import reliance for the four CRMs present in S355G10+M steel for offshore structures. Numbers shown are obtained from European Commission (2020c) and adjust for readability. No source country information was available due to lack of trade data for titanium and vanadium, therefore the main global producers are shown. Hence, for vanadium no import reliance could be determined. However, no vanadium is produced in the EU, therefore it can be assumed that the import reliance is 100%.

CRM	Source country for EU production	Import reliance	Recycling input rate
Niobium	Brazil (85%) Canada (13%)	100%	0%
Silicon metal	Norway (30%) France (20%) China (11%) Germany (6%) Spain (6%)	63%	0%
	Main global producer		
Titanium	China (45%) Russia (22%) Japan (22%)	100%	19%
Vanadium	China (55%) South Africa (22%) Russia (19%)	n.a. *(100%)* *84%*	2% 44%

Silicon metal criticality is relatively low for a CRM, as it is associated with minor supply risks due to the fact that is produced in the EU. However, European production does not fulfil consumption and in combination with its economic importance the element is considered critical (European Commission, 2020c). Silicon metal is present in all steel types as it increases hardness and strength and functions as a deoxidiser in the primary steel making process (American Welding Society, 2009). Its main drawback is the effect it has on welding performance, as silicon concentrations >0.3% negatively affect the steel's surface layer and can lead to cracking. Best welding capabilities are achieved with silicon concentrations at approximately 0.1%. The silicon concentration in S355G10+M steel is close to the maximum of 0.3%, see Table 14. Silicon concentrations in other steel applications can be found up to 1%. In order to keep the silicon concentration below its maximum, it should be considered not to mix steel scrap from OWT structures with steel scrap from other applications. Silicon metal dissolves in iron and cannot be effectively removed from a solution. Reducing silicon metal concentrations in a steel composition is only economically achieved by dilution with high purity iron (Yang, 2019).

The addition of titanium to steel has significant influence on the hardness and toughness of steel alloys. Its main advantage comes from its limiting effect on the grain size in the cooling of the thermo-mechanically rolled steel (El-Faramawy, Ghali & Eissa, 2012). Titanium is added to the CRM list since 2020, where in 2017 the material was not considered critical. Weather this is due to increased consumption or supply instability is not mentioned in the European Commission (2020c) report. Titanium is used as an light-weight steel replacement in the aerospace and automotive industries, but characterised by very low material efficiency, which can be as low as 20% (Takeda & Okabe, 2019). Recycling systems for titanium are most developed considering the alloying elements under assessment. However, recycled titanium mainly originates from titanium new scrap from the aerospace industry and no examples were found where titanium is recovered from steel alloys or old scrap. Recycling input rates in titanium making are 19% on average, see Table 14.

Vanadium is used in higher strength steel grades, as it increases hardenability – and therefore positively influences tensile and yield strength – of thermo-mechanically rolled steels very effectively (American Welding Society, 2009). This effect is so strong that for vanadium concentrations >0.05%

the hardenability effects become disadvantageous and a steel alloy can become brittle. Roughly 85% of globally produced vanadium is used in the steel industry which makes its economical importance relatively high (Satyendra, 2020). Furthermore, it is not produced in the EU and – even though import reliance could not be calculated through a lack of data – consumption is assumed to be fully reliant on imports (European Commission, 2020c). Vanadium has been on and off CRM lists between 2011 and 2020, being on the list in 2011 and 2014, off the list in 2017 and then added again to the CRM list published in 2020. Vanadium can be recovered from molten steel, even though its concentrations are very low. Recovered vanadium can be recycled by recovering and adding it to varying steel alloys. This is limitedly applied, which can be seen in Table 14 as the recycling input rate for Vanadium is only 2% (European Commission, 2020c). Interestingly, an earlier report by the EC shows EOL-RiR at 44% contribution of vanadium recycling to meet EU demand of CRMs (European Commission, 2017). Given that the former mentioned source is of later publishing date, this source is assumed to be correct.

From the above, it can be concluded that four critical materials – niobium, silicon metal, titanium and vanadium – are present in the offshore structure steel, albeit in low relative quantities. Each metal is added to the steel alloy for specific reasons, with the effect of enhancing tensile and yield strength, toughness, ductility and weldability properties. Niobium is lost in steel recycling through dilution with lower grade steel scraps and in the formation of slags. Oppositely, silicon cannot be effectively removed from a steel alloy through which accumulation could take place. This can be harmful, as silicon concentrations >0.3% can lead to crack formation during welding. Titanium is only recently added to the CRM list and recycling systems for new scrap are available but these mainly focus on the recycling of new scrap. Vanadium is only used in higher steel grades and very effective in very small quantities. In contrast to the other CRMs, vanadium can be recovered from steel alloys so that its concentration can be regulated. All CRMs are very much reliant on imports.

Based on the very specific and large effects of the CRMs even in low quantities, low replaceability, low recycling input rates and large homogenous steel volumes in use for OWT structures, a recycling system specifically for OWT structure steel could be considered. Generally steel is well recyclable, as it is characterised by a recycling efficiency of >95% in EAFs (Yang, 2019). In BF-BOF processes, impurities are removed from the molten iron through oxidation and slag forming, which can trap some amount of the Iron resulting in losses. For BFs, Iron content in the slag is quite low at approximately 0.5 wt%, but for every ton of molten iron produced 200-300 kg of slag is created. Combined, this leads to an Iron passing efficiency of >99%. Converter slag contains a much higher Iron content, at 16-18 wt% with 100-150 kg of slag produced per ton steel. The BF-BOF combined iron passing efficiency is similar to that of EAFs, at >95%.

These high recycling efficiencies hold true for the bulk Iron fraction in the steel composition, but not for the specific alloying metals required for the steel to be of sufficient grade for offshore use. The purpose of such a system would be to retain CRMs in the steel alloy as much as possible through remelting using electric arc furnaces. When OWT support structure steel scrap is recycled in blast furnaces or converters it is likely that the many CRMs are lost. Quick assessment of an Ellingham diagram suggests that elemental Ti, Nb, Zn, Al, Cr, Si, Mn, P and S will be lost due to oxidation and removed from the steel melt through slag formation. Other elements like Cu, Ni and Sn do not oxidise and remain in the steel melt, potentially adding to the accumulation of tramp elements. Dilution with other metal grades and the loss of niobium in slags would require relying on continuous imports to sustain European high grade steel production for OWT support structures. No comment regarding financial feasibility of such a system can yet be made. Further insight would be required into minimal throughput and the effect of transportation distances on recycling cost compared to the cost of

conventional recycling practices. Considering CRMs, three end-of-life recycling scenarios can be considered, in increasing order of CRM retainment:

- No physical separation of coating, paints and marine growth. Structures are recycled, but scrap quality is low. It needs to be recycled in traditional BF-BOF processes to remove impurities. Alloying elements are lost in BF and/or BOF slag or off-gasses.
- Physical separation of coating, paints and marine growth. Structures are recycled and homogeneous high quality scrap is obtained. This is then recycled by traditional EAF recycling processes.
- Physical separation of coating, paints and marine growth. Structures are recycled and homogeneous high quality scrap is recycled in a separate EAF recycling process.

A4: Steelmaking and the steel recycling process

In steel production there are two main processes. The first process is called the primary steel production process and takes place in blast and basic oxygen furnaces (BF-BOFs) or in electric arc furnaces (EAFs). In the former, iron ore is converted to pig iron in a blast furnace. Here, high temperatures are required to oxidize the iron ore, oxidize harmful impurities – like sulphur and phosphorus – from the iron melt and to reduce the carbon content to roughly 4% (Yang, 2019). This part of the steel making process is very energy intensive and mainly uses cokes obtained from coal as energy source. Next, pig iron and steel scrap are mixed and treated in a basic oxygen furnace – or converter, see Figure 32 – to further reduce the carbon content to 0.1-2.0% and remove remaining impurities from the ore or added steal scrap. In the converter steel scrap is added as a coolant, as the exothermic reactions taking place in the steel converter release more heat than is necessary in this step. The added scrap content in primary BF-BOF production processes is commonly 20-30% (Björkman & Sandelsson, 2014).The EAF process uses only steel scrap as feed for an electric arc furnace. The steel is heated to above melting point using electricity, allowing mixing a limited amount of impurities to be removed. Steel recycling is integrated in the primary production of steel making.

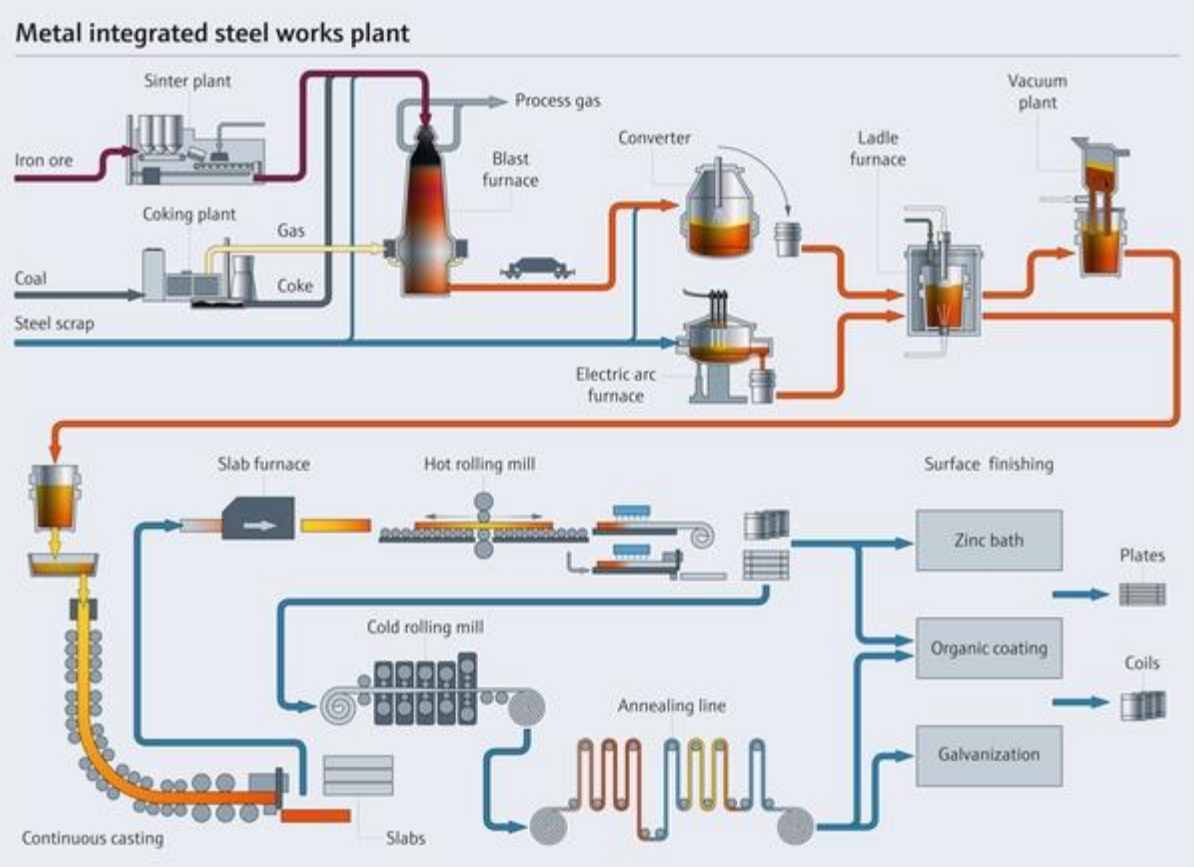

Figure 32: Process overview of primary and secondary steel production processes. This image is retrieved from: https://www.endress.com/en/industry-expertise/mining-minerals-metals/Cost-efficient-steel-production

Secondary steel making takes place in a ladle furnace. Here, molten steel from either the blast furnace route and/or electric arc furnace route is refined to its final composition. The final steel composition depends on the steel characteristics required for the final product and can be influenced by adding alloying elements. Next, the steel is casted into slabs, which are then further processed using cold or hot milling techniques to obtain plates, sheets or coils. As a final step, the steel surface is commonly coated in either zinc, nickel or chromium to decrease weathering of the embedded iron. An overview of process steps in steel making is shown in Figure 32.

Considering production capacity, the EU is the second largest steel producer in the world at roughly 10% of global production in 2018. Globally, steel is the most produced metal with an annual production of 1808 million (10^6) ton in 2018 (World Steel Association, 2019). European production in the same year was 168 million ton. European steel production is characterised by the high use of electric arc furnaces in primary steel production at 40% of total production, compared to 25% globally. An advantage of this production method is that it consumes electricity instead of cokes as its energy source. A disadvantage is that it solely uses steel scrap as feedstock, as it is not possible to convert iron ore into pig iron using electric arc furnaces (Yang, 2019). Within the EU28, the largest steel producers are Germany (25%), Italy (15%), France (9%), Spain (9%) and Poland (6&), based on 2018 production data (EuroFer, 2019).

A5: Technical design and modelling details

A final substructure design is the product of many design iterations. In each step, more information is considered in the design, decreasing uncertainty and adding to the level of detail and complexity. Environmental conditions, like wind regime, water depth, waves, currents, tides and especially the soil composition play a major role the design of OWTs. Hence, in practice for each wind turbine a specific design is made. For the purpose of this research, this is not feasible due to the amount of work, time and expertise required. To reduce the number of computations, environmental conditions near available development zones are characterised.

In this appendix, the development of a mass estimation tool is elaborated. The tool aims to estimate the steel demand for offshore wind turbine monopile and jacket support structures using change in water depth and turbine rated power as the main research parameters. A classification of the North Sea is made based on available development zones and environmental conditions. The sub-question related to this and the following three sections is as follows:

SQ3: How does the material demand for main support structure technologies change with increasing water depth and rated power?

OWT development zones

As can be seen in Figure 4 and 13, areas available for future wind turbine development are numerous in the North Sea basin. The North Sea can be coarsely divided into three regions, namely the Southern Bight, the Central North Sea and the Northern North Sea. The development areas available in each of these regions are separately assessed, in order to distinguish varying environmental conditions that are characteristic for each region. That varying conditions apply for these regions will become clear in the following paragraphs. Main variations can be seen in water depth and wave climate.

Classification of regions

The first region is selected as the development zones in the Southern Bight, being the bottom four regions between the coasts of France, Belgium, the Netherlands and the UK plus the Dogger Bank, see Figure 13. The second region is selected as the five development zones West of the Danish and South of the Norwegian coasts. The third region is selected as the development areas along the northern coast of the UK.

Water depth

An important parameter in the support structure design is the water depth at which a turbine is aimed to be build. It influences construction material requirements, suitability of support structure typology and cost of the support structure. In this research, water depth is a leading research parameter and is used to determine the interface height. Bathymetry is the visualisation of water depth for a given region. The bathymetry for the North Sea basin is shown in combination with available development zones in Figure 13 and a more detailed version of currently known development areas can be found in Figure 4.

For Region 1, water depths vary between 20 and 50 meter. For Region 2, water depths vary between 20 and 80 meter. For Region 3, water depth varies between 50 and 200 meter. However, bottom fixed designs are currently considered up to 80 meter depth, after which floating design are considered to become more economical (Wang et al., 2018; Perez-Collazo, 2018). Taking potential technological advancements into account, the water depth for bottom-fixed structures will be assessed up to 100 meter if water depths >80 meter are present in a region.

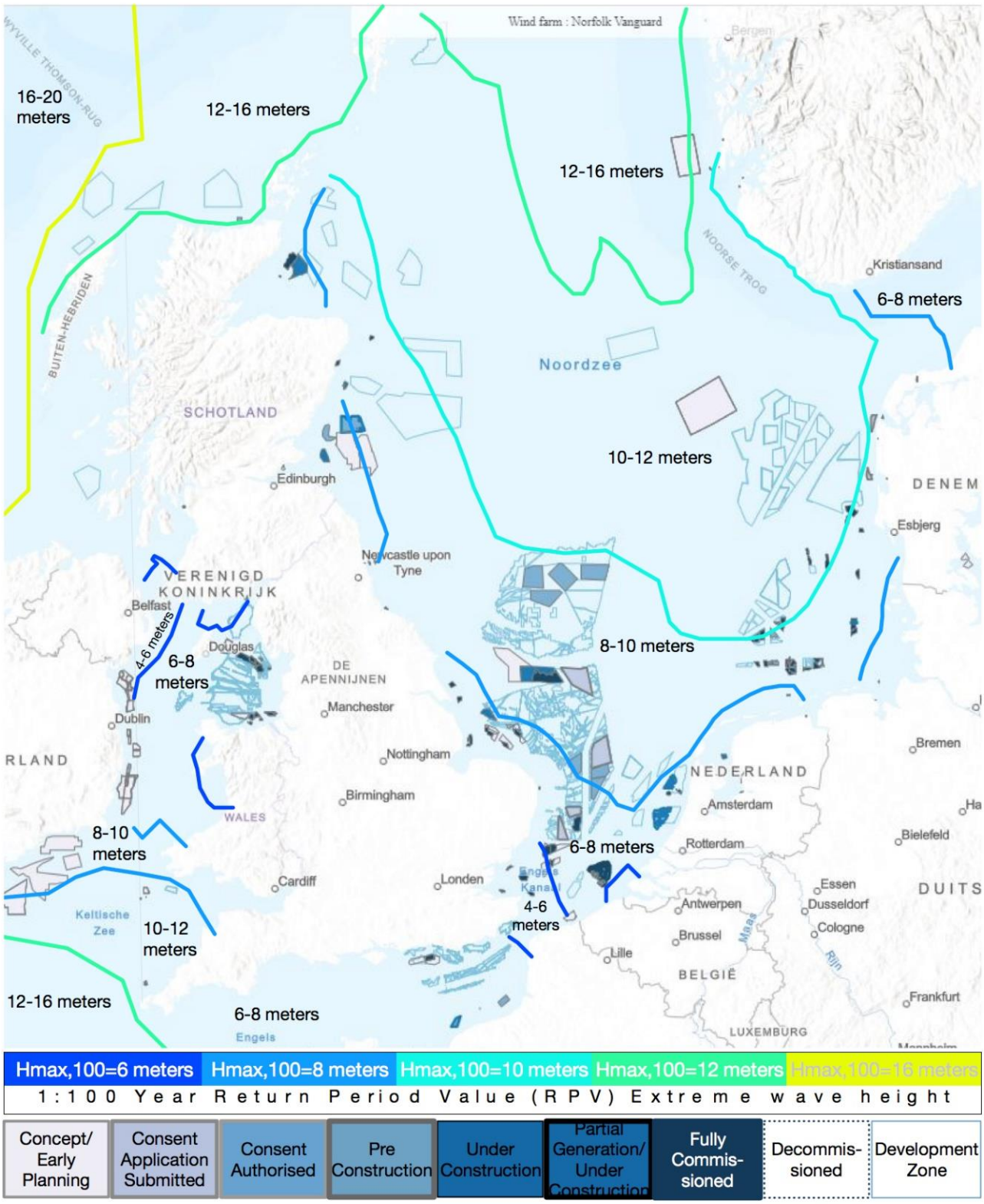

Figure 33: Extreme wave height on detailed OWT development zones. Development zone base map is obtained from the 4Coffshore website, available at: https://www.4coffshore.com/offshorewind/. 1:100 RPV extreme wave height are obtained from the Meteorological Service of New Zealand ocean viewer and shown as contours (MetOceanView, available at: https://app.metoceanview.com/hindcast/). Number indications shown black text indicate the extreme wave height in between contours.

Extreme and significant wave height

The significant and extreme wave height are sea state parameters used to describe waves that could occur given specific return period, often set to 10, 50 or 100 years. The return period does not indicate that a wave will not be encountered again after a single occurrence in that time, but is used a statistic indicator. For example, the one year significant wave height is defined as that significant wave height one would encounter ten times in a reference period of ten years, regardless of the time in between encounters. Similarly, the 100 year significant wave height would only be encountered 0.1 time in a reference period of ten years (Holthuijsen, 2009).

Wave height is important in the design process as it determines the water level to which waves affects a support structure. Wave height is, to a degree, correlated with water depth hence the terms 'shallow water' and 'deep water' are introduced. Deep water is where waves do not interact with the sea floor and the full cyclic movement of water particles is allowed. In shallow water, the water depth is not sufficient to allow full cyclic movement, which results in waves to get more steep and to eventually break and dissipate their embedded energy (Holthuijsen, 2009). The significant wave height is defined as the average wave height of the 1/3 largest waves in a data set and is a common parameter for offshore design. The extreme wave height shows the largest waves expected to occur given a reference period. In practice, significant and extreme wave height are found through long time series of measurements, but this falls out of scope for this research (DNVGL-ST-0437, 2016). Instead, the latter of the mathematical relations between the significant and extreme wave height suggested by Arany et al. (2017) is used and as follows:

$$H_{max} = H_s * \sqrt{0.5 * \ln(N)} \approx 1.87 * H_s$$

, where H_{max} is the extreme wave height, H_s is the significant wave height and N is the number of waves measured in a three hour wave record. Hmax are taken as the 1:100 year RPV extreme wave heights obtained from the Meteorological Service of New Zealand which are – combined with available development zones – shown in Figure 4. In practice, the use of 1:50 year RPV extreme wave heights is more common, but were unavailable. Hence, the slightly more conservative 1:100 year RPV values are used.

The wave period associated with extreme wave heights is found through the following formula:

$$11.1 * \sqrt{\frac{H_{max}}{g}} \leq T \leq 14.3 \sqrt{\frac{H_{max}}{g}}$$

, where g is the gravitational constant at 9.81 m/s^2 and T is the wave period in seconds. From Arany et al. (2017, pg26) it is concluded that "the most severe wave loads are produced by the lowest wave period, and the dynamic amplification is also highest since the frequency is closest to the natural frequency of the structure". Therefore, the peak wave period ($T_{max,\ peak}$) and peak wave frequency ($f_{max,\ peak}$) for extreme waves are taken taken as:

$$T_{max,\ peak} = 11.1 * \sqrt{\frac{H_{max}}{g}}, \qquad f_{max,\ peak} = \frac{1}{T_{max,\ peak}}$$

The same formulas are applied for the calculation of the significant wave period (Ts) and frequency ($f_{s,\ peak}$), where H_{max} is replaced with H_s and $T_{max,\ peak}$ with $T_{s,\ peak}$. The peak wave frequencies are required as inputs for the JONSWAP spectrum, which is elaborated in a later paragraph within this appendix.

Extreme and significant wave height per region

To limit the overall number of computations, the extreme wave height is specified for water depths of 20-40 meter, 50-70 meter and 80-100 meter areas. For Region 1, the extreme wave height varies between 6 meter in the English Channel and 10 meter in the northern Dogger Bank area. Extreme wave height for 20-40 meter water depth in the total region is set to 9 meter, representing more shallow areas in the English Channel. Extreme wave height at water depth of 50-70 meter is set to 10 meter representing the northern Dogger Bank area. For Region 2, extreme wave height varies between 8 meter near the Danish coast and 12 meter south of the Norwegian coast. Extreme wave height for water depths of 20-40 meter is set to 10 meter, to represent conditions near the Danish coast. For 50-70 meter depth areas the extreme wave height is set to 11 meter. For areas at 80-100 meter depth, extreme wave height is taken as 12 meter. For Region 3, extreme wave height varies between 8-11 meter east of the UK and 12-16 meter in the north-west. The range of the extreme wave height values for this region is substantial and in ideal conditions the region would be specified further to minimize the difference, but due to available time this is considered out of scope. No areas are present at 20-40 meter depth. For areas of 50-70 meter depth an extreme wave height of 13 meter is taken, for 80-100 meter depth this is set to 16 meter. An overview of the extreme and significant wave heights and their associated peak wave periods can be found in Table 17 and Table 18.

Table 17: Extreme wave height in meter and associated peak wave period in seconds for the three assessed regions in the North Sea. Associated peak frequency [-] are shown between brackets.

	Region 1		Region 2		Region 3	
Water depth [m]	H_{max} [m]	$T_{max,peak}$ [s]	H_{max} [m]	$T_{max,peak}$ [s]	H_{max} [m]	$T_{max,peak}$ [s]
20 30 40	9.0	10.6 (0.094)	10.0	11.2 (0.089)	*n.a.*	*n.a.*
50 60 70	10.0	11.2 (0.089)	11.0	11.8 (0.085)	13.0	12.8 (0.078)
80 90 100	*n.a.*	*n.a.*	12.0	12.3 (0.081)	16.0	14.2 (0.070)

Table 18: Significant wave height in meter and associated peak wave period in seconds for the three assessed regions in the North Sea. Associated peak frequencies [-] are shown between brackets.

	Region 1		Region 2		Region 3	
Water depth [m]	H_s [m]	$T_{s,peak}$ [s]	H_s [m]	$T_{s,peak}$ [s]	H_s [m]	$T_{s,peak}$ [s]
20 30 40	4.8	7.8 (0.128)	5.4	8.2 (0.122)	*n.a.*	*n.a.*
50 60 70	5.4	8.2 (0.122)	5.9	8.6 (0.116)	7.0	9.4 (0.106)
80 90 100	*n.a.*	*n.a.*	6.5	9.0 (0.111)	8.6	10.4 (0.096)

As a validation to the wave heights and periods literature was assessed. A study regarding potential wave energy exploitation in the North Sea was conducted by Beels et al. (2007). In this study, characteristic sea states were formulated for 34 locations in the North Sea basin, using various measurement stations and time series ranging from 1979 to 2005. In their paper, characteristic sea states were formulated for Belgium, the Netherlands, Germany, Denmark, Norway and the United Kingdom. Significant wave height data and energy period data were collected for varying sea states and show significant variation for the various countries. The Belgium, Dutch, Danish and German continental shelfs show significant wave heights in the order of magnitude of one to five meters for water depths up to 40 meter, whereas the significant wave height in Norway reaches up to almost 10 meter. The wave period associated with these wave climates range between four and ten seconds and fall in a frequency range of 0.07 to 0.17 Hz. The wave heights and periods indicated by Beels et al. (2007) compare well with values chosen for Region 1,2 and 3.

Wave frequency domain and the JONSWAP spectrum

Sea states are hard to model, but several modelling attempts have been made and are currently used in practice. Two examples of these models are the Pierson-Moskovitz and JONSWAP models (Holthuijsen, 2009). These models aim to describe a sea state, in particular the spectral occurring wave height and frequency, for a given wind speed and fetch. The Pierson-Moskovitz spectrum was created to give insight into sea states and is useful for offshore design by being able to determine spectral density, and with that wave height and frequency, for a fully developed sea. However, wind turbines are often built in areas characterized by young sea states, e.g. where the sea has not fully developed. The JONSWAP spectrum provides insight into younger sea states, which better describes North Sea wave conditions, and will be used to determine the frequency domain required for alter design steps. The JONSWAP spectrum shows the spectral energy per wave frequency of a given sea state. Fetch is the length of open water where wind can interact with the water surface, leading to the formation of waves (Holthuijsen, 2009).

The JONSWAP spectral energy density is described by the following formula:

$$S(f) = \frac{\alpha * g^2}{16 * \pi^4} * f^{-5} * \exp\left[-\frac{5}{4} * \left(\frac{f}{f_{peak}}\right)^{-4}\right] * \gamma^b, \qquad with:$$

$$b = exp\left[-\frac{1}{2 * \sigma^2}\left(\frac{f}{f_{peak}} - 1\right)^2\right], \quad \sigma = \begin{cases} \sigma_1 \, for \, f \leq f_{peak} \\ \sigma_2 \, for \, f > f_{peak} \end{cases}$$

, where S(f) is the spectral density in [m^2/Hz], α is a dimensionless energy scale, g is the gravitational constant, f_{peak} is the peak wave frequency, γ is a dimensionless peak enhancement factor that distinguishes the JONSWAP spectral curve from the Pierson-Moskovitz spectral curve and σ are dimensionless peak-width parameters. Commonly applied values for these parameters reflecting the North Sea are suggested by Holthuijsen (2009), namely:

$$\alpha = 0.2044\,[-], \qquad g = 9.81\left[\frac{m}{s^2}\right], \qquad \gamma = 3.3\,[-], \qquad \sigma_1 = 0.07\,[-], \qquad \sigma_2 = 0.09\,[-].$$

The JONSWAP spectral analysis assumes fetch limited deep water conditions, which are assumed to apply for OWT development areas. This, in reality, might not always be the case. However, the effect of shallow water conditions are left out of scope in this research.

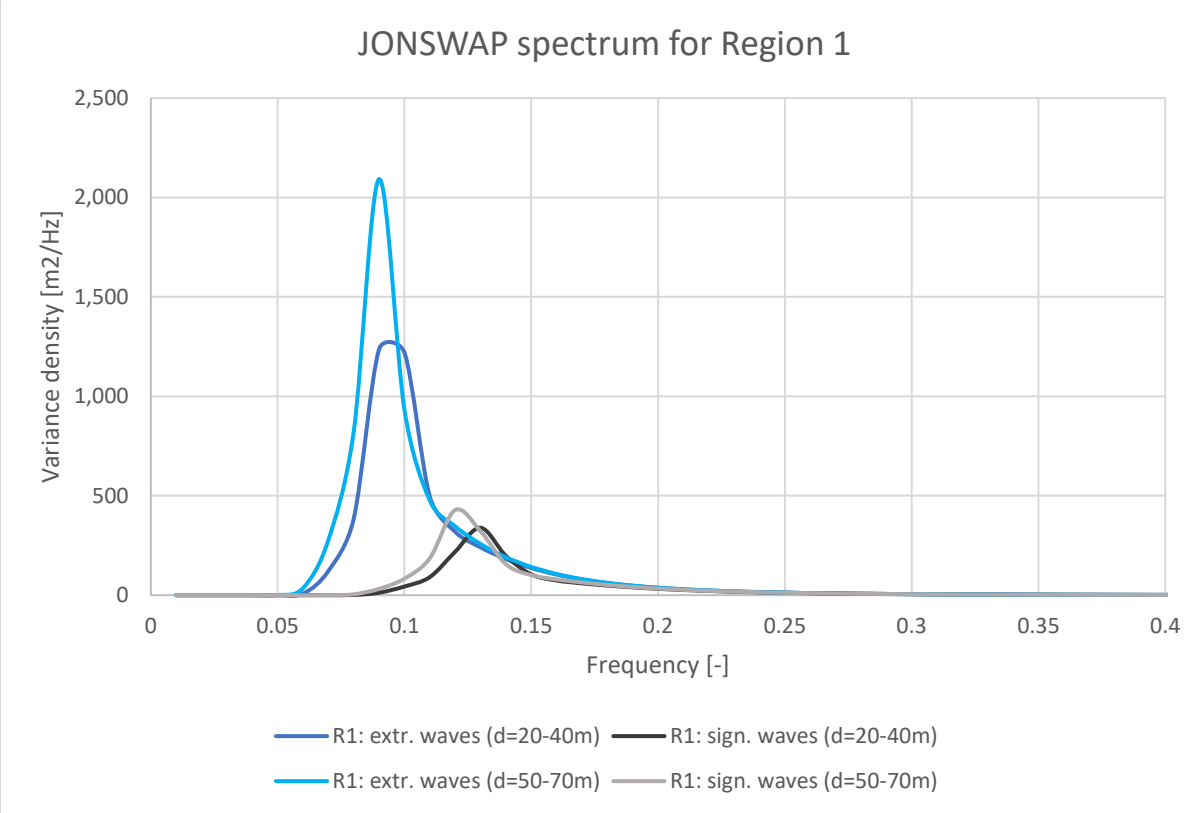

Figure 34: Energy variance density compiled with the JONSWAP spectrum curve for Region 1, based on prior discussed peak wave frequencies. In blue, spectral density of extreme waves. In grey, spectral density of significant waves.

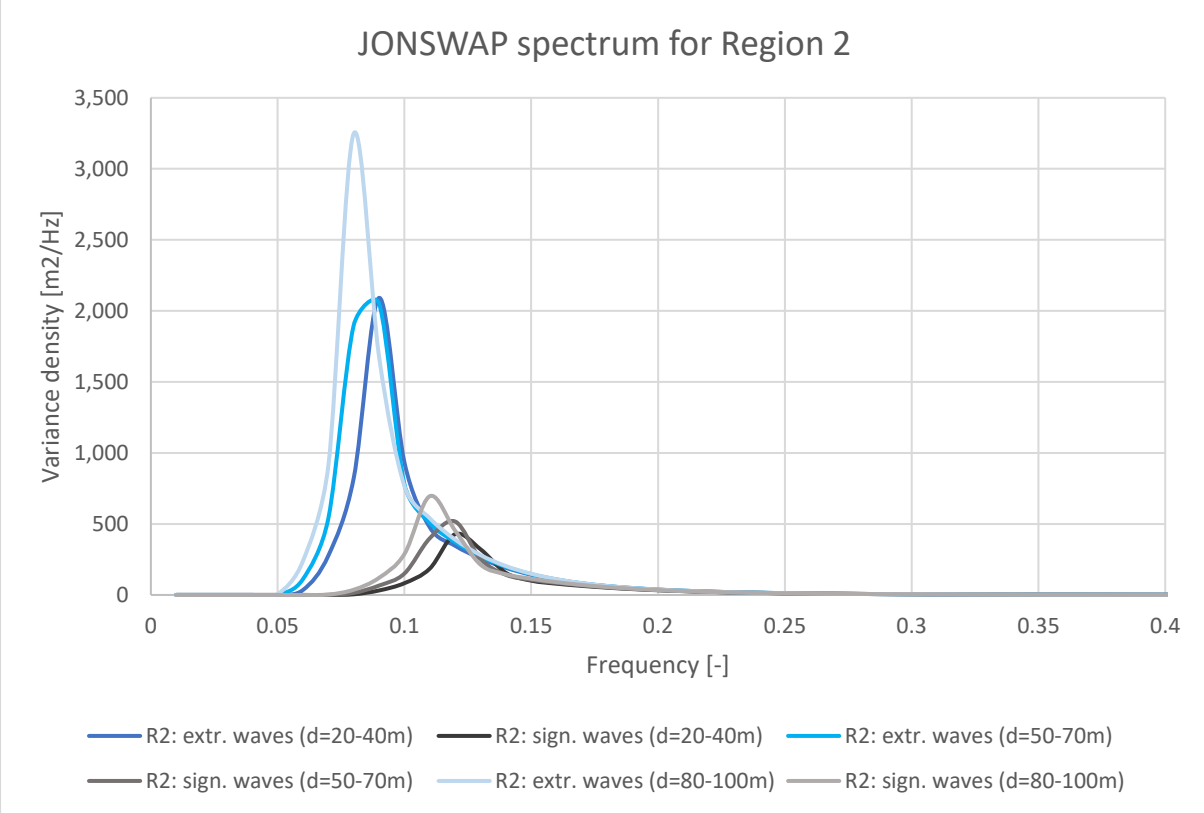

Figure 35: Energy variance density compiled with the JONSWAP spectrum curve for Region 2, based on prior discussed peak wave frequencies. In blue, spectral density of extreme waves. In grey, spectral density of significant waves.

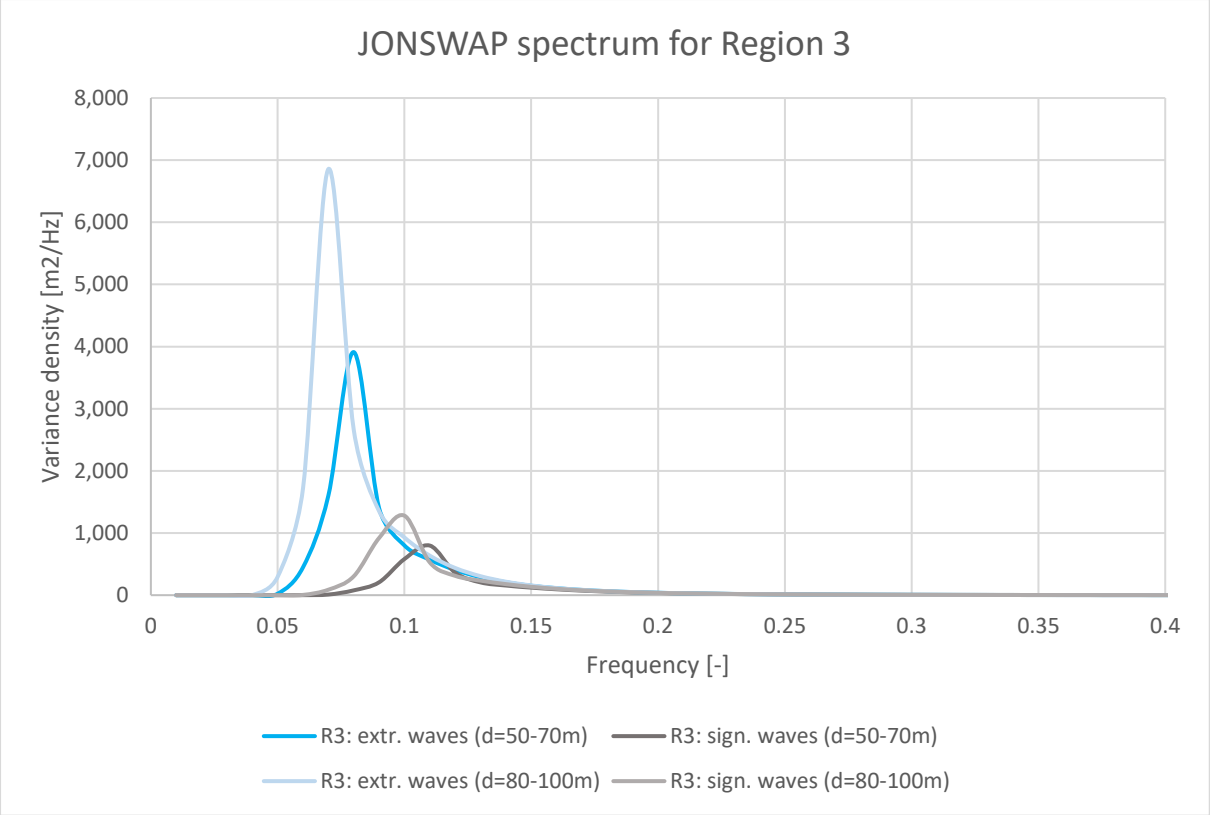

Figure 36: Energy variance density compiled with the JONSWAP spectrum curve for Region 3, based on prior discussed peak wave frequencies. In blue, spectral density of extreme waves. In grey, spectral density of significant waves

From Figure 34, Figure 35 and Figure 36 it can be seen that the wave energy associated with extreme waves is much higher than those of the significant waves, as wave energy increases exponentially with wave height (Holthuijsen, 2009). The highest energy waves are observed in lower frequencies, as was previously discussed and stated by Arany et al. (2017).

Currents

The currents in the North Sea are predominantly caused by the horizontal movement of water related to tidal waves. In contrast to wind waves which are characterized by wave periods of 1-30 seconds, tidal waves are characterized by a higher wave period in the order of magnitude of 12 to 24 hours. Tidal range in the North Sea varies per location but occur within a range of 0-4 meter in the Central and Northern North Sea, see Figure 37 on page 88. In the Southern Bight tidal ranges of 3-5 meter can be observed due to a funnelling effect, where large masses of water are pushed through the relatively narrow English Channel. Amphidromic points – where the tidal range is close to zero – are located West of Denmark and West of the Netherlands. Hence, for Region 1, 2 and 3, tidal variations are set to +4 meter, +2 meter and +3 meter respectively.

Soils

The soil on the construction site is very important to determine a turbine design, as it needs to provide balance the external forces applied on the wind turbine to guarantee structural stability. Even within the area of a wind farm, soil conditions can vary greatly (Lourens, 2019b). The soil composition influences turbine design, as it determines the foundation depth required. In densely packed sandy soils the penetration depth is more limited, less densely packed sand layers or clay layers require increased foundation depths. In the North Sea region many soil types occur and in practice detailed

soil investigation is required to determine the specific soil composition for each wind turbine installed (Lourens, 2019b). An overview of soil compositions in the North Sea can be found in Figure 38 on the next page. In this research, distinction is made between two soil types, namely loose-medium packed sandy soils and medium-dense packed sandy soils. The two soil types are present in all three regions. Clay soils are kept out of scope, as these are known to be susceptible to creep when exposed to long term loading (Lourens, 2019b). Hence clay soils are considered less favourable for OWT foundations.

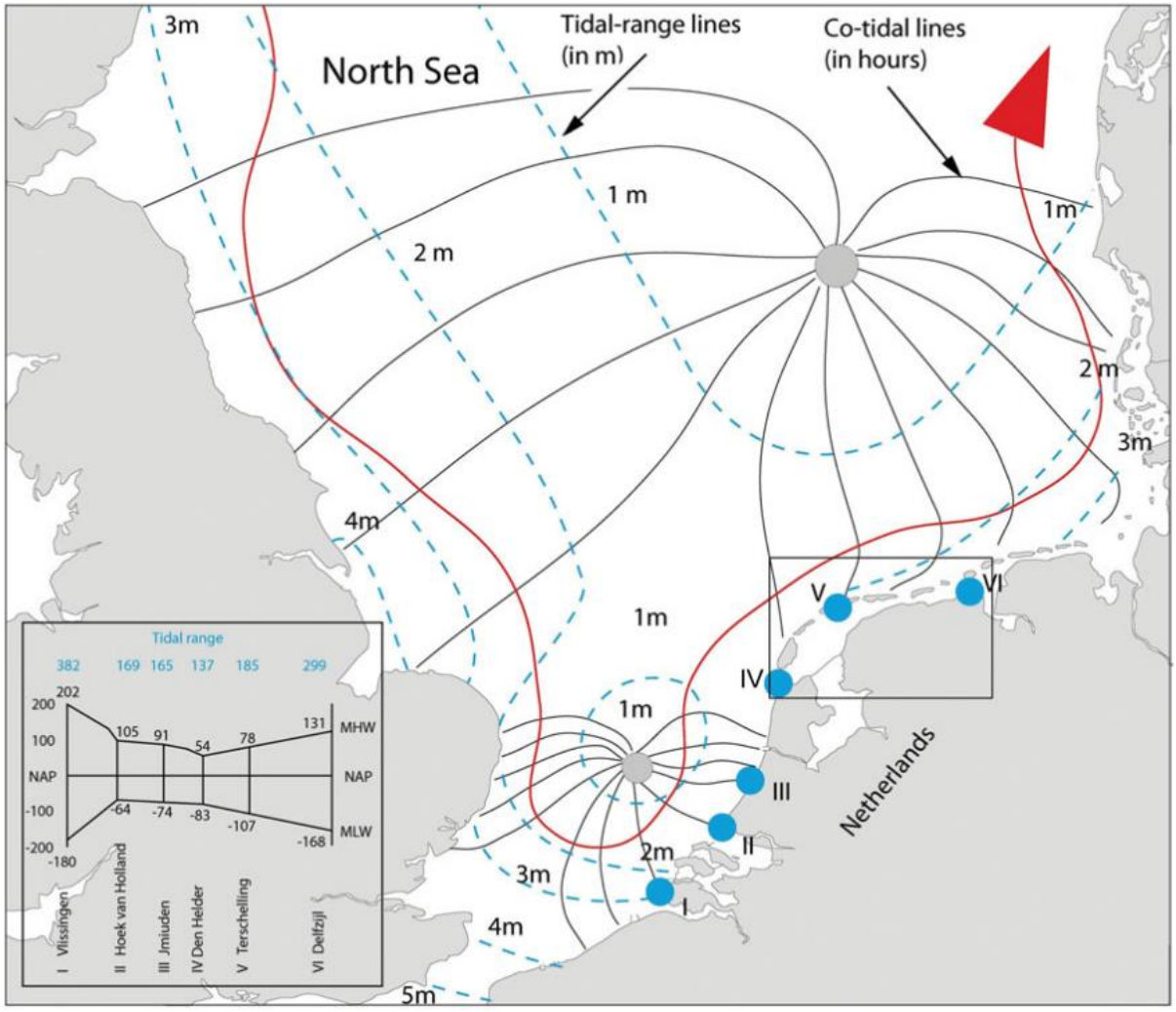

Figure 37: Differences in tidal ranges and the levels of high and low tides in the North Sea. Amphidromic points shown as grey dots. Inset in left bottom corner: Mean High Water, Mean Low Water and tidal range in centimetre of six locations along the Dutch coast compared to average water depth at NAP. This image is obtained from Vos (2015).

Concluding remarks

An overview of environmental conditions for available OWT development zones is created. The North Sea is coarsely divided into three regions, characterised by varying environmental parameters. Various parameters of influence, like wave height, peak wave period, peak wave frequency are introduced. The soil composition is elaborated and a distinction is made between two soil types, namely loose-medium packed sandy soils and medium-dense packed sandy soils. Relevant environmental parameters are specified for the three regions under assessment.

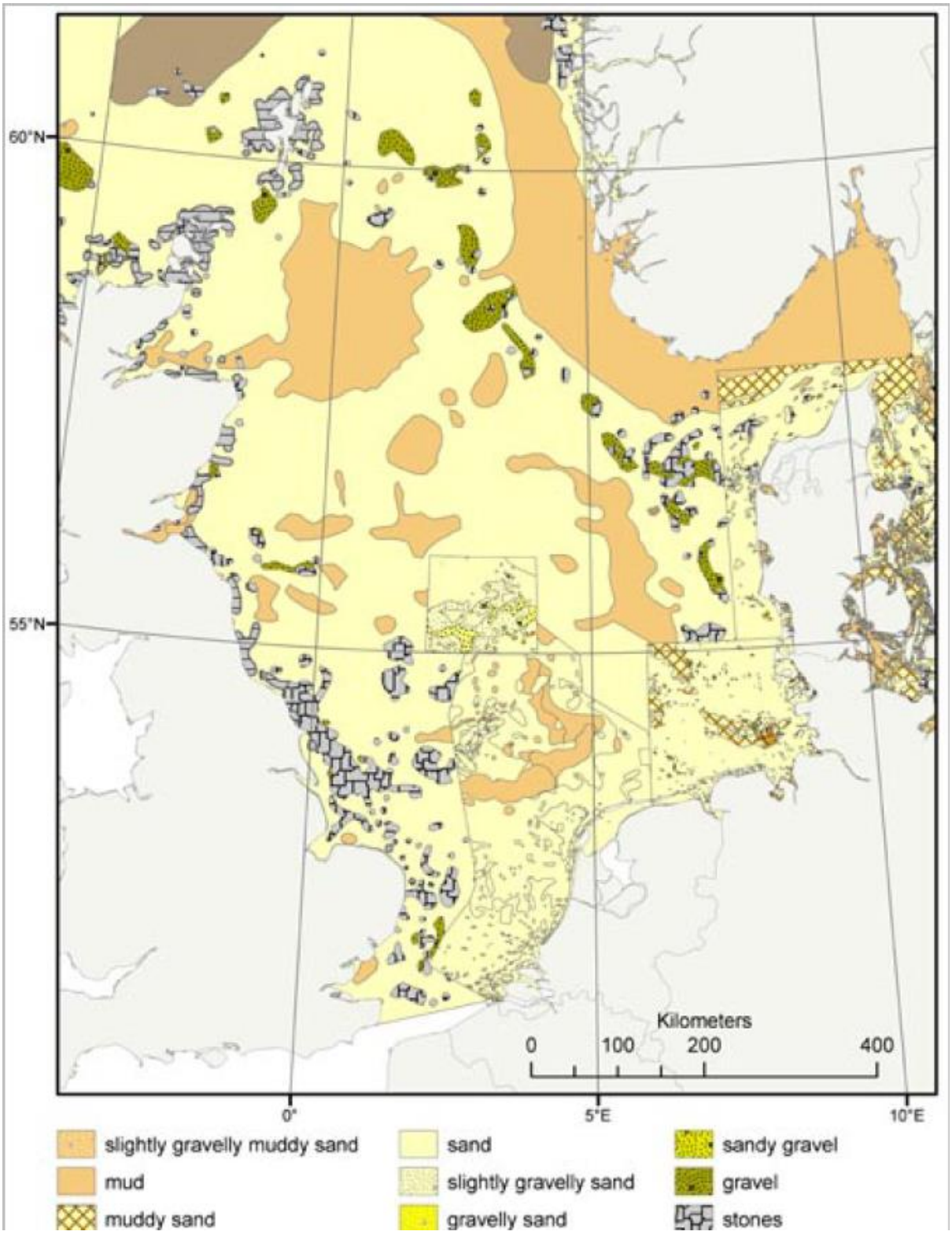

Figure 38: Image obtained from Alfred Wegener Institute (2009)

MONOPILE DIMENSIONING AND MASS ESTIMATION

With the environmental parameters for each region priorly obtained, the initial geometry of the support structures for various turbine and site combinations can estimated. First, the hub and interface height will be determined for each combination. Then monopile and tower dimensions follow from an iterative natural frequency assessment, followed by associated masses estimates.

Reference turbine parameters

Several turbine parameters are required to estimate dimensions of the support structures, like hub height, interface height and NRA mass. In the following paragraphs these are elaborated for five reference turbines. Reference turbines are created by researchers and developers, to provide insight into characteristics of future OWTs, see section 'Development of rated power until 2050' on page 23. The reference turbines under assessment and their respected sources are shown in Table 19.

Hub height

The hub height for each turbine is shown in Table 19. The hub height is defined for each turbine brought to market and determined by its manufacturer. The hub height is the height level where the nacelle connects to the tower of the support structure. In general, a higher rated capacity correlates with a larger hub height.

Table 19: Hub height and nacelle-rotor-assembly mass for the reference turbine models under assessment.

Turbine model	Hub height [m]	M_{NRA} [t]	Source
NREL-5MW-ref	90	350	Jonkman et al. (2009)
LW-8MW-ref	110	480	Desmond et al. (2016)
DTU-10MW-ref	119	677	Bak et al. (2013)
IEA-15MW-ref	150	1017	Gaertner et al. (2020)
IEA-20MW-ref	168	1730	Jensen et al. (2017)

Interface height

The interface level is where the tower of the OWT support structure connects with the substructure. It is defined as the height that water will not reach considering extreme waves, tidal range, storm surge and soil settlement in a given reference period. The formula describing the interface height is as follows:

$$z_{interface} = MSL + {}^{1}/_{2}\,\Delta z_{tide} + \Delta z_{surge} + z_{air\,gap} + \zeta^{*}, \qquad with$$

$$LAT = MSL - {}^{1}/_{2}\,\Delta z_{tide} = HAT - \Delta z_{tide}$$

, where LAT is the lower astronomical tide, Δz_{tide} is the tidal difference, Δz_{surge} is the storm surge, Δz_{gap} is the air gap above the wave crest and ζ^* is the highest wave elevation above the still water level, all expressed in meters height. The interface height can be expressed relative to low (LAT), mean (MSL) and high astronomical tide (HAT). The storm surge can be positive or negative depending on the wind direction and bathymetry. The storm surge is assumed to be +1.5/-0.5 m for all regions, as suggested by Hoving (2017, slide 37). The wave crest height is calculated as 0.65 times the highest expected wave height, e.g. the 1:100 year extreme wave height. Figure 39 presents a visual overview of the

components that influence the interface height. An overview of parameters for each region is shown in Table 20. Region specific interface height per water depth is shown in Table 21.

Figure 39 (right): Visual representation of the Interface level and the components of influence. Retrieved from Lourens (2019b, slide 37).

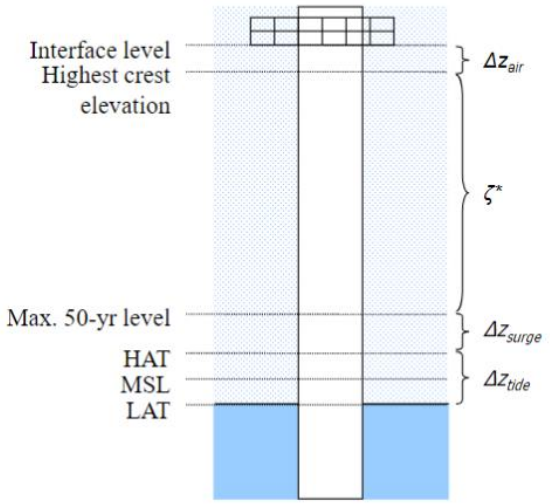

Table 20 (below): Region specific environmental parameters used to determine the interface height at various water depths.

Water depth [m]	Region 1				Region 2				Region 3			
	Δz_{tide} [m]	Δz_{surge} [m]	Δz_{gap} [m]	ζ^* [m]	Δz_{tide} [m]	Δz_{surge} [m]	Δz_{gap} [m]	ζ^* [m]	Δz_{tide} [m]	Δz_{surge} [m]	Δz_{gap} [m]	ζ^* [m]
20												
30	+4.0	+1.5	1.5	5.9	+2.0	+1.5	1.5	6.5	*n.a.*			
40												
50												
60	+4.0	+1.5	1.5	6.5	+2.0	+1.5	1.5	7.2	+3.0	+1.5	1.5	8.5
70												
80												
90	*n.a.*				+2.0	+1.5	1.5	7.8	+3.0	+1.5	1.5	10.4
100												

Table 21: Interface height for the varying water levels specified for each region.

Water depth [m]	Interface height [m] (relative to sea floor)		
	Region 1	Region 2	Region 3
20	32.9	31.5	
30	42.9	41.5	
40	52.9	51.5	
50	63.5	62.2	64.5
60		72.2	74.5
70		82.2	84.5
80		92.8	96.4
90			106.4
100			116.4

Rotational and blade passing frequencies

The rotor speed range of a wind turbine is specific for each wind turbine model. At relatively low wind speeds, the turbine rotors are so called torque driven. This means that the rotor torque generated by the wind is the limiting factor for the rotation speed and thus the energy captured and converted (Jarquin Laguna, 2019). At the rated wind speed, the turbine produces its rated power. At wind speeds higher than the rated wind speed, the turbines are so called pitch driven. This means that through adjusting the yaw and pitch of the blades, the rotor speed is kept constant. From this point, the turbine will generated a constant power output until the cut-out – or maximum operating – wind speed. When wind speeds exceed the cut-out speed of a turbine, the turbine is shut off. The minimum, nominal and maximum rotor speed are supplied by the turbine manufacturer and are largely dependent on the speed of the blade tip. To avoid large pressure drops in the wake of a rotating blade, which could result in formation of ice, the tip speed is constraint by a maximum value. As a result, larger diameter rotors are constraint in their maximum rotational speed (Natarajan, Stolp & Njomo Wandji, 2019).

The importance of the rotor speed in the support structure design is due to wind induced vibrations. The rotational frequency of the rotor imposes cyclic loads on the support structure, resulting in excitation of the structure due to small offsets or imbalances in the rotor blades. The range between the minimum and maximum rotational frequency is denoted as the 1P range. In order to avoid large dynamic forces due to resonance, the eigenfrequency of the support structure should not be chosen to be within the 1P range. The same holds for the blade passing frequency. Each time one of the blades passes the turbine tower, it imposes a force on the support structure leading to excitation and vibrations (Lourens, 2019b). The range between the minimum and maximum blade passing frequency is denoted as the 3P range and should be avoided when the eigenfrequency of the support structure is chosen. A typical one-dimensional representation of the 1P and 3P range is shown below.

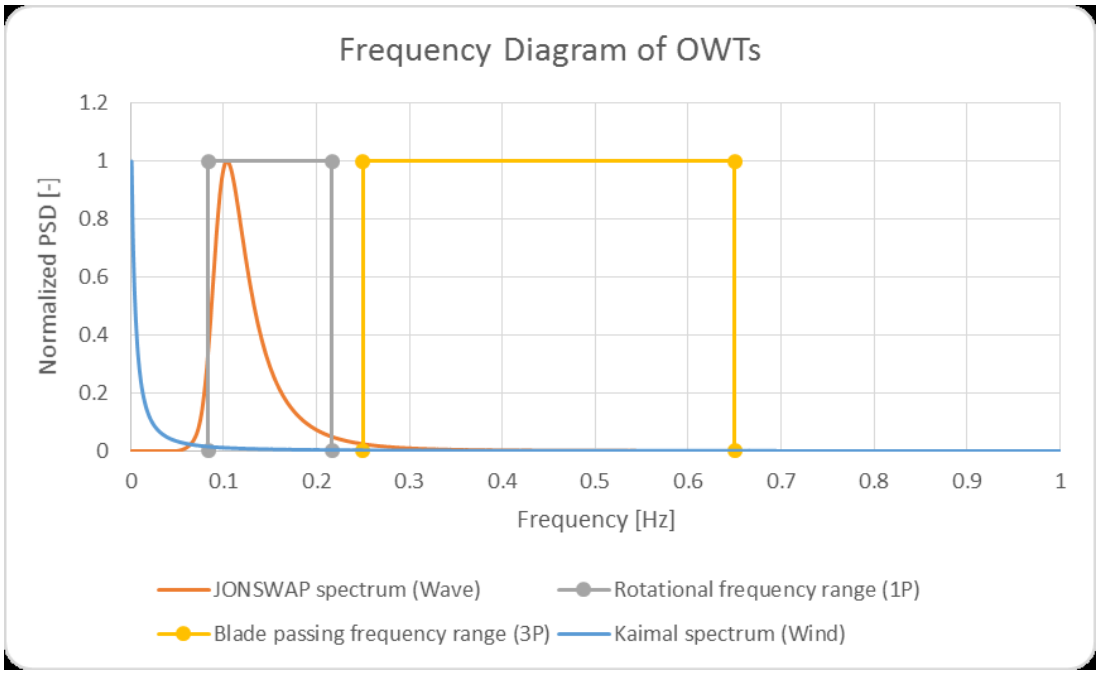

Figure 40: Illustration of typical excitation frequencies by environmental conditions like wind, waves and the rotor and blade passing frequencies of a wind turbine. This image is obtained from Arany et al. (2016).

Due to the 1P and 3P frequency constraints, three potential target ranges for the design natural frequency of the support structure emerge, namely the soft-soft range, the soft-stiff range and the stiff-stiff range. The soft-soft support structure's eigenfrequency is situated below both the rotational

and blade passing frequency domains. Soft-soft towers are usually lighter in mass, but require more dynamic analysis to guarantee a sufficient fatigue life time (Lourens, 2019b; Arany et al., 2017). Soft-stiff support structures have their eigenfrequency in between the rotational and blade passing frequency. Currently, soft-soft and soft-stiff support structure designs are most commonly found. The eigenfrequency of stiff-stiff support structures is located above both the rotational and blade passing frequencies. Stiff-stiff designs are usually not economically feasible due to the high mass requirements of the support structure. The minimal, nominal and maximum rotation speed for the turbines assessed in this research are shown in the table below.

Table 22: Rotational and blade passing frequency for the reference turbines under assessment.

Reference turbines	Rated power [MW]	Rotor diameter [m]	Rotor speed [rpm]		1P frequency [Hz]		3P frequency [Hz]		Soft-stiff range [Hz]
			Min	Max	Min	Max	Min	Max	
NREL-5MW-ref	5	126	6.9	12.1	0.12	0.20	0.35	0.61	0.20-0.35
LW-8MW-ref	8	164	6.3	10.5	0.11	0.18	0.32	0.53	0.18-0.32
DTU-10MW-ref	10	178	6.0	9.6	0.10	0.16	0.30	0.48	0.16-0.30
IEA-15MW-ref	15	240	4.6	7.6	0.08	0.13	0.23	0.38	0.13-0.23
IW-20MW-ref	20	252	4.2	7.1	0.07	0.12	0.21	0.36	0.12-0.21

Support structure target frequency

As discussed in the previous section, the design natural frequency of a support structure is limited by wind induced vibrations. This holds as well for wave induced vibrations, which were obtained via the JONSWAP spectrum. In this paragraph the target natural frequency for support structures in the various water depths assessed will be formulated.

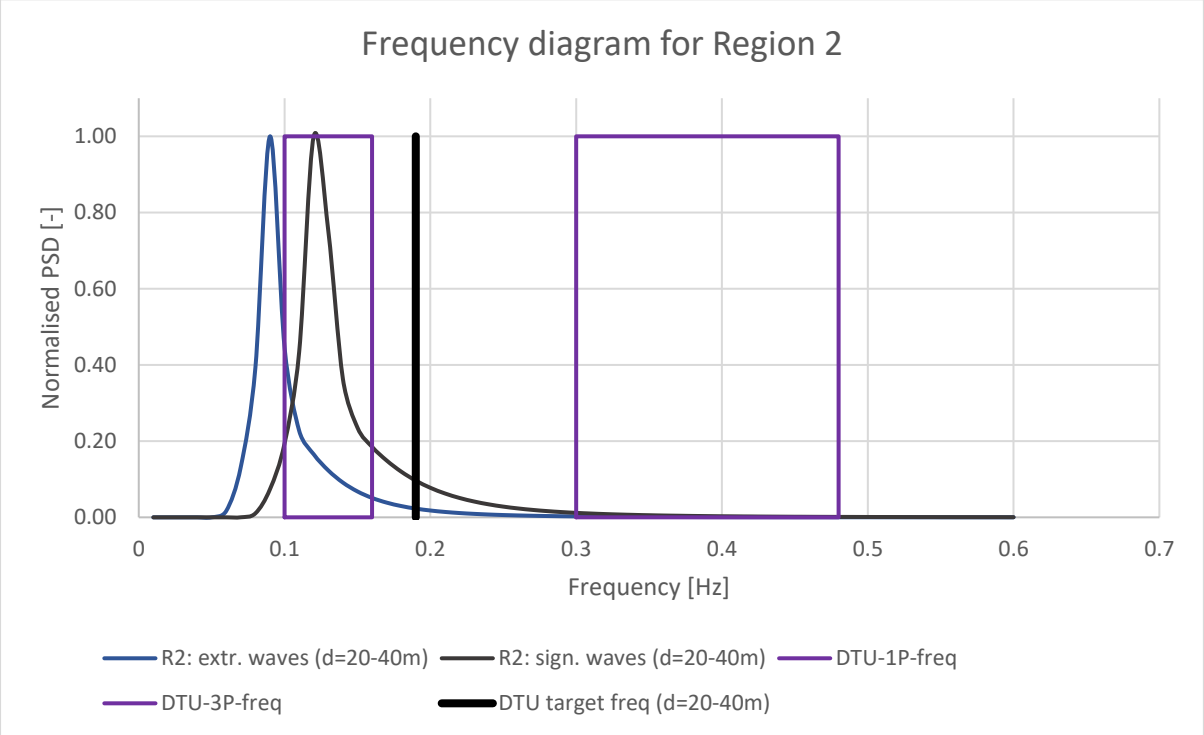

Figure 41: Frequency diagram for DTU-10MW at 20-40m water depth in Region 2. On the vertical axis, normalised energy variance density in m2/Hz. In this specific situation, the minimum target frequency is determined by wave induced frequencies. An overview of target frequencies for other turbine- water depth combinations is shown on the next page.

Dynamic effects, like resonance, determine for a large part the minimum dimensions of a monopile-tower combination and can be considered a leading design criterium. Therefore, a target natural frequency has to be determined for each turbine-water depth combination. In current practice, the target natural frequency of a monopile support structure is set to be 10% higher than the 1P maximum frequency (Lourens, 2019b, slide 15). This was common practice for monopile foundations placed in relatively shallow waters up to 30 meter water depth. However with increasing rotor diameters and the shift towards lower 1P and 3P frequency ranges – see Table 22 – the soft-stiff range becomes more narrow and could start to overlap with wave induced frequencies. In this case, wave induced vibrations provide the lower limit of the support structure target frequency. The upper limit for soft-stiff designs is found 10% below the 3P minimum frequency. In general, a low target frequency is preferable as this result in less material intensive – and hence more economical attractive – designs. An example of a frequency diagram obtained for the DTU-10MW reference turbine located in Region 2 at 20-40 water depth can be seen in .

Table 23: Target frequencies for monopile support structures specified per turbine and water depth combination, for each of the three regions. In grey cells: required pile length exceeds manufacturing capabilities. Target frequency is determined by the lower bound of two options:
a) wind induced vibrations: the upper limit of turbine 1P range +10% [-], depicted as underlined values
b) wave induced vibrations: normalised energy variance density < 0.10 [-], depicted as regular values

	Water depth [m]	Region 1	Region 2	Region 3
NREL-target frequency	20-40	0.22	0.22	
	50-70	0.22	0.22	0.22
	80-100		(0.22)	(0.22)
LW-target frequency	20-40	0.20	0.20	
	50-70	0.20	0.20	0.20
	80-100		(0.20)	(0.20)
DTU-target frequency	20-40	0.20	0.19	
	50-70	0.18	0.18	0.18
	80-100		(0.18)	(0.18)
IEA-target frequency	20-40	0.20	0.19	
	50-70	0.18	0.18	0.17
	80-100		(0.17)	(0.15)
IW-target frequency	20-40	0.20	0.19	
	50-70	0.18	0.18	0.17
	80-100		(0.17)	(0.15)

Natural frequency for support structure design

There are several approximation methods to determine the natural frequency of a monopile structure, varying in computation speed, complexity and accuracy. One way to approximate the natural frequency of a monopile founded wind turbine is to assess the structure as a stick model with a top mass and a fixed connection to the sea bed. The natural frequency can now be approximated using Rayleigh's method. In Rayleigh's method one makes use of the fact that the natural frequency of a structure is equal to the rate of the exchange of kinetic and potential energy within the structure. The kinetic energy is associated with the motion of mass and the potential energy is stored by strains during deformation. When these forms of energy are made equal, the natural frequency can be determined for a given mode shape. Second, the tower and monopile can be divided into segments with roughly equal mass and moment of inertia. The natural frequency is then calculated as the square

root of the generalized stiffness (k*) divided by the generalized mass (m*) of each segment and described by the following formula:

$$\omega = \sqrt{\frac{k^*}{m^*}} = \sqrt{\frac{\int_0^L EI(x) * (\frac{d^2\psi}{d\,x^2})^2 dx}{\int_0^L m(x) * \psi^2(x) dx}}$$

, where L is the total monopile and tower length, ψ is the mode shape of vibration, E is the modulus of elasticity, I is the moment of inertia and m is the mass for a segment of the tower or monopile. The mode shape for a single-side-fixed-support beam is assumed as:

$$\psi = 1 \cos(\frac{\pi * x}{2 * L})$$

In each segment, ψ(x) and its second derivative are assumed to be constant. For each segment, an equivalent mass per unit length ($m_{equivalent}$) and moment of inertia ($I_{equivalent}$) is formulated:

$$m_{equivalent} = \frac{\sum_{j=1}^{n} m_j * L_j * (1 - \cos\left(\frac{\pi x_j}{2 * L}\right))^2}{L}$$

$$I_{equivalent} = \frac{\sum_{j=1}^{n} I_j * L_j cos^2(\frac{\pi x_j}{2 * L})}{L}$$

Substituting the formulas above leads to the expression used to determine the natural frequency:

$$f_{natural} = \frac{\pi}{8} * \sqrt{\frac{EI_{equivalent}}{\left(m_{top} + m_{equivalent} * L\right) * L^3}}$$

Here, m_{top} is the weight of the rotor-nacelle assembly and varies per turbine model. The equivalent mass ($m_{equivalent}$) depends on the diameter (D) and wall thickness (t) of a segment.

Diameter and wall thickness

With a natural frequency expression obtained and target frequencies determined per water depth, rotor-nacelle assembly mass for the turbines and total tower and monopile length, the diameter and thickness of the wall segments are determined. In this calculation, the ratio between the diameter and thickness for the tower and for the monopile are modelled to be constants. However, in reality the diameter and thickness are empirically determined in more detailed load and natural frequency analyses.

Suggested D/t ratios for both tower and monopile are not consistently applied in available literature. Arany et al. (2017) made an overview of monopile diameter and applied wall thickness for wind turbines installed in the North Sea region and included a design value suggested by the American Petroleum Institute as a dashed line, see Figure 42. In Table 24, an overview of D/t ratios used by various authors is presented. It can be seen that for increasing diameters, the D/t ratio for the tower increases. Hermans & Peeringa (2016) use a relatively low tower diameter in combination with a lower D/t ratio, which makes for a more slender design with relatively high wall thickness. For monopiles supporting turbines up to 10 MW, D/t ratios range between 60 and 100 [-]. Notably, Gaertner et al. (2020) use much higher D/t ratios for their 15 MW monopile design, but no other literature has been found supporting D/t ratios of this magnitude. D/t ratios applied in the modelling for this research

follow the API formula shown in Table 25, where $D_{monopile}$ is put into the formula in meter and t is obtained in millimetre.

Table 24: Diameter, wall thickness and D/t ratios from literature for towers and monopiles of various turbine sizes.

Turbine rated power [MW]	Tower		Monopile		Source
	$D_{tower,top}$ [m]	D/t_{tower} [-]	$D_{monopile}$ [m]	$D/t_{monopile}$ [-]	
2 MW	3.0	160-250	n.a.	n.a.	Senvion Wind (2016)
<5MW	2.3-4.2	75-250	4-10	80-110	Lourens (2019b, slide 15)
5 MW	3.87	190-225	n.a.	n.a.	Jalbi et al. (2019)
8 MW	5.0	214-227	n.a.	n.a.	Desmond et al. (2016)
10 MW	4.2	140	9.6	100	Hermans & Peeringa (2016)
10 MW	5.5	218-275	n.a.	n.a.	Desmond et al. (2016)
10 MW	5.5	220-245	9.5	63-95	DTU Wind (2013)
15 MW	6.5	260-280	10	240-270	Gaertner et al. (2020)
20 MW	7.8	215-280	n.a.	n.a.	Pontow et al. (2017, pg28)

Table 25: Design D/t ratios for towers used in the modelling for this research.

Turbine rated power [MW]	D/t_{tower} [-]	$t_{monopile}$ [mm]
<10 MW	220	$t_{monopile} = \frac{6.35 + 10 * Dmonopile}{1000}$
10 MW	240	
15 MW	260	
20 MW	260	

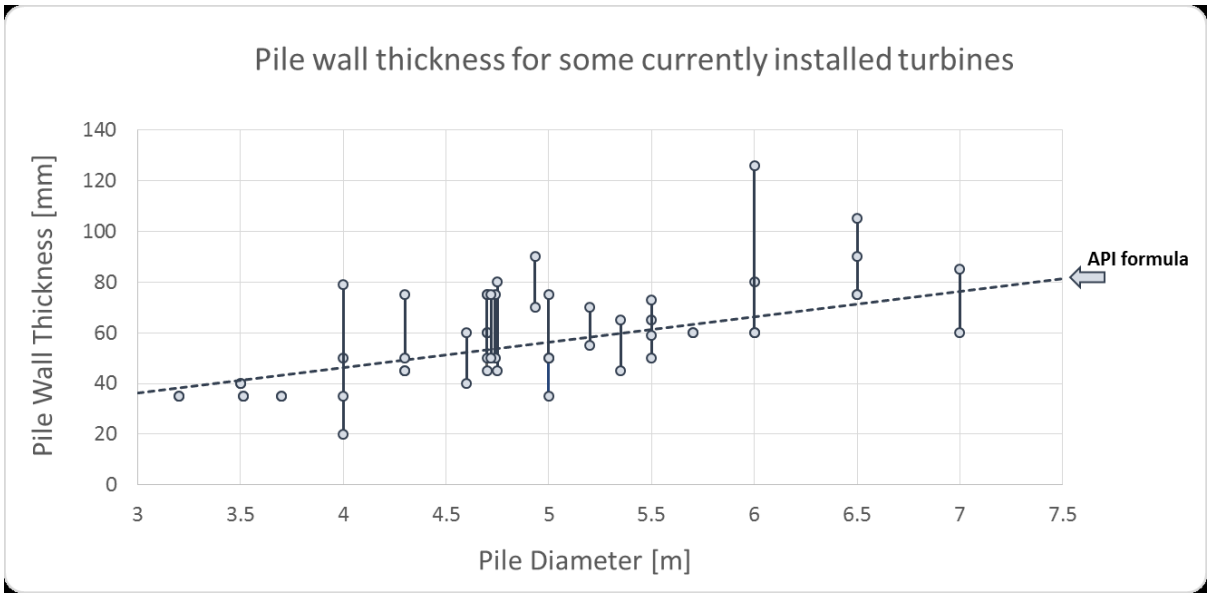

Figure 42: Monopile diameter and wall thickness for several installed turbines in the North Sea region. The dashed line shows the D/t ratio for fixed offshore platforms suggested as an initial value by the American Petroleum Institute (API, 2005). Most case study D/t ratios are in a range of 70 to 110 [-], regardless of monopile diameter. This figure was obtained from Arany et al. (2017).

Embedded monopile length

There are three main design criteria for the minimal embedded pile length of a OWT, of which one has to be satisfied; the zero toe-kick criterion, the vertical tangent criterion or the critical pile length criterion. Given that internal pile stresses need to be known for the first two criteria, the critical pile length criterium is most applicable for this research. The critical pile length can be expressed as a ratio between the necessary embedded pile length $L_{emb,pile}$ and the pile diameter D_{pile} (Arany et al., 2017). This is because after this critical embedded length, the pile can be considered infinitely long and will not show any displacement or force-transfer to the soil. The minimum embedded pile length can be determined using the following expression:

$$L_{emb,pile} \geq 4.0 * \left(\frac{E_{pile} * I_{pile}}{n_h}\right)^{0.2}, with:$$

$$I_{pile} = \frac{1}{8}\left(D_{pile} - t_{pile}\right)^3 * \pi * t_{pile} \quad and \quad n_h = \frac{A * \gamma'}{1.35}$$

, where E_{pile} is the Young's modulus of the steel grade at 210 [GPa], I_{pile} is the moment of inertia of the pile cross section in m^4, n_h is the soil's coefficient of subgrade reaction in kN/m^3, A is a dimensionless parameter pertaining the level of soil compactness and γ' is the soil's submerged unit weight in kN/m^3. The soil's coefficient of subgrade reaction is assumed to be linearly increasing with depth. In the previous section a D/t ratio was elaborated, which can be substituted in the above formula to obtain a relation between exclusively the embedded pile length and diameter. Relevant soil parameters are shown in Table 26.

Table 26: Soil parameters describing compactness, submerged weight and coefficient of subgrade reaction for loose-medium packed sand and medium-dense packed sand.

	A [-]	γ' [kN/m³]	n_h [kN/m³]
Loose-medium packed sand	400	8	2.4E+03
Medium-dense packed sand	800	10	5.9E+03

Monopile dimension and mass estimation

With the mathematical relations priorly discussed, the initial dimensions and mass of the total structure can be computed. This is done for two embedded monopile lengths to account for varying soil characteristics. In the natural frequency optimization, the tower bottom diameter is iteratively adjusted to align the support structure's natural frequency with the target frequency. This is repeated for each water depth and turbine combination. The bottom diameter and embedded length are catalogued, as are the tower and monopile masses. The iteration process is cut off when the target frequency is reached, or the tower dimensions exceed the manufacturing limits. Current maxima for monopile cumulative mass, length and diameter are 2250 ton, 120 meter and 11 meter respectively (Sif Group, 2018). Larger tower and monopile diameters are not yet possible to manufacture but this might be the case in the future. Same holds for the lifting capacity for cranes on board of installation ships. During a presentation by Van Oord – a company specialised in amongst other things OWT installation – a maximum expected lifting capacity of 1600 and 2500 ton are mentioned for ships available now and by 2030 (Van de Brug, 2019). Therefore, the iteration process is stopped at maximum mass, cumulative length and/or diameter of 2500 ton, 130 meter and/or 12 meter

respectively. It is considered unlikely that multiple monopile segments will be combined to obtain larger monopile dimensions, as hammer and drilling equipment are operated emerged from the water. Second, alternative support structure typologies are assumed to be more feasible and competitive at that stage.

Monopile model results

An overview of the support structure masses acquired per turbine-water depth combination is shown in Figure 44 on page 99. Mass estimates obtained from the model are shown, excluding designs that surpass manufacturing constraints discussed in the previous paragraph. In Figure 43, an overview of the number of viable designs and the number of manufacturing constraints encountered is shown. It can be seen that most designs were considered unviable due to the maximum mass constraint of 2500 ton.

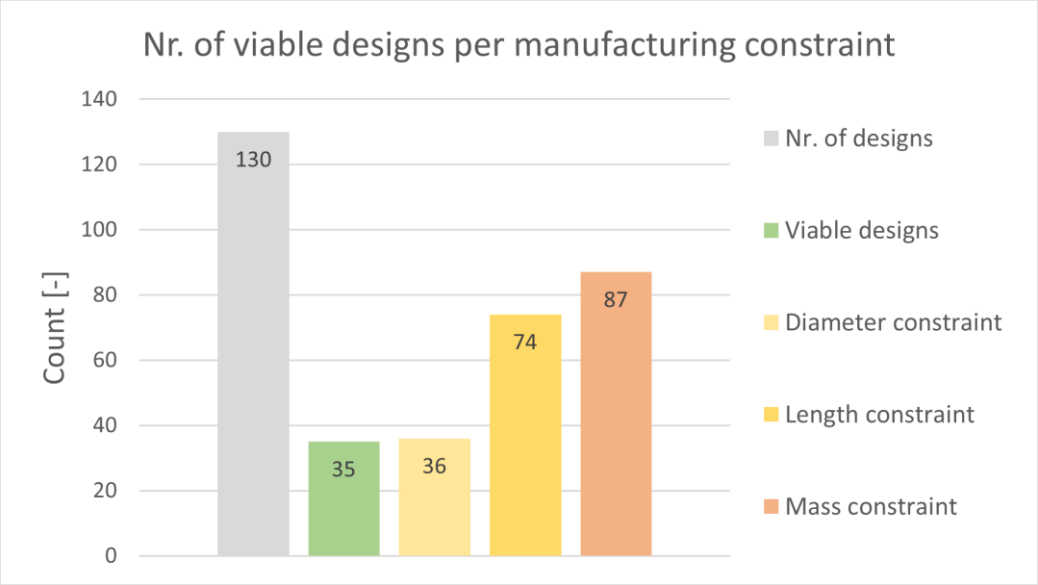

Figure 43: Nr. of viable designs due to manufacturing constraints.

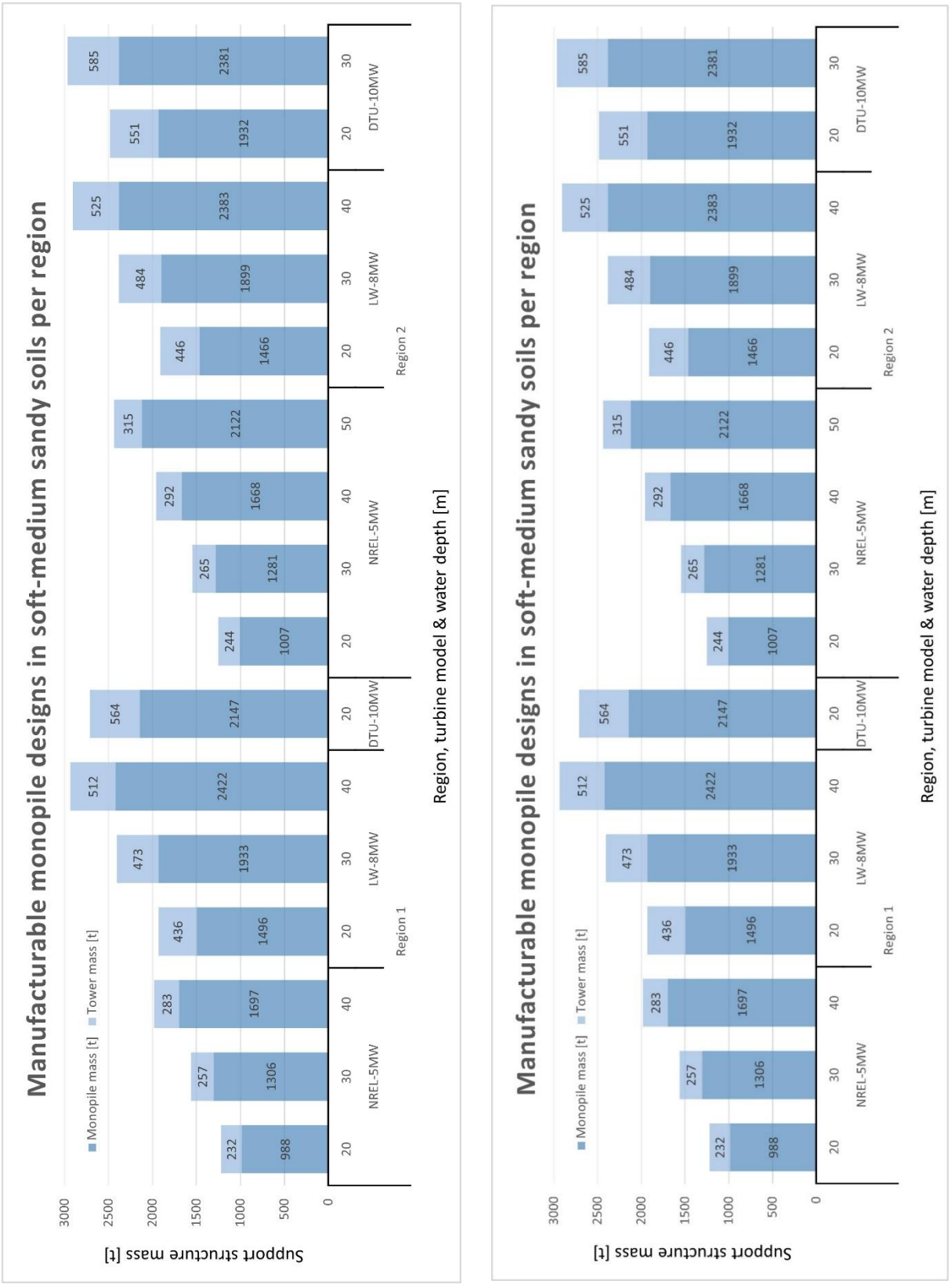

Figure 44: Overview of monopile and tower support structure mass in tons per turbine model, region and water depth. All designs shown meet manufacturing constraints as discussed in previous sections within this chapter. More designs proved possible in dense soils, as soft soils required larger monopile dimensions. Monopile mass shown in dark blue, tower mass shown in lighter blue. No monopile designs proved viable for the IEA-15MW and IW-20MW turbines mostly due to the maximum mass constraint.

JACKET DIMENSIONING AND MASS ESTIMATION

Next, the initial geometry of jacket structures are assessed. Hub height and interface level for the various reference turbines were priorly discussed – see Table 19, 19 and 20 – and are used in the geometry and mass estimates for the jacket support structures. Jacket dimensions follow from design steps provided in the Bottom Founded Offshore Structures course (Hoving, 2017). Initial geometry is obtained based on rule-of-thumb member size assumptions, not on structure optimization or stress and limit state checks. For the jacket design, towers of similar dimensions are used that were obtained in the dimensioning of the monopiles rather than those suggested by literature. Transition piece dimensions are estimated based on recommendation from a paper by Lee, Gonzalez & Lee et al. (2016). Total jacket support structure mass is then estimated based on initial jacket dimensions, transition piece, foundation and tower masses.

Tower mass and dimensions

Tower masses provided for the NREL-5MW, LW-8MW and DTU-10MW reference turbines are associated to onshore placement and do not hold true for offshore application. Desmond et al. (2016) use tower diameter dimensions suggested for the NREL reference turbine – based on Jalbi et al. (2019) – to estimate tower dimensions for the LW-8MW reference turbine. However, they neglect the significant difference in tower height between offshore and onshore locations, being 70.4 meter for offshore turbines and 87 meter for onshore turbines. Hence, a better fitting tower mass needs to be determined for the reference turbines. Comparing tower parameters from literature is somewhat difficult as the interface height for a tower depends on location specific environmental site conditions. Desmond et al. (2016) refer to a report by De Vries et al. (2011) who assume tower dimensions in order to construct a preliminary jacket design for the NREL-5MW turbine at a 50 water depth location in the North Sea. The proposed tower has the following characteristics:

Table 27: Comparison of tower parameters used by De Vries et al. (2011) for the NREL 5MW reference turbine at 50 meters water depth in the North Sea and parameters obtained in tower design. Values shown correspond to a monopile tower for the NREL-5MW reference turbine located in Region 1, at 30 meter water depth and medium-dense sandy soils. Absolute difference is due to considering different hub heights. Relative difference is considered significantly small for tower dimensions to be viable in jacket dimensioning.

Source:	h_{hub} [m] (w.r.t. MSL)	$h_{interface}$ [m] (w.r.t. MSL)	L_{tower} [m]	$D_{tower,\ top}$ [m]	$D_{tower,\ bottom}$ [m]	D/t_{tower} [-]	M_{tower} [t]
De Vries et al. (2011)	82.75	14.75	68	4	5.5	160-200	216
MP tower dimensions	90.0	12.9	77.1	3.9	6.5	220	237

Taking the difference in tower length into account – caused by the consideration of different hub heights – the difference in tower mass is relatively small, being 3.18 ton/meter for De Vries and 3.08 ton/meter. Therefore, tower dimensions and associated masses related to monopile towers at 50 meter water depth and medium-dense sandy soils will be used for dimensioning of transition pieces and jackets. An overview of tower dimensions for each reference turbine is shown in Table 28. Here it can be seen that the bottom diameter associated with the IW-20MW reference turbine exceeds the current maximum manufacturable value for monopile diameters. However, in contrast to monopiles the tower is not exposed to hammering forces during installation. Furthermore, the tower does not have to be manufactured upfront to be installed in one piece, but can be transported in segments and assembled on site. Lastly, the mass of the IW-20MW tower is lower than the maximum lifting capacity

indicated by Van Oord and therefore assumed to be viable from an installation perspective (Van de Brug, 2019).

Table 28: Overview of tower properties used for the jacket mass calculations. Values correspond with tower design values used in the monopile mass calculations for the case of 50 meter water depth and medium dense sandy soils.

Turbine	L_{tower} [m]	$D_{tower,\ top}$ [m]	$D_{tower,\ bottom}$ [m]	$t_{tower,\ bottom}$ [mm]	M_{tower} [t]
NREL-5MW	77.1	3.9	6.5	29.5	217
LW-8MW	97.1	5.0	7.6	34.5	436
DTU-10MW	106.1	5.5	8.7	36.3	556
IEA-15MW	134.2	6.7	11.4	43.8	1063
IW-20MW	155.1	7.8	14.3	55.0	1840

Transition piece mass and dimensions

In order to connect the turbine tower to the jacket support structure, a transition piece is required. The transition piece connects the cylindrical shape of the tower to the four jacket legs. An example of tower-to-jacket transition piece is shown in Figure 45. In their study, Lee et al. (2016) look into typology optimization for tower-to-jacket transition pieces and conclude that a straight tubular brace with inclination between 45 and 60 degrees would be optimal. Therefore, the transition pieces used in the model comprise of a cylindrical section with similar diameters to the tower bottom ($D_{TP,top}$), horizontal bracing and tubular cross bracing between the jacket legs and to the tower cylinder. The height of the cylindrical section ($L_{TP,cylinder}$) is chosen to be 1.5 times the tower diameter, so that the brace inclination equals 56 degrees and is within the range provided by Lee et al. (2016). The wall thickness of the TP tower segment ($t_{TP,top}$) is assumed to be somewhat larger than that of the turbine tower ($t_{tower,bottom}$) due to potential concentration of forces. Therefore, the wall thickness of the TP tower segment is to 1.5 times the wall thickness of the tower bottom. Sizing and geometry of the transition piece are momentous as it affects the geometry of the jacket structure in further design steps. The mathematical relations applied are shown below:

$$D_{tower,bottom} = D_{TP,top}, \quad L_{TP,cylinder} = 1.5 * D_{TP,top}, \quad t_{TP,top} = 1.5 * t_{tower,bottom}$$

Figure 45: Illustration of tower-to-jacket transition pieces. On the left: OWEC Quattropod® for the Beatrice Offshore Wind Project in Scotland 2007. On the right: a design for Thortonbank wind farm in Belgium 2012. These images are obtained from Lee et al. (2016).

For the width of the transition piece structure (b_{TP}), from Figure 45 it can be seen that the slanting braces directly connect the TP's cylindrical segment to the jacket legs. The diagonal distance between two diagonally opposing jacket legs is determined by the tower bottom diameter. This needs to be 3 times the tower bottom diameter and two times the jacket leg diameter for the angle of 56° to uphold. Therefore, applying simple geometry, the width of the transition piece can be found as:

$$b_{TP} = \frac{3 * D_{tower,bottom} + 2 * D_{jacket\ leg}}{\sqrt{2}}$$

For the horizontal braces supporting the cylindrical tower section, the diameter ($D_{TP,braces}$) is assumed to be equal to that of the jacket leg piles ($D_{jacket,leg}$). The jacket leg diameter is elaborated in the **Jacket dimensions and mass** section on the next page, but depends on the required length of jacket pile**.** For the wall thickness of these segments, a diameter over thickness ratio of 25 [-] is used which is common for tubular members located in or near the splash zone (BOFS, 2019). Mathematical expressions for the transition piece braces and wall thickness are:

$$D_{TP,braces} = D_{jacket,leg}, \quad t_{TP,braces} = \frac{D_{TP,braces}}{25}$$

With the parameters described above, the volume of steel required for the transition piece can be calculated. As the TP tower segment, horizontal and cross braces are tubular members the volume and mass of each tubular segment are calculated as:

$$M_{member} = V_{member} * \rho_{steel} = 0.25 * \pi * (D_{outer} - D_{inner})^2 * L$$

, where D_{outer} and D_{inner} are the outside and inside diameter of a member and L is its length. The mass of each member (M_{member}) can be found by multiplying the volume (V_{member}) with the mass density of steel (ρ_{steel}) at 7800 [kg/m^3]. As the transition piece width is dependent on the jacket leg diameter and hence the water depth, a transition piece mass is calculated for each water depth and turbine combination. It should be mentioned that this approach counts overlapping areas between members double. However, this overlapping volume is very small and considered negligible compared to the material volume associated with the overall support structure. The transition piece masses for each turbine-water depth combination are shown below in Table 29.

Table 29: Transition piece masses in tons for each turbine-water depth combination following from dimensions elaborated above. Transition piece mass depends, amongst other parameters, on the jacket leg diameter which is discussed in the next section.

Water depth	Transition piece mass [t]				
[m]	NREL-5MW	LW-8MW	DTU-10MW	IEA-15MW	IW-20MW
20	150	183	222	340	513
30	241	288	341	493	703
40	359	424	494	689	944
50	530	620	715	971	1292
60	710	826	945	1263	1651
70	921	1065	1214	1602	2067
80	1213	1396	1584	2069	2636
90	1495	1715	1940	2515	3179
100	1812	2072	2337	3011	3782

Jacket dimensions and mass

To determine the jacket dimensions, individual components and members are assessed. A jacket is constructed from multiple geometrically equal bays. Bays are geometrically equal as it eases the manufacturing in such a way that angles between legs and diagonal or cross braces are identical for each bay. This can be seen in the figure below, as are important variables like the batter angle (α), the jacket top width (b_0) and consecutive bay widths (b_1, b_2, .. , b_N), bay heights (h_0, h_1, .. , h_N) and brace angle (θ). Here, i is the number index for each sequential bay and N the index for the last required bay. The estimated number of bays is found through dividing the interface height – with respect to sea level – by the estimated jacket top width, rounded down and as integers. This because optimal structural configuration is achieved at bracing angels of approximately 45°. Due to the size of welding equipment brace angles may never be smaller than 30° (Hoving, 2017). It should be noted that the batter angle can be assessed in a 2D-plane – denoted as the batter angle – or in 3D-space – denoted as the true batter angle. In the remainder of the report, a reference to the batter angle always indicates the true batter angle in 3D-space. Mathematical relations between the variables mentioned above are as follows:

$$dim_{i+1} = m * dim_i\,, \qquad m = \left(\frac{b_N}{b_0}\right)^{\frac{1}{N}}, \qquad \tan(\theta) = \frac{h_i}{b_i - h_i \tan(\alpha)}$$

$$\left.\begin{aligned} h_{total} &= \sum_{i=1}^{N} h_i = h_1 + mh_1 + \cdots + m^{N-1}h_1 \\ h_{total} &= h_1 \sum_{i=1}^{N} m^{i-1} = h_1 \frac{m^N - 1}{m - 1} \end{aligned}\right\} \rightarrow h_1 = h_{total} * \frac{m-1}{m^N - 1}$$

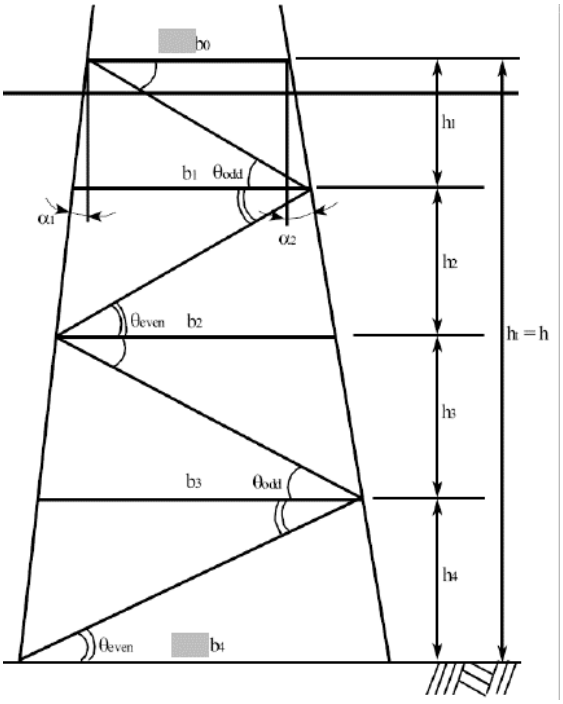

Various detailed jacket designs are consulted to decide on the batter angle, as this heavily influences the final jacket mass. Historically, the maximum batter angle was limited to 9.5°, as foundation piles were hammered through the jacket legs into the sea bed and hammering equipment prevented any slighter angles (Hoving, 2017). A reference jacket designed during the INNWIND.EU programme, used a batter angles of 12.4° to support a DTU-10MW reference turbine located at 50 water depth (van Borstel, 2013). Estimated jacket mass for this design was 1210 ton. A later study by provided the insight to reduce member dimensions which resulted in a 540 ton preliminary design while keeping an overall similar geometry (Stolpe, Wandji & Natarajan et al., 2017). Then, following their own recommendations, in another design iteration the jacket top width was increased – from 14 to 18 meter – and the batter angle reduced to 4° (Sandal, Verbart & Stolpe, 2018). Through this, the jacket bottom width was reduced from 34 to 24 meter and the optimised jacket mass would be reduced from 540 to 484 ton. Therefore, in this report the batter angle is similarly taken as 4° for estimating jacket dimensions and masses.

The member sizes can be estimated using the fact that generally – due to stability requirements – member stiffness is greater than member strength. Consequently, member diameter selection is based on slenderness. Slenderness of a member is described by the following formula:

$$\lambda = \frac{K * L}{r_g}, with: \begin{cases} L = member\ length & [m] \\ K = Effective\ buckling\ coefficient & [-], \\ r_g = Radius\ of\ gyration & [m] \end{cases} \quad and: \quad r_g = \sqrt{\frac{I}{A}} = \frac{D}{2\sqrt{2}}$$

Buckling length coefficients differ for various members, depending on a member being a leg pile, diagonal brace or cross brace. Furthermore, members located in the splash zone – that area where both water and air can interact with the structure – generally require larger wall thickness to account for wave impact and potential environmental weathering (Hoving, 2017). Applied buckling coefficients and member wall thicknesses are depicted in Table 30. Using commonly applied slenderness values and buckling coefficients, a ratio between a member's length and its diameter can be obtained by:

$$\left\{\frac{L}{D} = \frac{\lambda}{2\sqrt{2} * K}\right\} \rightarrow D = \frac{2\sqrt{2} * K}{\lambda} * L$$

Important to note, is that generally suggestions provided in a lecture by Hoving (2017) were respected, notably for suggested D/t ranges at 24-60 [-], λ and K values. However, the lecturer suggested to use a D/t ratios for the jacket legs at 60 [-] but this resulted in an underestimation of leg wall thickness. Instead, a D/t ratio of 25 is applied, which corresponds well with overall encountered values found in literature. Considering the length of the jacket leg, the formula on the next page applies.

Table 30: Design rules-of-thumb applied in jacket dimensioning. Values are obtained from Hoving (2017).

Member type	Member zone	λ [-]	K [-]	L/D [-]	D/t [-]
Diagonal brace	Splash zone	80	0.5	57	25
	Fully submerged	80	0.5	57	25
Cross brace	Splash zone	80	0.8	35	25
	Fully submerged	80	0.8	35	40
Horizontal member	Splash zone	100	0.8	44	25
	Fully submerged	100	0.8	44	40
Jacket legs	-	100	1.0	71	25

$$L_{jacket,leg} = \sqrt{{h_{total}}^2 + {}^1\!/_4\,(b_N - b_0)^2 + h_{bottom,min}}$$

, where $L_{jacket,leg}$ is the length of a single jacket leg in meter, b_N and b_0 are the bottom- and top frame width in meter and $h_{bottom,min}$ is the minimal vertical distance between the bottom frame and the sea bed taken as 0.5 meter. Member wall thickness is expressed as a constant ratio with respect to a member's diameter, and expressed as:

$$t_{member} = \frac{D_{member}}{\left(\frac{D}{t}\right)_{member}}$$

, where t_{member} is a member's wall thickness in meter and the dimensionless D/t values for various components are depicted in Table 30.

Jacket member configuration

Considering the jacket configuration, several options are possible. General configuration options consist of TP-to-jacket connection lay-out, the number of legs, the bay lay-out and mudline configuration facilitating the number of required foundation piles. For the bay lay-out, further options consist of horizontal braces (between diagonally opposing legs), horizontal members (between in-plane opposing legs), in-plane diagonal- or cross braces and finally diagonal or cross braces between diagonally opposing jacket legs. Each configuration choice presents advantages and disadvantages. For example, increasing the number of member connections for each bay effectively increases overall jacket stiffness, but increases material requirements, the number of welds – and their respective chance of failure – manufacturing time and labour cost. Furthermore, using multiple members of smaller dimensions increases the overall surface exposed to environmental conditions, inherently increasing the need of protective coatings and/or paints and associated labour time and cost. Other requirements mentioned in literature address the need to avoid fatigue problems in the uppermost *emerged* horizontal frame due to waves and buoyancy. Therefore, its minimum elevation should at least be six meter above mean sea level. Next, the minimum elevation of the uppermost *submerged* horizontal frame should be chosen such that it remains flooded at all times (Hoving, 2017).

Overall, it should be kept in mind that in practice the final design will always be selected on cost effectiveness, unless stated otherwise in project commissioning requirements, even if that design entails higher material requirements. The focus of this research, however, covers the assessment of expected material requirements and not optimalisation of material efficient design. Configuration suggestions by Hoving (2017), van Borstel (2013), Stolpe et al. (2017) and Sandal et al. (2018) are largely respected and proved decisive in the final choice of jacket configuration. The final configuration is considered to be balanced and likely to be cost effective now and up to 2050. In the model the design configuration are applied as follows:

- TP / Upper bay:
    - horizontal members between in-plane jacket legs (horizontal orientation)
    - horizontal cross braces between jacket legs (diagonal orientation)
    - in-plane cross braces between jacket legs (vertical orientation)
- Intermediate bays:
    - in-plane cross braces between jacket legs (vertical orientation)
- Mudline bay:
    - in-plane cross braces between jacket legs (vertical orientation)

It can be seen that no diagonally orientated cross braces are present, as these increase the number of welds in already high weld-density areas on the jacket legs. No horizontal members are added in intermediate bays for similar reasons. Also, no horizontal members are added at the mudline bay to account for installation delays due to a potential uneven seabed and to minimize scour potential associated with members in close proximity of the seabed. Scour is a result from increased water particle velocity, which occurs when water has to move around an encountered obstacle. Overall, cross braces are picked over diagonal braces, as this leads to the formation of an increased number of statically determinate 'triangles', resulting in a higher material utilization factor at the cost of increasing exposed surface area.

Jacket foundation dimensions and mass

For jackets, each leg needs to be fixed to the sea bed in order to achieve overall successful force transfer and stability of the OWT. In contrast to monopile foundations – which transfer external forces to the soil through bending and deflection – jacket foundations are predominantly strained in axial direction. In general, jacket foundation piles are of smaller diameter than is the case for monopiles. In reference literature, pile penetration depths of up to 50 meter are mentioned for the IW-20MW turbine (Pontow et al., 2017). This is based on assumed soil conditions which show a suitable force carrying sand layer at 40 meter below seabed. However, soil profiles are known to vary greatly even within the area of one wind farm and it might not always be the case that such a carrying sand layer occurs at 40 meter below seabed (Lourens, 2019b). On the other hand, it is considered unlikely that foundation piles of extreme lengths will remain economically feasible. Therefore, the maximum embedded pile length is assumed to be 70 meter. In this research, two soil types are assessed, namely soft-medium packed sandy soils and medium-dense packed sandy soils. The formula used to calculate pile length is as follows:

$$L_{foundation} = minimum \begin{cases} 8.0 * \left(\frac{E_{pile} * I_{pile}}{n_h}\right)^{0.2} \\ 70 \end{cases}$$

, where Epile is the Young's modulus of the steel at 210 GPa, Ipile is the moment of inertia and dependent on pile dimensions and nh is the coefficient of subgrade reaction. A visual representation of the embedded pile length is shown in Figure 46. Resulting foundation pile length values compare well to values found in literature (Van Borstel, 2013; Pontow et al., 2017; Stolpe et al., 2017).

Next, considering ease of installation the pile diameter of foundation piles is taken slightly larger than that of the jacket legs (Hoving, 2017) This is to allow for a grouted connection between the foundation pile and the jacket structure. A common applied grout thickness (t_{grout}) is 75 mm, and applied as such in the model. The pile thickness of the foundation pile is calculated with the API suggested formula priorly discussed. Both mathematical relations are shown below:

$$D_{foundation} = D_{jacket,leg} + 2 * t_{grout} = D_{jacket,leg} + 0.15m$$

$$t_{foundation} = \frac{6.35 + 10 * D_{jacket,leg}}{1000} \; [mm]$$

, where $D_{jacket,leg}$'s is supplied to the formula in meter but $t_{foundation}$ is obtained in millimetre. The mass of the foundation is then found through calculating the volume of the hollow cylinders and multiplying with the mass density of steel at 7800 [kg/m^3].

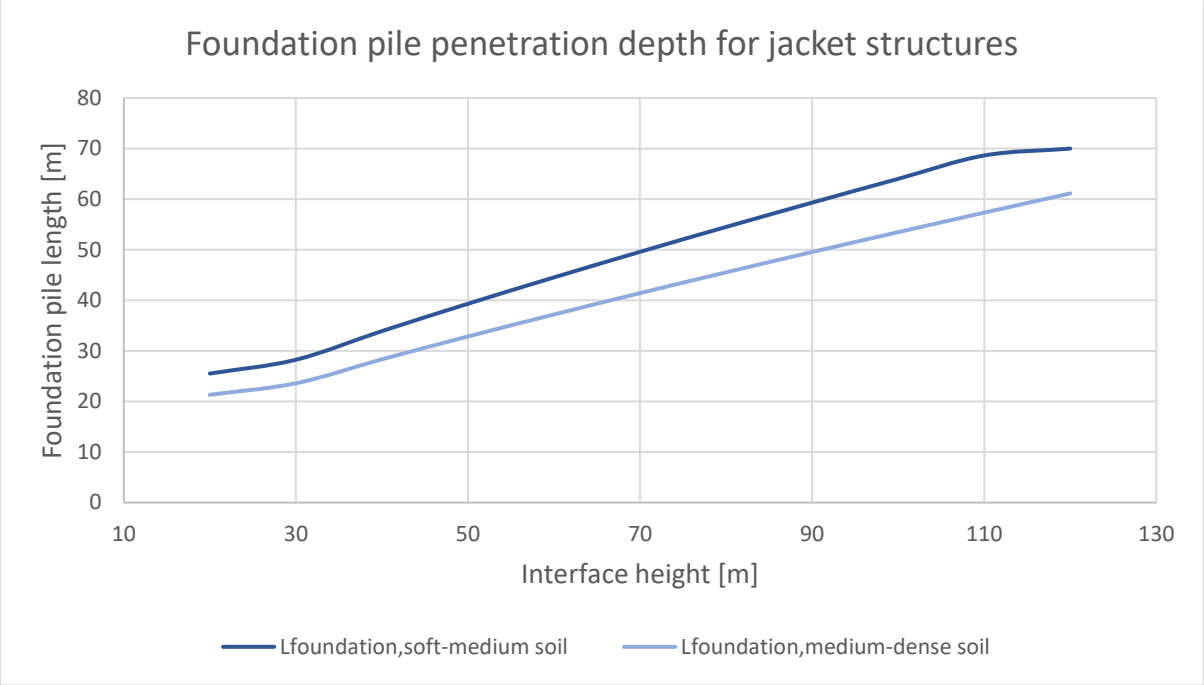

Figure 46: Relation between pile penetration depth and interface height applied to model embedded foundation pile length. In dark blue, pile length associated with soft-medium packed sandy soils. In lighter blue, pile length associated with medium-dense packed soils. No stress or limit state calculations are applied, but pile length compares well with reference literature.

Jacket model results

In the next pages, results of the jacket support structure mass estimation model are shown. Results are divided per region and soil type, showing the breakdown of component mass – e.g. tower, transition piece, jacket and foundation – for each turbine-water depth combination. On the horizontal axis, turbine-water depth combinations are shown. On the vertical axis, component mass resulting from the mass model is shown in ton steel. The table below each figure indicates specific component mass in tons.

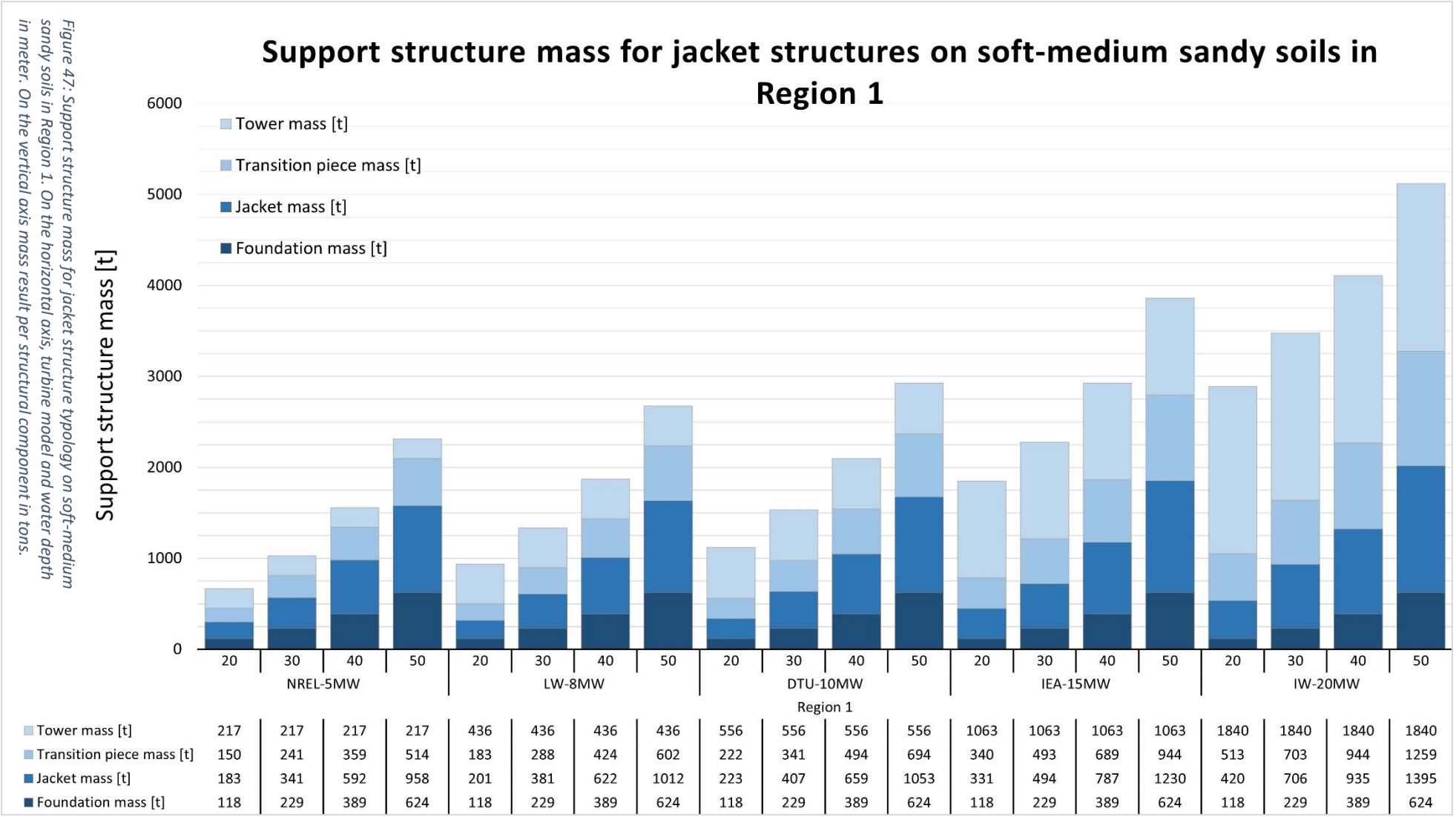

Tower mass [t]	217	217	217	217	436	436	436	436	556	556	556	556	1063	1063	1063	1063	1840	1840	1840	1840
Transition piece mass [t]	150	241	359	514	183	288	424	602	222	341	494	694	340	493	689	944	513	703	944	1259
Jacket mass [t]	183	341	592	958	201	381	622	1012	223	407	659	1053	331	494	787	1230	420	706	935	1395
Foundation mass [t]	118	229	389	624	118	229	389	624	118	229	389	624	118	229	389	624	118	229	389	624

Figure 47: Support structure mass for jacket structure typology on soft-medium sandy soils in Region 1. On the horizontal axis, turbine model and water depth in meter. On the vertical axis mass result per structural component in tons.

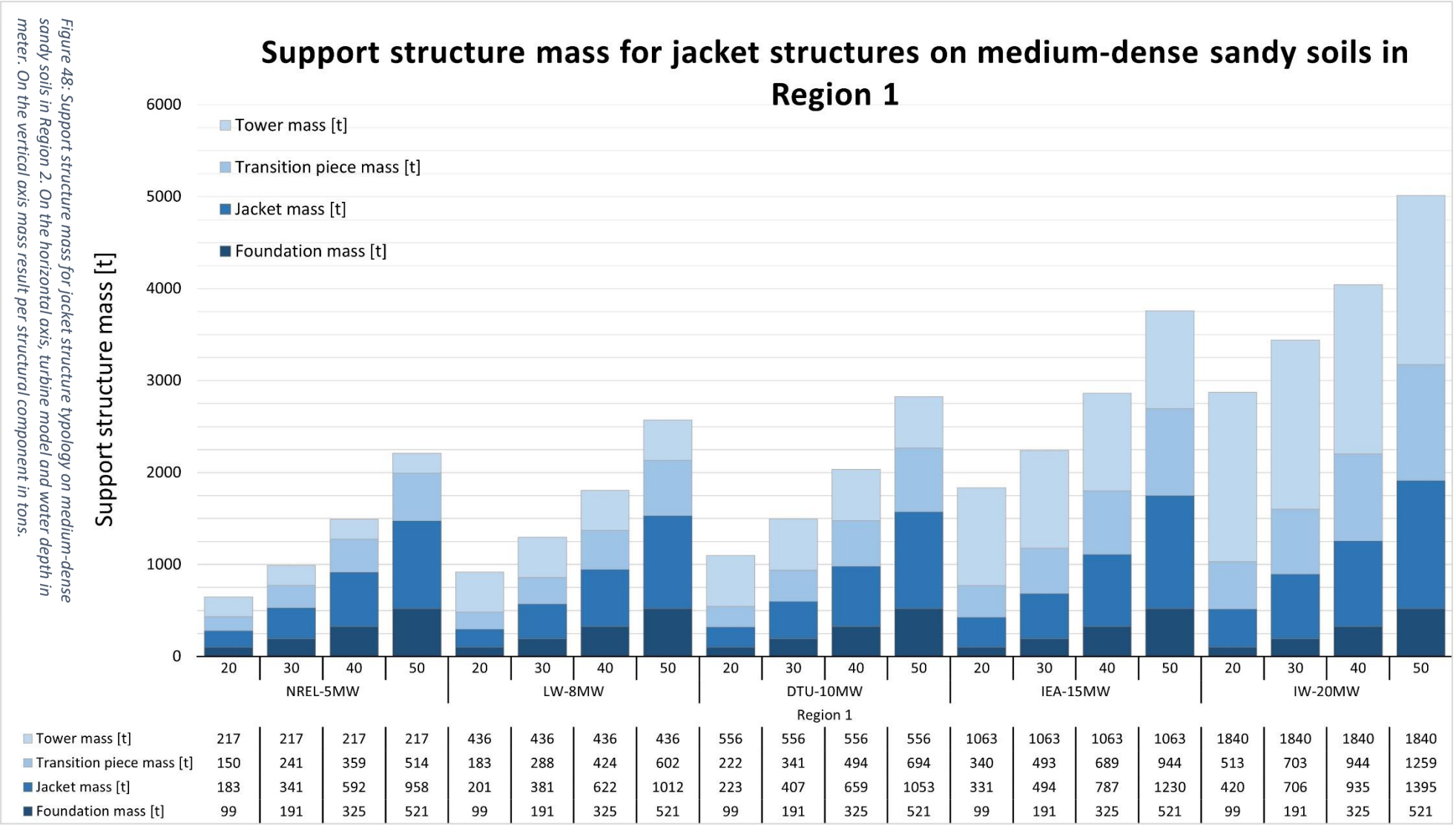

Figure 48: Support structure mass for jacket structure typology on medium-dense sandy soils in Region 2. On the horizontal axis, turbine model and water depth in meter. On the vertical axis mass result per structural component in tons.

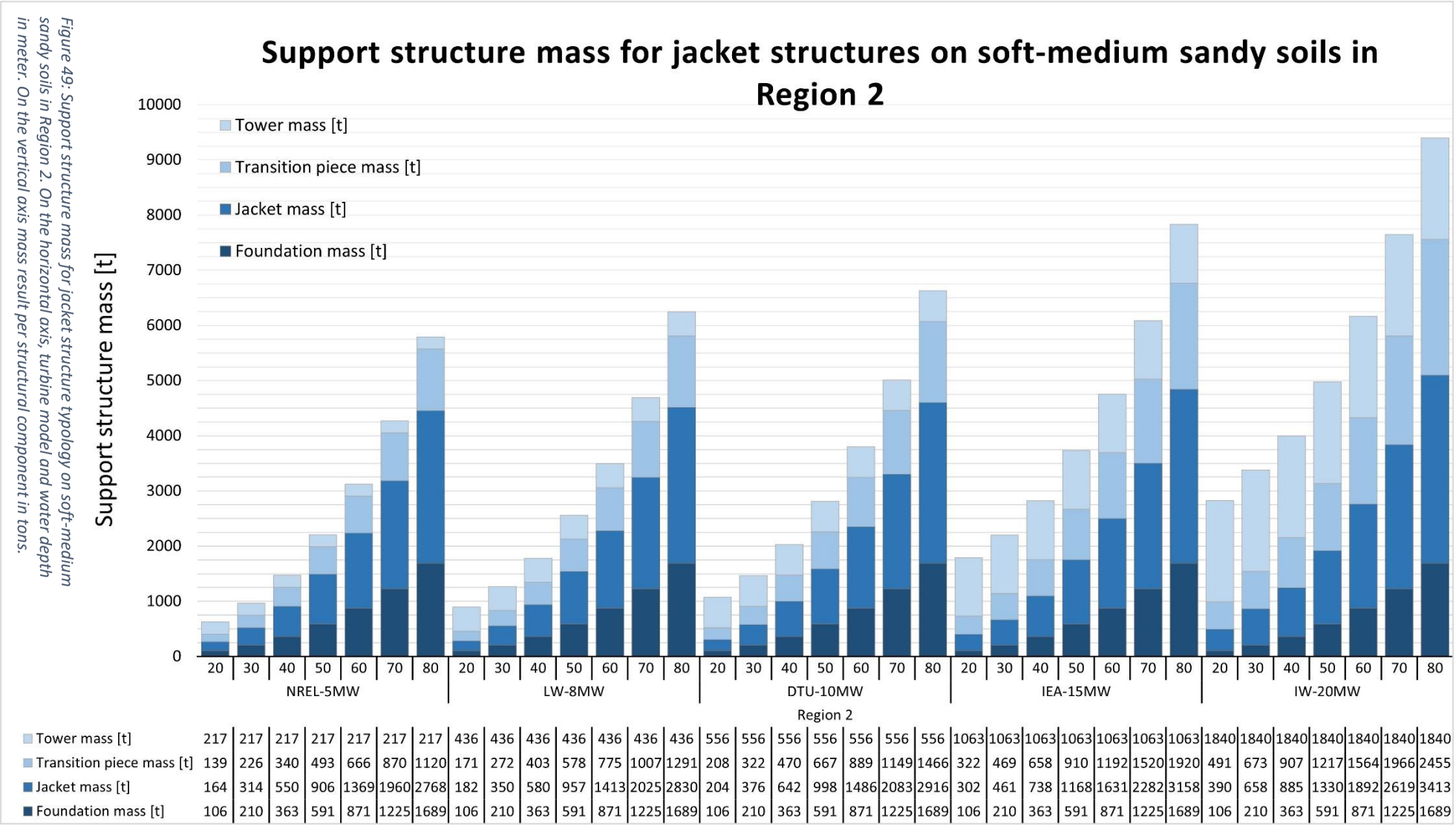

	NREL-5MW							LW-8MW							DTU-10MW							IEA-15MW							IW-20MW						
Region 2	20	30	40	50	60	70	80	20	30	40	50	60	70	80	20	30	40	50	60	70	80	20	30	40	50	60	70	80	20	30	40	50	60	70	80
Tower mass [t]	217	217	217	217	217	217	217	436	436	436	436	436	436	436	556	556	556	556	556	556	556	1063	1063	1063	1063	1063	1063	1063	1840	1840	1840	1840	1840	1840	1840
Transition piece mass [t]	139	226	340	493	666	870	1120	171	272	403	578	775	1007	1291	208	322	470	667	889	1149	1466	322	469	658	910	1192	1520	1920	491	673	907	1217	1564	1966	2455
Jacket mass [t]	164	314	550	906	1369	1960	2768	182	350	580	957	1413	2025	2830	204	376	642	998	1486	2083	2916	302	461	738	1168	1631	2282	3158	390	658	885	1330	1892	2619	3413
Foundation mass [t]	106	210	363	591	871	1225	1689	106	210	363	591	871	1225	1689	106	210	363	591	871	1225	1689	106	210	363	591	871	1225	1689	106	210	363	591	871	1225	1689

Figure 49: Support structure mass for jacket structure typology on soft-medium sandy soils in Region 2. On the horizontal axis, turbine model and water depth in meter. On the vertical axis mass result per structural component in tons.

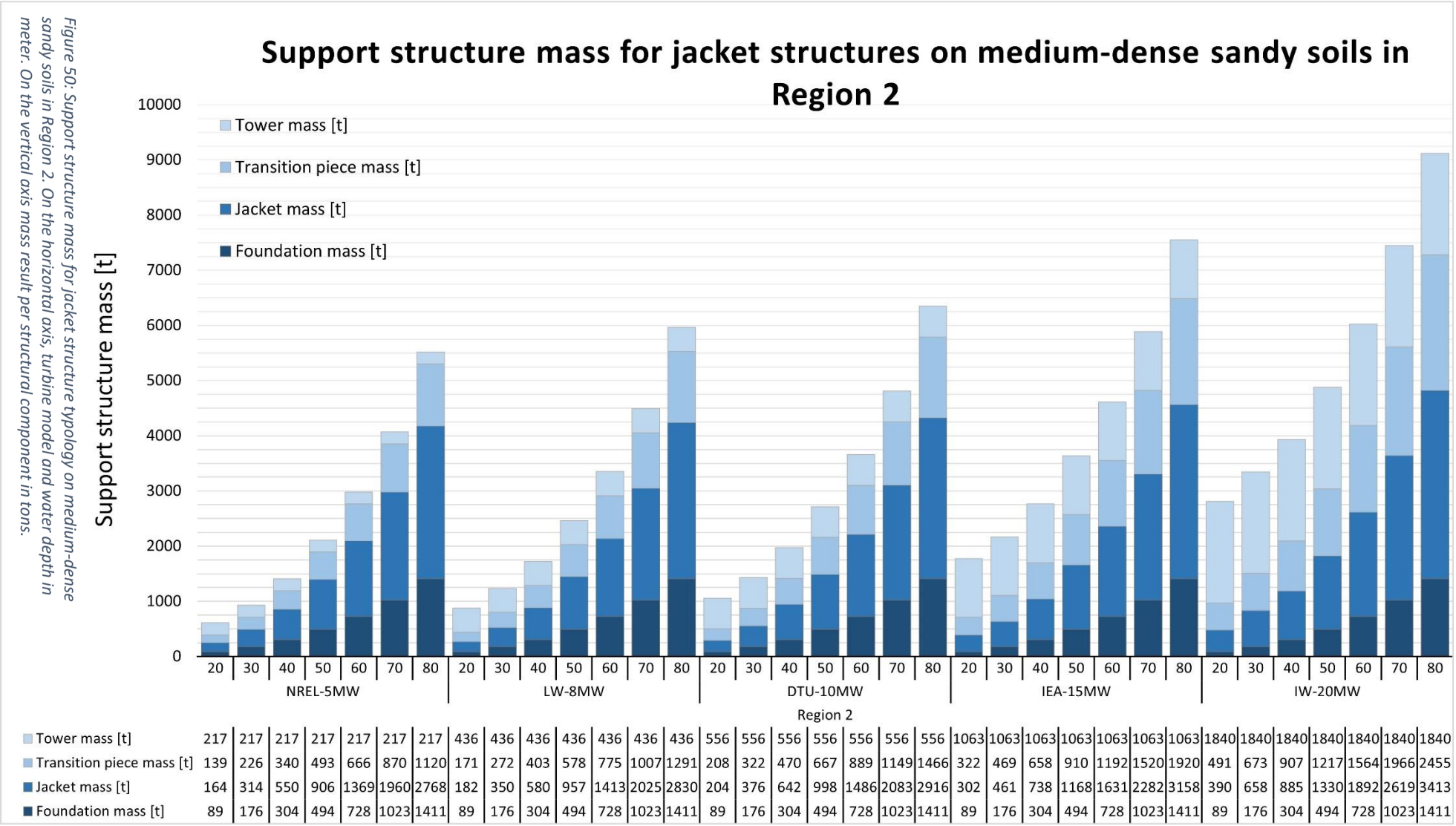

	NREL-5MW							LW-8MW							DTU-10MW							IEA-15MW							IW-20MW						
Region 2	20	30	40	50	60	70	80	20	30	40	50	60	70	80	20	30	40	50	60	70	80	20	30	40	50	60	70	80	20	30	40	50	60	70	80
Tower mass [t]	217	217	217	217	217	217	217	436	436	436	436	436	436	436	556	556	556	556	556	556	556	1063	1063	1063	1063	1063	1063	1063	1840	1840	1840	1840	1840	1840	1840
Transition piece mass [t]	139	226	340	493	666	870	1120	171	272	403	578	775	1007	1291	208	322	470	667	889	1149	1466	322	469	658	910	1192	1520	1920	491	673	907	1217	1564	1966	2455
Jacket mass [t]	164	314	550	906	1369	1960	2768	182	350	580	957	1413	2025	2830	204	376	642	998	1486	2083	2916	302	461	738	1168	1631	2282	3158	390	658	885	1330	1892	2619	3413
Foundation mass [t]	89	176	304	494	728	1023	1411	89	176	304	494	728	1023	1411	89	176	304	494	728	1023	1411	89	176	304	494	728	1023	1411	89	176	304	494	728	1023	1411

Figure 50: Support structure mass for jacket structure typology on medium-dense sandy soils in Region 2. On the horizontal axis, turbine model and water depth in meter. On the vertical axis mass result per structural component in tons.

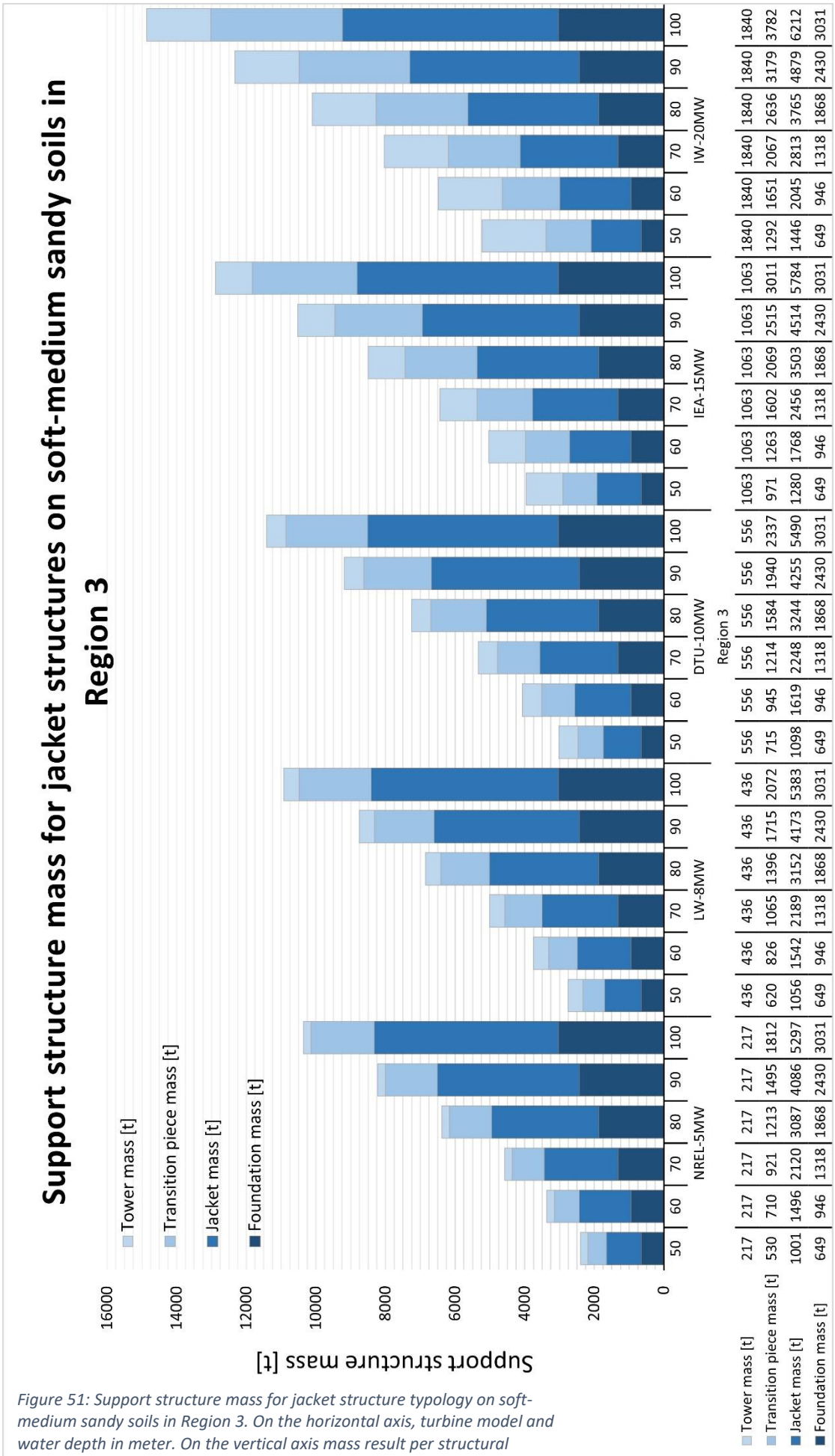

Figure 51: Support structure mass for jacket structure typology on soft-medium sandy soils in Region 3. On the horizontal axis, turbine model and water depth in meter. On the vertical axis mass result per structural

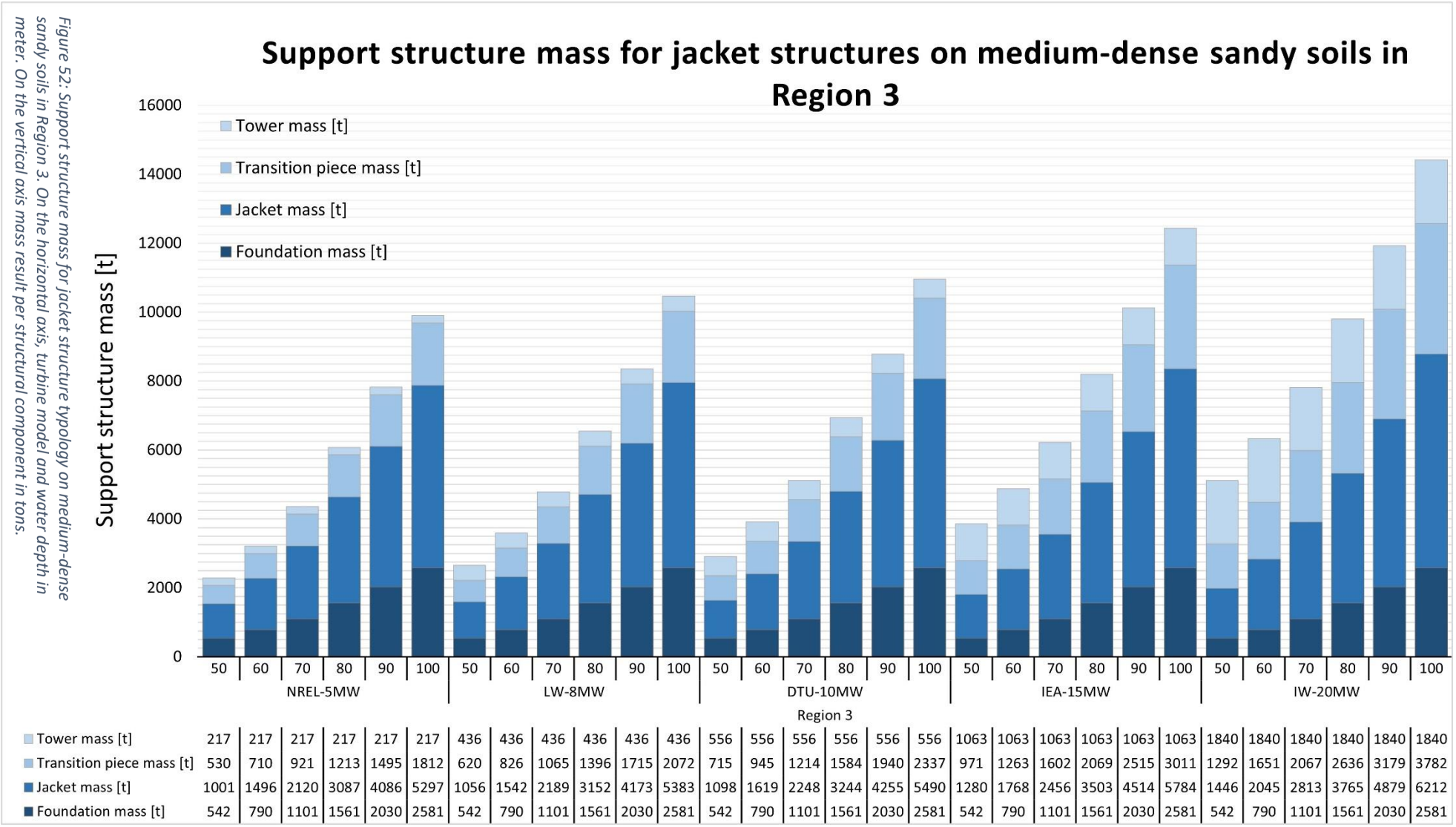

Region 3	NREL-5MW						LW-8MW						DTU-10MW						IEA-15MW						IW-20MW					
Tower mass [t]	217	217	217	217	217	217	436	436	436	436	436	436	556	556	556	556	556	556	1063	1063	1063	1063	1063	1063	1840	1840	1840	1840	1840	1840
Transition piece mass [t]	530	710	921	1213	1495	1812	620	826	1065	1396	1715	2072	715	945	1214	1584	1940	2337	971	1263	1602	2069	2515	3011	1292	1651	2067	2636	3179	3782
Jacket mass [t]	1001	1496	2120	3087	4086	5297	1056	1542	2189	3152	4173	5383	1098	1619	2248	3244	4255	5490	1280	1768	2456	3503	4514	5784	1446	2045	2813	3765	4879	6212
Foundation mass [t]	542	790	1101	1561	2030	2581	542	790	1101	1561	2030	2581	542	790	1101	1561	2030	2581	542	790	1101	1561	2030	2581	542	790	1101	1561	2030	2581

Figure 52: Support structure mass for jacket structure typology on medium-dense sandy soils in Region 3. On the horizontal axis, turbine model and water depth in meter. On the vertical axis mass result per structural component in tons.

RECYCLING POTENTIAL OF OWT SUPPORT STRUCTURES

The recycling potential of a product expresses the share of product mass that can be retrieved after end-of-life. The end-of-life recycling rate (EOL-RR) can be computed as the product of the collection rate, separation rate and recovery rate, all expressed as percentages. The collection rate expresses how many of the originally placed support structures are retrieved at the decommissioning stage of an offshore wind park. The separation rate relates to the recoverable material quantity after the structures are retrieved to shore at end-of-life. The recovery rate is determined by the efficiency of a recycling process. The EOL-RR, expressed as a percentage, indicates the level of recyclability of a product and is derived as shown in the formula below. In the following paragraphs each of these terms is elaborated for the case of OWT support structure steel.

$$EOL - RR = \%_{collection} * \%_{separation} * \%_{recovery}$$

Collection of support structures at end-of-life

Considering the collection rate, for offshore structures "the removed components of a wind farm should generally be disposed of entirely on land taking into account the waste management hierarchy of avoidance, reduction, re-use, recycling, recovery and residue disposal" (Smith, Garrett & Gibberd, 2015, p2). Typically, the decommissioning plans need to be included by the developers prior to starting construction. More importantly, steel scrap has – albeit susceptible to price fluctuations – relatively high monetary value, in the range of 150 to 450 euro per ton steel scrap considering prices in the last 15 years (World Steel Association, 2019). Topham et al. (2019) show that the scrap value of 'the average monopile' currently embedded in the North Sea covers 4-7% of the decommissioning cost considering scrap prices of 150-250 euro per ton. The tower and NRA were not separately assessed, but decommissioning cost reduction for these components varied between 11-13% of total decommissioning cost, of which roughly 8-10% could be allocated to steel components. In short, as decommissioning of OWTs is considered from the start of the development process and recoverable value can add up to 20% of decommissioning cost, the collection rate of OWT support structures is assumed to be near 100%.

Retrievable steel quantity

Considering separation rate, some parts of the OWT's foundation may be left at sea, following the reasoning that the environmental disruption created to remove foundation piles completely would be disproportionate. In practice, this leads to foundation structures being cut-off at 1-2 meter below the mudline, such that the remaining stumps do not become exposed over time (Topham et al., 2019; Smith, Garrett & Gibberd, 2015). Keeping this in mind, the overall recycling potential is to a large extent determined by the amount of material that can be successfully retrieved from a OWT support structure in decommissioning. In terms of retrievable components, monopile and jacket in-soil embedded foundations can be expected to be left at sea after the decommissioning stage, while the substructure, transition piece and tower can be retrieved.

For the support structure designs obtained, the ratio of retrievable material is calculated. Generally this found to be higher for jacket structures than for monopile structures, at 72-87% and 54-55% respectively. The influence of soil conditions on the foundation mass is substantial for both monopile and jacket structures and is shown in Table 31. Interesting to see is that soil conditions affect jacket design more than monopile design, showing a larger variation in relative retrievable mass per soil type. This can be due to the fact that the jacket is supported on four smaller sized foundation piles compared to the single monopile and that embedded pile length directly depends on soil conditions through the coefficient of subgrade reaction.

Table 31: Relative share of retrievable mass compared to total support structure mass per typology and soil type, in percentages.

Turbine	Monopiles			Jackets		
	Soft-medium soils	Medium-dense soils	Average	Soft-medium soils	Medium-dense soils	Average
NREL-5MW	62%	48%	55%	85%	58%	72%
LW-8MW	60%	48%	55%	90%	62%	76%
DTU-10MW	56%	51%	54%	92%	64%	78%
IEA-15MW	-	-	-	95%	69%	83%
IW-20MW	-	-	-	97%	74%	87%

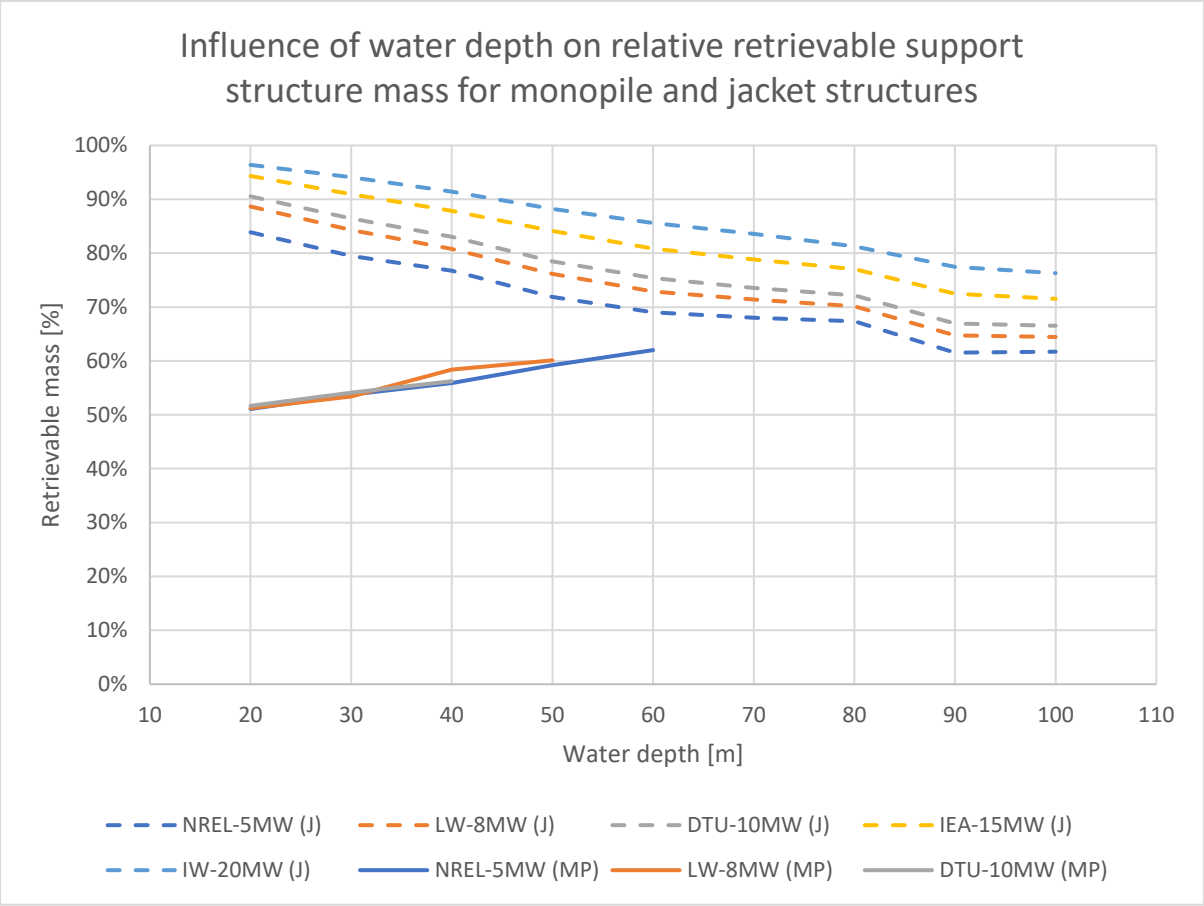

Figure 53: Influence of water depth on relative retrievable support structure mass. Values are based on support structure dimensioning and calculation results.

The influence of water depth on the share of retrievable material is shown in Figure 53. It can be seen that an increase in water depth results in lower retrievable support structure mass, roughly following a linear correlation. Monopiles and jackets seem to be similarly affected by water depth variation, as – disregarding the higher overall values for jacket structures – relative retrievable mass declines at an even rate for both typologies.

The influence of the turbine rated power on the relative retrievable mass is negligible for monopile structures, while a clear difference can be seen for jacket structures. Interesting to see is that the relative share of retrievable mass increases for structures at greater depth. Logic dictates that an absolute increase in structure size above the mudline results in an increased structure size below the mudline, considering the structure's stability requirements. The relative increase of retrievable mass

can be explained by the fact that the embedded monopile length does not increase linearly for deeper water structures. In other words, for every ton of steel added above ground less than a ton of soil-embedded foundation is required. For the obtained monopile designs, tower dimensions depend on the NRA mass and the natural frequency of the tower and monopile structure combined. Therefore, it would be expected that the reference turbine models influence the relative retrievable mass. The fact that it seemingly does not, could be the result of the applied modelling method, but the cause remains unknown and could be reason for further study. For tower and monopile combined, the variation of relative retrievable mass is roughly 10% for water depths of 20 and 60 meter, being approximately 50% and 60% respectively.

For the jacket typology, a decrease in relative share of retrievable mass is observed in relation to turbine rated capacity increase and increase in water depth. The former follows from the fact that a single tower mass was chosen for each reference turbine. Hence, the relative difference between the NREL-5MW and the IW-20MW ranges between 10-15% and is constant with respect to water depth. In contrast, substructure and foundation dimensions are modelled to be depend on turbine tower dimensions, water depth and soil type. It stands out that the relative share of retrievable mass for jacket structures consistently decreases for greater water depths, whereas the opposite was observed for monopile structures**.** In other words, for every ton of steel added above ground, more than a ton of soil-embedded steel is required for jacket foundations. Variation in water depth affects retrievable mass in the range of 15-20%. For combinations of >10MW capacity turbines and water depths up to 30 meter, retrievable mass is found to be in the order of magnitude of 90%. For a water depth range of 30-80 meter – in which jackets are mostly likely to be deployed – the retrievable mass varies between 70-90%.

It can be concluded that the average retrievable support structure mass for various turbines and water depths up to 2050 will be in the order of magnitude of 55% and 80% for monopile and jacket typologies.

Recyclable steel quantity

As priorly mentioned, the EOL-RR is a function of the collection, separation and recovery rate. The quantity of recyclable mass for each water depth and turbine combination is calculated as the product of said rates and the cumulative support structure masses. A collection rate of 100% for both monopile and jacket structures, separation rates for the specific turbine-water depth combinations and a recovery rate of 95% for all steel available for recycling are applied. The development of retrievable masses and loss of material for each turbine and water depth combination is shown in Figure 54 and Figure 56 respectively to be found on page 117 and 118.

From Figure 54 it can be seen that recoverable steel roughly follows a second-order polynomial increase for both monopile and jacket topologies. Rated capacity influences recoverable mass by means of vertical translation. Specifically, increase in rated capacity results in an increase of to-be-recycled material at end of life. For monopiles, the trend seems to follow a linear relation, even though the number of data points to base this conclusion on is quite low. For jackets, this trend does not follow a linear relation, as the relative increase of recyclable steel between 5 and 10 MW rated capacity is smaller than the relative increase between a 15 and 20 MW rated capacity. This is most easily observed by comparing jacket structure retrievable mass at 70 meter depth, comparing the difference between light blue and yellow dashed lines and the orange and dark blue dashed lines, in Figure 54. Increase of water depth also results in increase of recyclable material at end of life. Water depth influences recyclable mass by means of a 2nd order polynomial for both monopile and jackets.

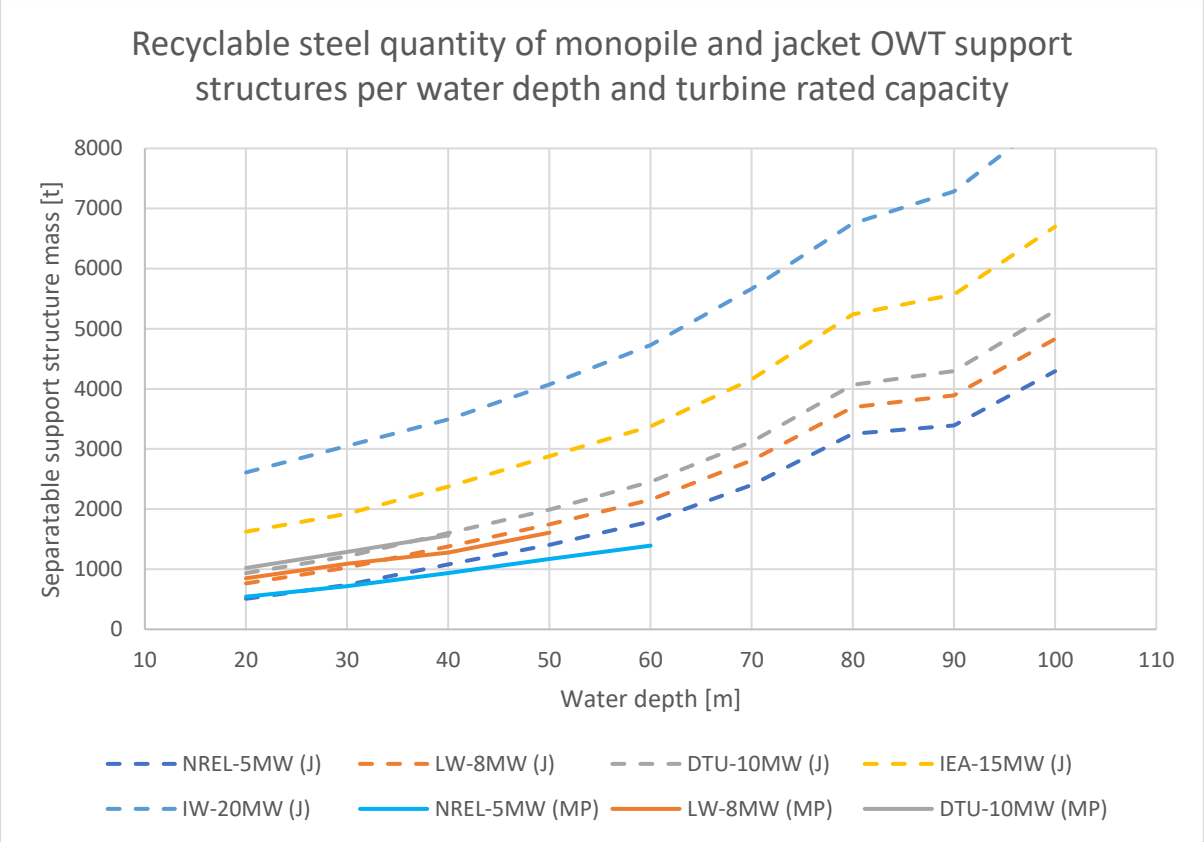

Figure 54: Overview of retrievable mass development for monopile and jacket support structure typologies with respect to turbine rated capacity and water depth. Mass values are given in tons of steel.

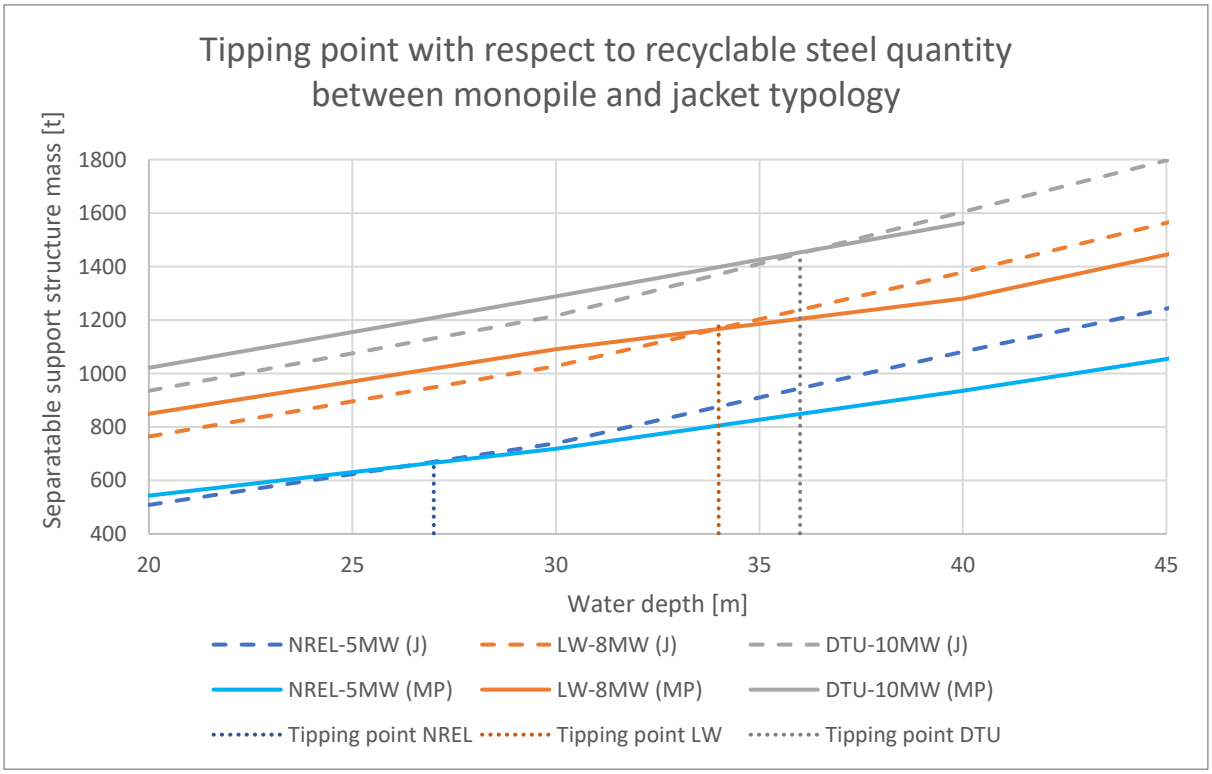

Figure 55: Tipping point of retrievable mass between monopile and jacket support structures. This visualisation is a cut-out of the figure presented above. For the NREL-5MW, LW-8MW and DTU-10MW tipping points are found at water depths of 27, 34 and 36 meter respectively.

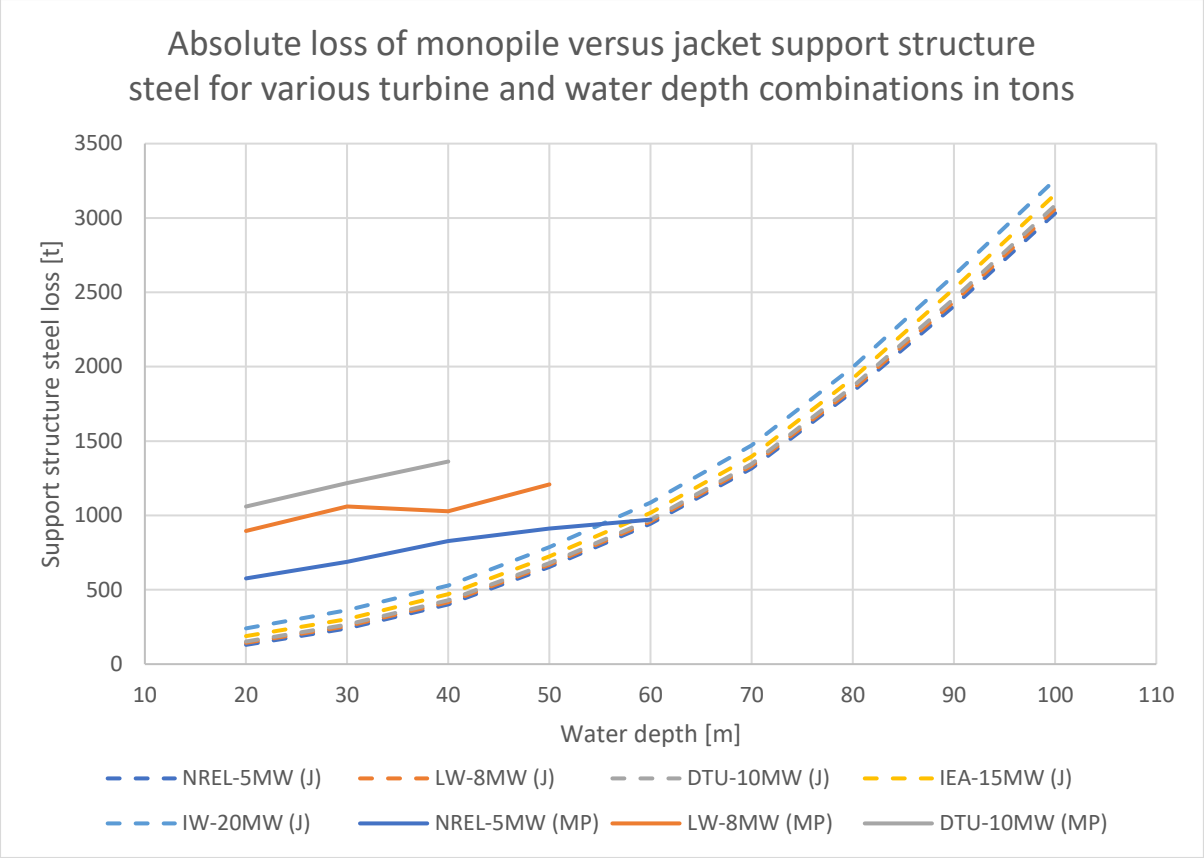

Figure 56: Material loss over a single lifetime for monopile and jacket support structures related to multiple turbine capacities and water depths.

To avoid confusion, it is emphasised that the aforementioned trend regarding rated capacity and retrievable mass is not well visible in Figure 55. Here, only the NREL-5MW, LW-8MW and DTU-10MW are displayed which makes the former comparison between 5-10 and 10-20MW turbines irrelevant and harder to observe. The trend, however, does still hold. Figure 55 shows tipping points between monopile and jacket recyclable mass. It can be seen that the water depth at which this tipping point occurs, increases with turbine rated capacity. More specifically, the to-be-recycled mass for monopiles is higher than for jackets below the tipping point water depth. Tipping points between monopile and jacket typologies for the NREL-5MW, LW-8MW and DTU-10MW are found as 27, 34 and 36 meter respectively.

Considering the main research question of this research, more interesting to know are the support structure steel losses related to the reference turbines and water depths combinations. An overview of the absolute steel loss occurring from the point of installation to post-recycling are shown in Figure 56. It can be seen that for almost all turbine-water depth combinations jacket typology structures are more favourable towards material losses.

For water depths of 20 to 60 meter, monopile steel losses occur in a range of 570-1360 ton depending on turbine rated capacity for which monopile designs proved manufacturable. For the same depth range and turbine selection, jacket typology steel losses occur in a range of 130-970 ton. Regarding steel losses per turbine rated capacity, higher rated turbines are consistently associated with higher steel losses. The same applies with respect to water depth, where water depth increase consistently results in higher steel losses.

A6: GHG emission indicator EU steel production

There are two common methods for primary steel production, namely BF-BOF and EAF methods. Steel production in the EU is characterised by relatively high EAF production. In 2017, the ratio of BF-BOF and EAF originated steel were 59.8% and 40.1% respectively. An assumption is made that the S355G10+M steel used for OWT support structures is also represented by this ratio.

In the BF-BOF method, cokes obtained from coal are used as fuel to convert a mixture of iron ore and steel scrap into molten iron. In this process, carbon from the cokes is oxidised releasing large amounts of energy required to break the chemical bonds between Iron and Oxygen present in iron ore. Furthermore, most impurities present in the molten iron are oxidised and are separated from the iron melt by slag formation or end up in off-gasses. The carbon and oxygen chemically react to form carbon dioxide, which is a potent green house gas. The amount of coke consumed in BF iron making is 0.45 ton coke / ton iron (World Steel Association, 2016). In turn, approximately 1.5 ton coking coal is required to produce 1.0 ton of BF coke where the average carbon content of a ton coking coal is 78 wt% (Schobert & Schobert, 2015). By multiplication of these numbers, carbon consumption per ton molten iron can be found as approximately 0.5 ton C/ton iron. The ratio between molecular mass of carbon dioxide and elemental carbon is found as 44/12 and, after unit conversion, amounts to 3.67 ton CO2/ton C. Based on the above, the carbon emissions related to one ton of BF molten iron are found as 1.84 ton CO2/ton BF iron.

EAF furnaces consume electricity instead of cokes, at a rate of 500 kWh electricity per ton molten EAF iron. Carbon emissions of grid-fed electricity vary between 0.48-0.63 kg CO2/kWh depending on, amongst other thing, the availability of renewable electricity and the share of nuclear electricity generation at a given point in time (CO2 Emissiefactoren, 2020). An average value for grey electricity is also provided as 0.56 kg CO2/kWh. An assumption is made that EAF electricity used is represented by these emission factors, which reflect the Dutch electricity mix but might differ in other countries. Combining these numbers, a carbon dioxide emission of 0.28 ton CO2/ton EAF iron is obtained.

In secondary steel making, no additional energy is supplied to the ladle furnace, as much excess heat is formed in the oxygen blowing processes taking place (Yang, 2019). In secondary steel making, carbon content of the steel is reduced from approximately 4% to the 0.06% present in the S355G10+M steel, which results in an additional 0.04 ton CO2/ton steel. Total carbon emissions allocated to BF-BOF and EAF steel production are 1.85 ton CO2/ton BF-BOF steel and 0.29 ton CO2/ton EAF steel. Combining this with an average steel composition of 59.8% BF-BOF and 40.1% EAF steels, this results in 1.22 ton CO2/ton steel.

It should be noted that during the steel making process some more emissions emerge related to mining and transport of iron and CRM ores and fossil coal, off-gas handling, milling and shaping of the steel, transport of the steel towards the manufacturing and assembly facility, assembly and welding, transport to final OWT installation and final assembly. Compared to GHG emissions emerging in steelmaking processes, Bonou et al. (2016) find that the before mentioned processes combine to approximately 22% of the total contribution to climate change.